DEVELOPMENT OF DUAL-WAVELENGTH AND PULSED FIBER LASERS BASED ON THULIUM-DOPED FIBERS

SALAM MAHDI AZOOZ

FACULTY OF ENGINEERING
UNIVERSITY OF MALAYA
KUALA LUMPUR

2015

DEVELOPMENT OF DUAL-WAVELENGTH AND PULSED FIBER LASERS BASED ON THULIUM-DOPED FIBERS

SALAM MAHDI AZOOZ

THESIS SUBMITTED IN FULFILMENT
OF THE REQUIREMENTS
FOR THE DEGREE OF DOCTOR OF PHILOSOPHY

FACULTY OF ENGINEERING
UNIVERSITY OF MALAYA
KUALA LUMPUR

2015

UNIVERSITI MALAYA

ORIGINAL LITERARY WORK DECLARATION

Name of Candidate: **SALAM MAHDI AZOOZ**   (I.C/Passport No: **A7221693**)
Registration/Matric No: **KHA120134**
Name of Degree: **Doctor of Philosophy (Ph.D)**

Title of Project Paper/Research Report/Dissertation/Thesis ("this Work"):
DEVELOPMENT OF DUAL-WAVELENGTH AND PULSED FIBER LASERS BASED ON THULIUM-DOPED FIBERS

Field of Study: **PHOTONIC & FIBER OPTIC**

I do solemnly and sincerely declare that:
(1)   I am the sole author/writer of this Work;
(2)   This Work is original;
(3)   Any use of any work in which copyright exists was done by way of fair dealing and for permitted purposes and any excerpt or extract from, or reference to or reproduction of any copyright work has been disclosed expressly and sufficiently and the title of the Work and its authorship have been acknowledged in this Work;
(4)   I do not have any actual knowledge nor do I ought reasonably to know that the making of this work constitutes an infringement of any copyright work;
(5)   I hereby assign all and every rights in the copyright to this Work to the University of Malaya ("UM"), who henceforth shall be owner of the copyright in this Work and that any reproduction or use in any form or by any means whatsoever is prohibited without the written consent of UM having been first had and obtained;
(6)   I am fully aware that if in the course of making this Work I have infringed any copyright whether intentionally or otherwise, I may be subject to legal action or any other action as may be determined by UM.

Candidate's Signature   Date

Subscribed and solemnly declared before,

Witness's Signature   Date

Name:
Designation:

ABSTRACT

A growing interest on lasers operating in the eye-safe two micron spectral region especially on dual-wavelength and pulse operations for a variety of applications motivated this PhD work. The scope of this thesis focuses on the development of new fiber lasers, which incorporates Thulium fiber as either gain medium or saturable absorber. At first, all-fiber dual-wavelength 2 μm fiber lasers are demonstrated based on three simple approaches; spatial filtering effect, inline microfiber Mach Zehnder Interferometer (MMZI) and multimode interference effect. The use of MMZI in the 2 μm laser cavity, for instance, successfully generates two simultaneous laser lines at 1952.93 and 1956.68 nm with a signal to noise ratio of more than 35 dB by using a cascaded commercial Thulium-doped fiber (TDF) and laboratory made double-clad Thulium-Ytterbium co-doped fiber (TYDF) as the gain media. Then, various Q-switched and mode-locked fiber lasers operating in 2 μm region were demonstrated using either the TDF or TYDF as the gain medium. Q-switched fiber lasers operating at 1949.0 nm and 1846.4 nm are successfully demonstrated based on nonlinear polarization rotation (NPR) technique and multi-walled carbon nanotubes (MWCNTs) saturable absorber (SA), respectively. A mode-locked fiber laser is also demonstrated by using a TYDF as the gain medium and commercial graphene oxide (GO) paper as SA. The mode-locked TYDFL has a repetition rate of 22.32 MHz and the calculated pulse width of 1.1 ns. Besides amplification purpose, a Thulium fiber can also be used as a SA in Erbium-doped fiber laser (EDFL) setups for both Q-switching and mode-locking applications. A dual-wavelength Q-switched EDFL EDFL operating at 1551.64 nm and 1534.8 nm was also demonstrated using the solid state TDF as the SA.

ABSTRAK

Terdapat pertambahan minat terhadap laser yang beroperasi pada panjang gelombang selamat mata 2-mikron terutamanya pada aplikasi laser denyut dan laser dua panjang gelombang. Skop thesis ini memberi tumpuan kepada pembangunan laser gentian baru yang menggabungkan gentian Thulium sebagai media pengganda atau penyerap boleh tepu. Pertamanya, laser dua panjang gelombang pada 2-mikron ditunjukkan melalui tiga cara mudah iaitu, melalui efek penapis ruang, 'Mach Zehnder' (MMZI) dan inteferens pelbagai mod. Sebagai contoh, kegunaan MMZI di dalam kaviti laser 2 mikron telah berjaya menjana dua laser sekaligus, iaitu pada 1952.93 nm dan 1956.68 nm, dengan nisbah signal-to-noise (SNR) melebihi 5 dB dengan menggunakan gentian optic Thulium (TDF) dan gentian optic terdop Thulium-Ytterbium (TYDF). Kemudian, pelbagai laser gentian Q-suis dan mod terkunci yang beroperasi di panjang gelombang 2 µm telah ditunjukkan menggunakan TDF atau TYDF sebagai media pengganda. Laser gentian Q-suis yang beroperasi pada 1949 nm dan 1846.4 nm berjaya ditunjukkan berdasarkan teknik pengutuban putaran tak malar dan karbon tiub nano berlapis dinding penyerap boleh tepu. Laser gentian mod terkunci juga ditunjukkan dengan menggunakan kertas graphene oxide sebagai penyerap boleh tepu dan TYDF sebagai media pengganda. Frekuensi yang dijanakan adalah pada 22.32 MHz dan lebar denyut yang dikira adalah 1.1 ns. Selain tujuan gandaan, gentian terdop Thulium juga boleh digunakan sebagai penyerap boleh tepu di dalam kaviti laser Erbium untuk tujuan Q-suis dan mod terkunci. Dua panjang gelombang Q-suis laser Erbium yang beroperasi pada 1551.64 nm dan 1534.8 nm juga ditunjukkan dengan menggunakan TDF sebagai penyerap boleh tepu.

ACKNOWLEDGEMENTS

LIST OF CONTENTS

LIST OF FIGURES

Chapter 4   Pulsed Fiber Lasers Operating at 2 Micron Region

LIST OF SYMBOLS AND ABBREVIATIONS

ASE   Amplified spontaneous emission

CCVD   Catalytic Chemical Vapor Depostion

CNT   Carbon Nano-Tube

CVD   Chemical Vapor Depostion

CW   Continues Wave

DIAL   Differential Absorbtion Lidar

DWFL   Dual-Wavelength Fiber Laser

DWQS   Dual-Wavelength Q-Switching

EDF   Erbium-Doped Fiber

EDFL   Erbium-Doped Fiber Laser

EPMA   Electron Probe Micro-Analyser

FBG   Fiber Bragg Grating

FC/PC   Fiber-Optic Connector/Physical Connector

FOLM   Fiber optic loop mirror

FWHM   Full-Width Half Maximum

GO   Graphene Oxide

GOP   Graphene Oxide Paper

GSA   Graphene Saturable Absorber

Hi-Bi   High-Birefringence

InGaAs   Indium Gallium Arsenide

LAGS   Lithium-Alumino-Germano-Silicate

LIDAR   Light Detection and Ranging

MCDV   Modified Chemical Vapor Deposition

MMC   Multi-Mode Combiner

MMF	Multi-Mode Fiber
MMI	Multi-Mode Interference
MMZI	Microfiber Mach-Zehnder Interferometer
MPE	Maximum phonon energy
MWCNT	Multi-Wall Carbon Nanotube
NA	Numerical Aparture
NPR	Nonlinear Polarization Rotation
OPO	Optical-Parometric-Oscillation
OSA	Optical Spectrum Analyzer
OSC	Oscilloscope
PC	Polarization Controller
PD	Photo-Detector
PEO	Polyethylene Oxide
PVA	Polyvinyl Alcohol
RBM	Radial Breathing Mode
RF	Radio Frequency
RFSA	Radio Frequency Spectrum Analyser
rGO	reduced-Graphene Oxide
SA	Saturable Absorber
SDS	Sodium Dodecyl Sulphate
Sech2	Hyberbolic Secant Squared
SESAM	Semiconductor Saturable Absorber Mirror
SHG	Second Harmonic Generation
SMF	Single Mode Fiber
SNR	Signal to Noise Ratio
SPM	Self-Phase Modulation

SWCNT	Single-Walled Carbon Nanotube
VOA	Variable Optical Attenuator
WDM	Wavelength Divission Muliplexer
XPM	Cross- Phase Modulation
dB	desible
dBm	desible per milliwatt
ms	millisecond
ns	nanosecond
ps	picosecond
fs	femtosecond
Hz	Hertz
KHz	Kilohertz
MHz	Megahertz
GHz	Gigahertz
W	Watt
mW	milliwatt
µW	microwatt

CHAPTER 1

Introduction

1.1   Background

Optics is a science that deals with the genesis and propagation of light, the changes that it undergoes and produces, and other phenomena closely associated with it (Inc., 2004). Since Euclid published his work: Katoptrik, several research works have brought a new revolution to optics research, such as Newton's "Opticks", Huygens's work on wavelet, Maxwell's equations, and Planc's theory of light quanta. However the birth of Laser triggered the biggest explosion of activities in optics. Laser was first invented in 1958 and since then many new technologies based on lasers were established for various applications. (Wu, 2005). It also opened several entirely new fields for scientists, such as nonlinear optics, fiber optics, and opto-electronics, because of its ability to generate an intense and very narrow beam of light of a single wavelength. Numerous researches, patents, and businesses have been established upon the applications of Lasers. Today instead of as a branch of fundamental physics, laser researches have been involved in various other fields such as information technology, medicine treatment, biological study, and entertainment.

The idea of laser originates from Albert Einstein's theory on "Stimulated emission" in which, when it encounters a photon, matter may lose energy by emitting an exactly same photon. As a result the amplification of light is achievable under condition of population inversion. In addition to the gain media, another essential element is optical cavity in which the light can circulate and get amplified. As long as the gain is larger than the losses, the power of the light in the laser cavity quickly rises. Significant power output is thus achieved only above the so-called laser threshold that is the power where the small-signal gain is just sufficient to compensate the cavity loss.

The first laser action is demonstrated by Theodore H. Maiman in 1960 at Hughes Research Laboratories in Malibu, California (Maiman, 1960),using 2 cm long ruby cylinder as the active gain medium. It used a flash lamp to pump the ruby rod to generate laser lasing at 694 nm. However, Gordon Gould was the first person to use the word "laser". Interestingly, in 1962 the first diode laser was developed by Robert N. Hall at the General Electric (Hall et al., 1962). It was a gallium-arsenide p-n junction emitting at the wavelength of 842 nm. The development of powerful and efficient diode laser has been essential for their use as pump sources. Meanwhile, the first visible wavelength laser diode was demonstrated by Nick Holonyak Jr later in 1962. (Holonyak Jr & Bevacqua, 1962). Since then laser physics has always been driven by a genuinely scientific quest to extend existing limits such as higher power, shorter pulse, narrower linewidth and new wavelength. Over the last fifty years, developments in the laser field have occurred at a rapid pace. Many new lasers have been discovered, each with its own special properties and applications, and their cost, performance, and practicality have all shown dramatic improvement.

Recently a great deal of researches on the 2- µm fiber laser have been conducted using a Thulium-doped fiber (TDF) as the gain medium. The TDF laser (TDFL) has drawn a great interest since it offers a possibility for combining high efficiency and high output power with eyesafe operation. In addition, it suggests a number of specific applications associated exclusively with its infrared wavelength, e.g. in the fields of remote sensing and biomedicine (Harun et al., 2012; Harun et al., 2012; Jiang, 2011; Zhang et al., 2011). The TDFL was firstly discovered by Hanna et al. in 1988 with a 797 nm dye laser as the pump source (Hanna et al., 1988). Meanwhile, the first 2 µm Q-switched TDFL was carried out in 1993 by acousto-optic modulator (Myslinski et al., 1993). This thesis aims to investigate and demonstrate two applications of Thulium fiber as a gain medium and saturable absorber (SA). In this work, various 2 micron fiber

lasers operating in CW, Q-switching and mode-locking modes are proposed and demonstrated. Various Q-switched Erbium-doped fiber lasers are also demonstrated based on TDF SA.

1.2   Motivation

A growing interest on lasers operating in the eye-safe two micron spectral region for a variety of applications motivated this research work. Recently a great deal of researches on the 2-micron laser have been conducted in both solid-state laser and fiber laser field because of its wide applications in medicine, remote sensing, lidar, range finder, and molecular spectroscopy (Esterowitz, 1990; Henderson et al., 1993; Miazato et al., 2000; Stoneman & Esterowitz, 1990). The strong absorption by water and the weak absorption by human tissues at 2 μm also nominate it as an ideal wavelength for biological and medical applications including laser angioplasty in the coronary arteries, ophthalmic procedures, arthroscopy, laparoscopic cholecystectomy and refractive surgeries. In addition, other features of 2 μm laser such as the lower atmospheric absorption, smaller scattering and "eye-safe" property make the wavelength desirable for material processing, ranging, low altitude wind shear and remote sensing, which includes Doppler lidar wind sensing and water vapor profiling by differential absorption lidar (DIAL). Such wavelength is also an ideal pump source for mid-infrared optical material.

All-fiber dual-wavelength fiber lasers have also gained a great attention in recent years due to their potential applications in microwave photonics, fiber sensing systems, optical instrument testing, and optical signal processing (Ahmad et al., 2009; Chan, 1997). Up to date, various methods have been suggested and demonstrated to achieve a dual-wavelength lasing operating in the region of 1 and 1.5 μm. These are the techniques that involve a dual-cavity configuration or a twin-peak reflection grating. However, for the longer wavelength region of 2 μm, the fiber components in need are

not as readily available as those suitable for the generation at 1.00 μm or even 1.55 μm. Very recently, Zhang et. al. have demonstrated a dual-wavelength solid-state microchip Tm, Ho:YVO4 laser that simultaneously operates at 2041.3 and 2054.6 nm (Zhang et al., 2010). Due to its compactness and robustness, an all-fiber laser able to generate in the 2 μm band is still urgently expected to materialise. In this thesis, at first, we aim to develop a room-temperature all-fiber dual-wavelength fiber laser operating near 1900 nm by using a homemade filter.

Likewise, pulsed lasers are used in a variety of applications, ranging from optical communications (Rulliere, 2005) to medical diagnostics (Dausinger et al., 2004) and industrial materials processing (Fermann et al., 2002). Development of new gain medium and saturable absorber technologies (Keller, 2003, 2004; Keller, 2010) have changed the outlook of Q-switched and ultrafast lasers over the past two decades. These advances, in particular the realization of new saturable absorbers, have pushed the applications of both Q-switched and mode-locked lasers to a realm broader than ever before. Q-switched and mode-locked fiber lasers demonstrated up to date are usually achieved using nonlinear polarization rotation (NPR) (Liu et al., 2011; Liu et al., 2008) semiconductor saturable absorbers (SESAMs) (Huang et al., 2009; Ji et al., 2007) and single-walled carbon nanotubes (SWCNTs) (Harun et al., 2012; Solodyankin et al., 2008) and graphene (Sun et al., 2010; Wei et al., 2012). These approaches are well-known and have been established over the years. Nevertheless, NPR induced lasers tend to be environmentally unstable and difficult to provide self-starting pulsed operation. SESAMs are complex quantum well devices, typically fabricated by molecular beam epitaxy on distributed Bragg reflectors. Furthermore, lasers assisted by SESAMs suffer from relatively narrowband operation. Lasers produced with the use of SWCNTs and graphene saturable absorbers are known to show distinct advantages in their ultra-fast recovery time and wide absorption bandwidth. Therefore, in this thesis, various Q-

switched and mode-locked fiber lasers are proposed and demonstrated based on new materials and technologies.

To date, only a few works on the generation of pulsed fiber laser near 2 μm wavelength region have been reported. For instance, Wang et. al. (F. Wang et al., 2012) reported a Q-switched generation with maximum pulse energy of 69 nJ and a repetition rate of 26 kHz using 1560 nm CW laser source and graphene saturable absorber (GSA). More recently, Jiang et. al. (Jiang et al., 2013). Achieved laser with a short pulse duration of 760 ns and a repetition rate of 202 kHz using graphene transferred to the HR mirror as SA. Works on GSA based Q-switched TDFLs are mostly related to free-space arrangement (Wang et al., 2012) and linear configuration (Lu et al., 2013). In this thesis, Q-switched 2 micron fiber lasers are proposed by using new passive saturable absorbers based on multi-walled carbon nanotubes (MWCNTs) and graphene oxide.

While constructing carbon nanotubes and graphene based SAs are relatively simple and cheap, they have a low damage threshold and thus limit the attainable pulse energy. Modulation of the Q-factor can also be realized using solid-state SA fibers (Dvoyrin et al., 2007; Kurkov et al., 2009; Tsai et al., 2009). The advantages of the fiber based SA are their relatively high damage threshold for high-power Q-switched pulses as well as their ability to hold enormous gain excited in the fiber from lasing. Only a few SA fibers have been demonstrated up to now in the literature, and most are for Ytterbium-doped fiber lasers (Dvoyrin et al., 2007; Kurkov et al., 2009). It is reported that Thulium fiber has a very broad emission wavelength range, from 1.6 to 2.1 μm, and an absorption band from 1.5 to 1.9 μm due to the energy transition between $^3H_6$ and $^3F_4$ energy levels. Furthermore, the absorption cross section of TDFs are larger than the emission cross sections of Erbium-doped fiber (EDF) at 1.6 μm region, suggesting a possible realization of a passively Q-switched EDF laser (EDFL) using a TDF as a

passive SA. In this thesis, we have also proposed Q-switched EDFLs by using a solid state Thulium fiber SA as a Q-switcher.

1.3   Thesis Objectives

The scope of this thesis focuses on the development of new fiber lasers, which incorporates Thulium fiber as either gain medium or saturable absorber. To achieve this, few objectives have been proposed to guide the research direction, i.e.:

1. To develop new all-fiber dual-wavelength 2μm fiber lasers using commercial Thulium-doped fiber (TDF), a newly developed Thulium-Ytterbium co-doped fiber (TYDF) or both fibers as the gain medium

2. To develop Q-switched and mode-locked fiber lasers operating in 2 micron region using both artificial and passive saturable absorbers as Q-switcher or mode-locker.

3. To develop Q-switched EDFLs operating in both single- and dual-wavelength modes using a short piece of TDF as a passive saturable absorber.

1.4   Thesis Overview

In this thesis, we focus on the study of two applications of Thulium fiber as gain medium and SA. In this work, two types of Thulium fibers were used; a commercial Thulium-doped fiber (TDF) and a newly developed Thulium-Ytterbium co-doped fiber (TYDF). This thesis is arranged into six chapters, where the background, motivation and objective of this study are described in this chapter. Chapter 2 devoted to some fundamental and literature review of fiber lasers especially on Thulium fiber laser and Thulium Ytterbium co-doped fiber as well as the discussion on pulse generation based on Q-switching and mode-locking and saturable absorber. The important graphene and carbon nanotubes characteristics are also discussed in this chapter.

Chapter 3 focuses on demonstrating all-fiber dual-wavelength 2 µm fiber lasers based on three simple approaches; spatial filtering effect, inline microfiber Mach Zehnder Interferometer (MMZI) and multimode interference (MMI) effect. Spatial filtering effect is the simplest approach where the mismatch at the splicing points of a TDF is used to generate mode-beating. By pumping the gain medium with an 800 nm laser and controlling the phase mismatch at the splicing points of a TDF, the two output lines are obtained at 1844.8 and 1852.0 nm in a TDFL setup. A homemade inline MMZI is used to generate dual-wavelength fiber laser operating in 1955 nm region using a cascaded commercial TDF and homemade double-clad TYDF as the gain medium. The MMI filter is fabricated by using a 13.5 cm long multimode fiber (MMF), which axially spliced at both its ends to identical single mode fibers. By using a TDF and homemade double-clad TYDF as gain media, an all-fiber dual-wavelength fiber laser operating at 1939.68 and 1959.60 nm is realized by using the filter in the ring configuration.

In chapter 4, various Q-switched and mode-locked fiber lasers operating in 2 micron region were demonstrated using either commercial TDF or a newly developed TYDF as the gain medium. In this work both artificial and passive saturable absorbers were used as Q-switcher or mode-locker. At first, a Q-switched fiber laser operating at 1949.0 nm is demonstrated based on nonlinear polarization rotation (NPR) technique. Then, a simple, compact and low cost Q-switched TDFLs operating at 1846.4 nm are demonstrated by exploiting a MWCNTs polymer composite film as the SA. A mode-locked fiber laser is also proposed and demonstrated in Chapter 4 by using a TYDF as the gain medium and commercial graphene oxide (GO) paper as SA.

Chapter 5 demonstrates the application of Thulium fiber as a SA. Various Q-switched EDFLs are proposed and demonstrated by using a short piece of TDF as a passive SA in a ring laser cavity. A dual-wavelength Q-switched EDFL was also demonstrated using the solid state TDF as the SA The finding of this work is

summarized and concluded in Chapter 6. Various potential future works are also suggested in this chapter.

CHAPTER 2

Literature Review

2.1 Optical fiber fundamental

Optical fiber has been extensively utilized in modern telecommunications. Since reasonably low loss optical fiber, 20 dB/km was reported in 1970 (Kapron et al., 1970) the loss of silica fibers continued to be reduced by improvement of fabrication methods (Okoshi, 1982) and nowadays optical fibers with propagation loss of less than 0.15 dB/km are ready available. Due to its guiding structure and intrinsic small propagation loss, optical fiber enables to carry signals to distant place with way small number of amplification compared to conventional electric wire communication networks. Figure 2.1 shows a schematic diagram of a typical standard optical fiber, which consists of a core and a cladding. The core has slightly higher index of refraction than the cladding as shown in the figure. Thus light launched in the core can be confined in the core by total internal reflections and propagate along the fiber.
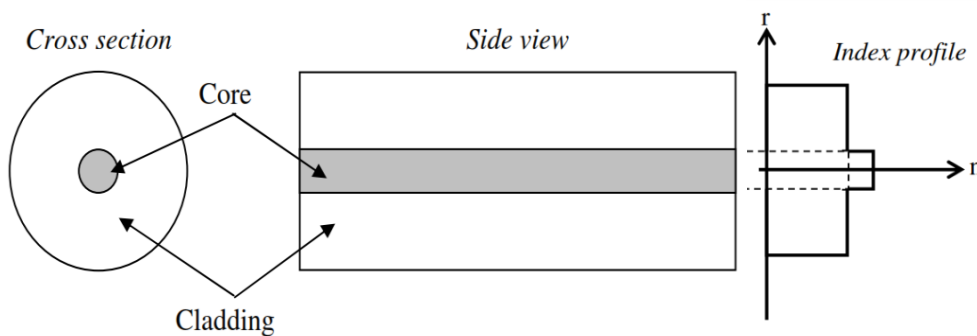
Figure 2.1: Schematic diagram of a step index optical fiber

Light can propagate in the core at different propagation modes depending on dimension, index profile of the optical fiber, and wavelength of the light. For a weakly

guiding fiber, there is a simple measure to find whether the fiber is able to confine one mode or more than one mode (Okoshi, 1982) It is called v-number or the normalized frequency, and expressed as following.

$$v = kn_1 a \sqrt{2\Delta} \qquad (2.1)$$

where $k = 2\pi / \lambda$, λ is a wavelength of the light, a is a radius of the core, $\Delta = (n_1 - n_2)/n_1$, and n_1 and n_2 are core and cladding refractive indexes, respectively. In general for a single mode operation, $v < 2.405$ must be satisfied. If v is greater than 2.405, the fiber is able to confine more than one mode. According to Eq. (2.1), it is easily understood that for a single mode operation either the core size or the index difference between core and cladding, Δ, needs to be small enough to satisfy the condition $v < 2.405$. Otherwise the fiber will be able to confine more than one mode. For telecommunication it is suitable to use a single mode fiber because a single mode fiber is able to avoid modal dispersion that distorts a signal during transmission although the core size will be relatively small and more difficult to launch light into the core and connect fibers each other. On the other hand, for applications, such as welding, that requires higher power but less modal quality of the output beam, a multimode fiber might be suitable.

Some of the advantages of optical fibers include light weight, immunity to electromagnetic interference, and nearly impossible to tap. In terms of telecommunication, it is important that optical fiber's attenuation is independent of the modulation speed differently from copper wires. It is also an advantage that the carrier frequency of optical fibers is quite high, ~190 THz at 1.55 µm wavelength because signal with higher modulation can be transmitted.

Optical fiber's excellent guiding structure is also attractive for laser applications. Actually in 1961, one year later than the first demonstration of a ruby laser, a fiber laser

was proposed and demonstrated by Snitzer (Snitzer, 1961A, 1961B). Fiber lasers are lasers that have at least optical fibers as gain media. Typically the gain medium is an optical fiber doped with rare earth elements such as erbium, ytterbium, neodymium, thulium, holmium etc. Fiber nonlinearities, such as stimulated Raman scattering or four-wave mixing can also provide gain and thus serve as gain media for a fiber laser.

2.2 Brief history of fiber laser

The laser is often grouped with the transistor and the computer as landmark inventions of the mid-20th century (Hecht, 2010).The invention of the laser trigged the development of new technologies such as fiber-optic, optoelectronics and sensors. This development has been affecting almost every aspect of our lives and has been pushing forward the progress of other scientific fields, such as communication, medical research, information technology, biological science, etc.. The first laser was demonstrated by Theodore H. Maiman at Hughes Research Laboratories in Malibu, California in 1960 (Maiman, 1960). Maiman used a flash lamp in his experiment to pump ruby crystal and generates laser in a visible wavelength. After this demonstration, a large variety of lasers were developed using different materials including helium neon (He-Ne) (Javan et al., 1961), Nd:YAG (Geusic et al., 1964), dye (Sorokin & Lankard, 1966), CO_2 (Patel, 1964), Argon Ion (Bridges, 1964), neodymium crystal (Johnson, 1962), semi-conductor (Hall et al., 1962), quantum well (Dingle & Henry, 1976), titanium sapphire (Moulton, 1986), etc. The earliest form of fiber laser was also developed by Snitzer et. al. in 1964 (Koester & Snitzer, 1964).

A fiber laser is an oscillator using an optical fiber as active medium in the cavity. The core of the fiber is doped with rare-earth elements such as erbium (Er), ytterbium (Yb), neodymium (Nd), dysprosium (Dy), praseodymium (Pr), thulium (Tm), holmium (Ho), and different synthesizers of these elements. Compared with other lasers, fiber laser has a lot of attractive advantages, including outstanding heat-dissipating capability, good

beam quality, compactness, robust operation and free of alignment, etc. Fiber lasers have been investigated and developed for more than fifty years. Laser researchers have always been working on building and developing better and cheaper fiber lasers: new operating wavelength, narrower linewidth (single frequency), shorter pulse duration, higher power/energy, etc.

A thulium has gained interest as a potential laser ion, for emission wavelength in the range of 1.4-1.5 and 1.9 - 2.1 μm regions. The first thulium doped silicate glass laser was demonstrated in 1967 (Gandy et al., 1967). However, thulium was never used for fiber lasers until the year of 1988 when the first thulium-doped fiber laser (TDFL) was reported. In the experiment, the Thulium-doped fiber (TDF) was pumped with a dye laser at 790 nm to achieve a few 10's of mW of power (Hanna et al., 1988). At first, TDF began to draw attention for the many other emission wavelength bands in both the S-band for telecommunications and in a blue upconversion band (Allen et al., 1993; Grubb et al., 1992). These fibers tend to be implemented in fluoride (ZBLAN) fibers. The first watt level TDFL operating in 2 micron region was quickly demonstrated soon after the first TDFL (Hanna et al., 1990), by simply scaling up pump power at the readily available Nd:YAG pump band of 1064 nm. This laser used a single clad TDF in conjunction with direct core pumping. The first mode-locked TDFLs were reported in 1990's (Nelson et al., 1995; Sharp et al., 1996).

2.3   Thulium-doped fiber laser

Interest in the Thulium-doped fiber laser (TDFL) originates from its emission band in the range of 1400-2700nm lying between the bands of Er^{3+} and Nd^{3+} ions. Since the advent of double-cladding configuration of fiber and the recent technological development of high-power laser diodes, output power (performance) of Tm^{3+}-doped fiber lasers has scaled exponentially. Up to date, the maximum output achieved in Tm^{3+}-doped fiber lasers has been comparable with that from Yb^{3+}-doped fiber lasers.

Laser beam in the 2 micron wavelength range has wide applications. First, it is a good candidate in laser microsurgery due to high absorption of water in this spectral region thus can provide high-quality laser tissue cutting and welding. In addition, this wavelength-range laser has potential applications in environment monitoring, LIDAR, optical-parametric-oscillation (OPO) pump sources, and so on. (Esterowitz, 1990; Henderson et al., 1993; Myslinski et al., 1993; Stoneman & Esterowitz, 1990).

For obtaining laser emission in the mid-infrared wavelength region, the Thulium-doped fiber (TDF) is an excellent candidate due to several unique advantages it possesses. First, the TDF has a strong absorption spectrum that has good overlap with the emission band of commercially available AlGaAs laser diodes, which have been significantly developed and are being developed with an unprecedented speed. Second, the specific energy-level structure of Tm^{3+} ions provides the TDFL with a special advantageous energy transfer process; the $^3H_4 + {}^3H_6 \rightarrow {}^3F_4 + {}^3F_4$ cross relaxation process. In this process, two excited state ions can be obtained with depletion of just one absorbed pump photon. With an appropriately high doping level, the cross relaxation process can offer a quantum efficiency close to two, which greatly improves the efficiency of the TDFL. Thirdly, the TDF has a very broad emission band, spanning over more than 400 nm. This feature offers the TDFL an especially high-degree wavelength tunability, which is very useful in applications such as spectroscopy, atmospheric sensing and so on.

For laser ions, the combination of the energy gaps between the excited level and the one just below it and the maximum phonon energy (MPE) plays an important role in the non-radiative relaxation rate, which in turn has a significant influence on the laser efficiency originated from the excited states. For Tm^{3+} ions, different host materials show a great difference in the maximum phonon energy (MPE) value. Two most common host materials used for Tm^{3+} fibers are silica and fluoride glass. Their MPE

differs about several times, being 1100 cm-1 (silicate) and 550 cm-1 (fluorides), respectively.(Vodopyanov, 2003). Large MPE of the silicate glass fiber limits its infrared transparency range less than 2.2 μm and improves its multi-phonon relaxation rates. Therefore, fluoride fibers are preferred as the host material for Tm^{3+} ions to achieve comparatively longer-wavelength emission. In TDFLs, the $^3F_4 \rightarrow {}^3H_6$ transition is usually exploited to achieve the ~2 μm high-power laser output. This transition can produce a very wide emission band, providing a broad tuning range for lasers and a wide optical bandwidth for amplifiers. However, the relaxation of the $^3F_4$ level is predominantly non-radiative. The measured lifetime of the $^3F_4$ level for Tm^{3+} doped silica fiber is just 0.2 ms (Hanna et al., 1990) showing a high non-radiative rate thus low quantum efficiency. Therefore, TDFLs usually have high laser thresholds. On the contrary, fluoride based TDFLs have comparatively lower thresholds due to a low MPE. The high non-radiative rate, however, does not impair laser slope efficiency, because stimulated emission will dominate non-radiative relaxation once the laser has been risen above threshold. Due to high damage threshold and the very effective modified chemical vapor deposition (MCVD) technique for fiber fabrication, silica based TDFs are usually chosen to construct high-power 2 μm fiber lasers.

TDFs can be either core pumped or cladding pumped. In the past, the fiber laser was usually core pumped. The fiber core areas are generally <100 μm which limit the power scalability because this method depend on expensive high-beam-quality pump sources. Since the invention of double cladding fiber configuration with a larger cladding area >10000 μm together with a high numerical aperture (NA) of 0.3-0.55, output power of Tm^{3+}-doped fiber lasers can be greatly improved by use of high-power diode-arrays as pumping sources. In the design of fibers for cladding pumping, the core of the fiber is usually made small (such as less than 5 microns) to guide a single-transverse mode (LP_{01}). The cladding generally has a much larger cross section

(several-hundred-micron diameter) for high-power launching, and the shape of the cladding can be flexible with novel consideration. The shape of the inner cladding of the fiber has a great impact on the absorption efficiency of launched pump light. In the past, the inner cladding is used to be circularly symmetric, which can be drawn with ease and is compatible with the pig-tail fiber of the pump laser diode. However, the circular symmetry will make large portion of the pump light to be skew light, greatly reducing the absorption efficiency of doping ions. In order to improve the utility efficiency of pump sources, and take the pump light shape into account (compatible with the inner cladding shape), various double cladding fiber structures are invented, by using these double cladding fibers, the pump efficiency is significantly enhanced.

Figure 2.2 shows the absorption spectrum of a Thulium-doped silica fiber (Agger et al., 2004).As shown in the figure, the fiber has strong absorption near 790 nm, which has good overlap with the emission band of present fully developed AlGaAs diode lasers. This feature of the TDFL makes the pump process comparatively easier and less expensive, offering an exciting potential for power scaling in the 2 µm wavelength range. Besides 790 nm pumping, we can also use 1200 nm and 1550 nm pumping schemes for the TDFL.
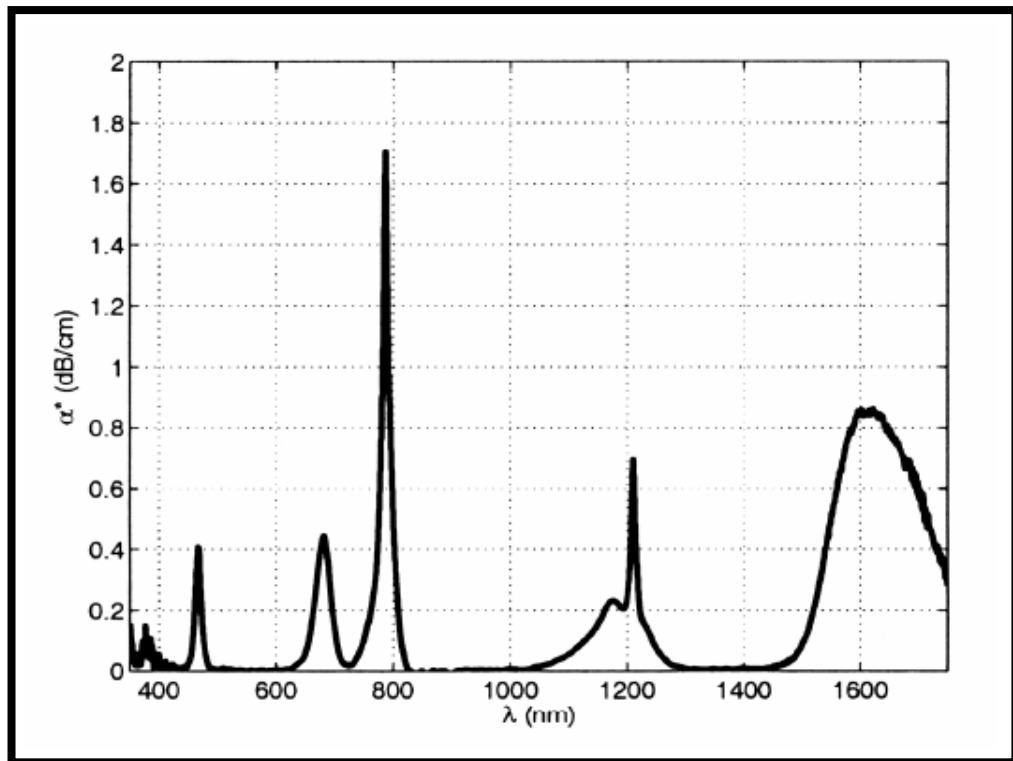
Figure 2.2: Absorption spectrum of a silica-based TDF (Agger et al., 2004).

Figure 2.3 shows the simplified energy-level diagram of Tm^{3+} ions. As shown in the diagram, the pump light at ~790 nm excites Tm3+ ions from $^3H_6$ to $^3H_4$, which then non-radiatively decay to the upper laser level of $^3F_4$ with a fluorescence lifetime of 0.55 ms (Gandy et al., 1967). The transition from $^3F_4 \rightarrow {}^3H_6$ will radiates photons at wavelength of ~2 μm due to large Stark splitting of the lower laser level (the ground state level), the TDFL is a quasi-four-level system.
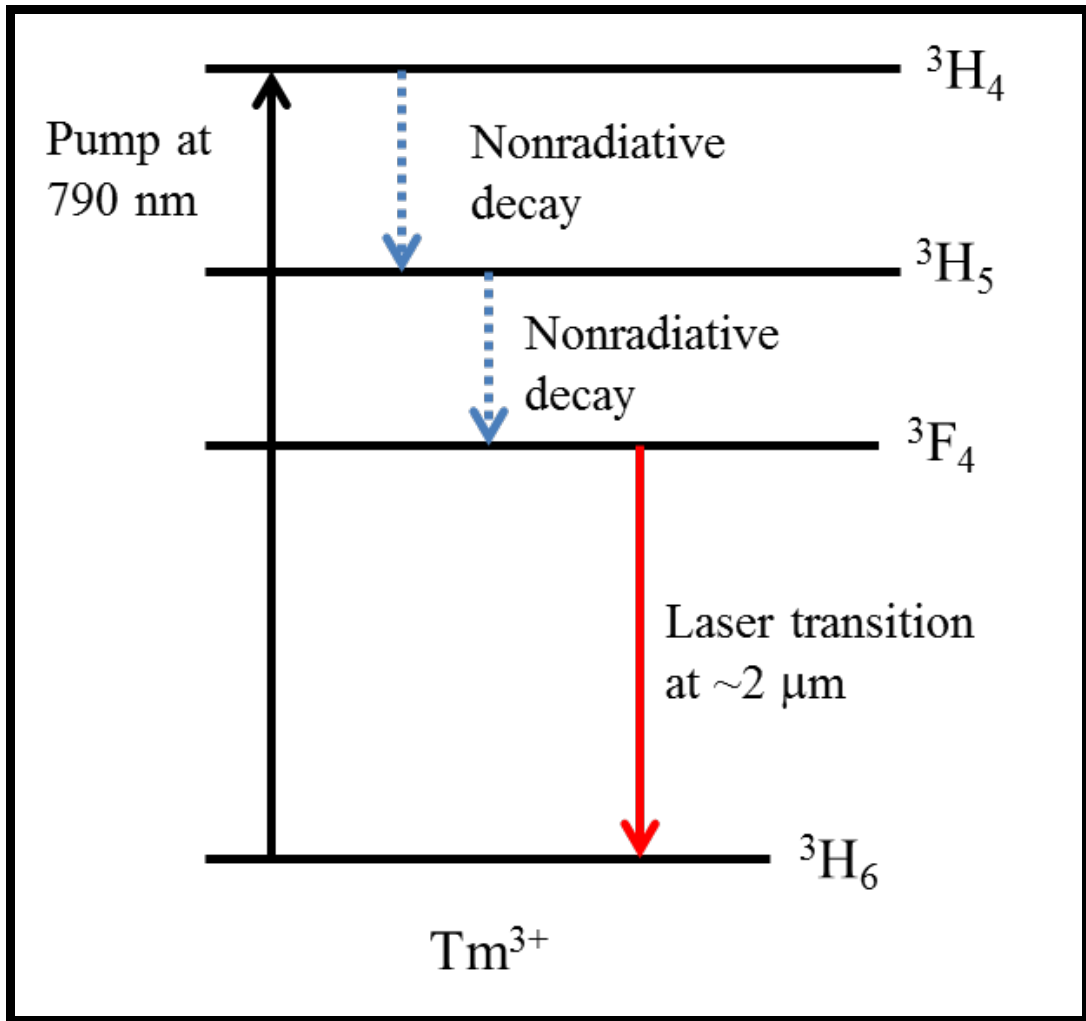
Figure 2.3: The simplified energy-level diagram of Tm3+ ions.

2.4   Thulium-Ytterbium co-doped fiber (TYDF)

Figure 2.4 shows a simplified energy level diagram of energy transfer between ytterbium-thulium ions. The Yb3+ ions absorbs 980 nm pump light to excite from ground level $^2F_{7/2}$ to $^2F_{5/2}$ level. Energy transfer occurred between Yb^{3+} to Tm^{3+} through radiative emission and Yb^{3+} decayed to ground level again. Tm^{3+} at the ground level absorbs the transferred energy and excites to $^3H_5$ but decay instantly to metastable state $^3F_4$ through non-radiative emission. 2μm laser is obtained electronic transition from level $^3F_4$ to ground level $^3H_6$.
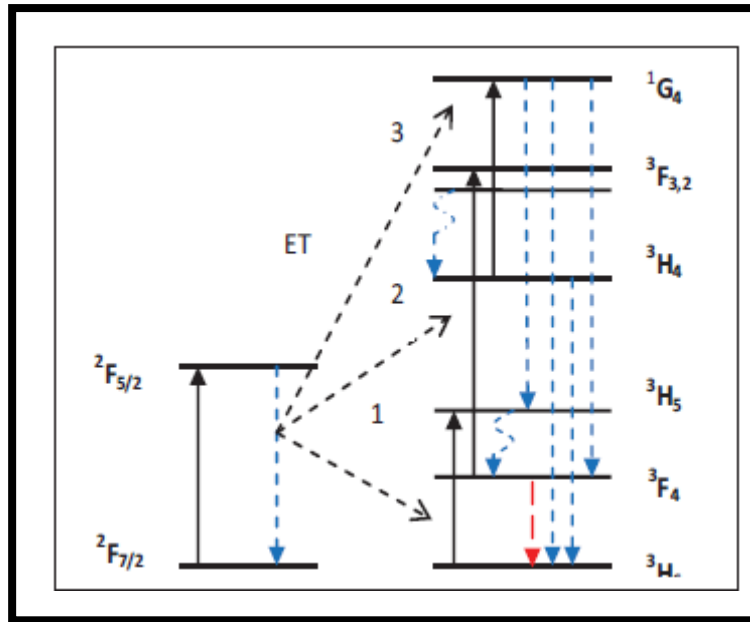
Figure 2.4: Energy diagram of Yb^{3+} and Tm^{3+} system with energy transfer from Yb^{3+} to Tm^{3+} (black dashed arrow), showing absorption (black solid arrow), luminescence emission (blue dashed arrow), non-radiative emission (wavy dashed blue arrow) and the expected 2μm laser emission (red dashed arrow).

2.5   Q-switching

Q-switching is a simple and well-known technique for achieving energetic short pulses from a laser by modulating the Q-factor of the laser resonator. The term Q represents the quality of the laser resonator which contains information regarding the cavity losses. The Q-factor portrays the ability of a laser cavity to preserve its energy. A higher Q indicates a lower intra-cavity loss. The Q-switching phrase describes the idea of switching the laser configuration from a low to high Q to create short pulse duration. In general, Q-switching technique generates pulses with durations typically in the range of microseconds to nanoseconds. The Q-factor value is defined as (Xinju, 2010).

$$Q = 2\pi v_o \left(\frac{W}{energy\, lost\, per\, second} \right) \qquad (2.2)$$

Where ν_o is laser's central frequency and W is energy stored in cavity. Energy lost per second is given by $\dfrac{\delta Wc}{nL}$, where δ is the energy loss rate for single-path propagation of light in the cavity, c is the light velocity, n is the refractive index of the medium and L is the length of the resonator. Thus, the above equation can be simplified as;

$$Q = 2\pi\nu_o \frac{W}{\delta Wc / nL} = \frac{2\pi nL}{\delta\lambda_o} \qquad (2.3)$$

where λ_o is a laser wavelength in the vacuum. From the above equation, it is clearly indicated that the Q-factor value is inversely proportional to the resonator loss (δ) when the value of λ_o and L are definite. It is also found that to change the threshold of the laser, we could suddenly change the loss (δ) of the resonator or Q-factor value.

The Q-switch operation is a simple approach that uses a certain methods to change the Q value of the resonator to vary with time in accordance with a definite procedure which involves rate equation of the gain medium. When the losses of a resonator are varied, the resonator Q-factor is also varied, resulting in a so-called Q-switched operation. The intra-cavity loss-modulation can be performed actively using, for example, modulators, or passively with saturable absorbers. Originally, the Q-factor is kept at low level (i.e. high losses), preventing any potential for lasing. The gain medium provides an accumulation of spontaneous emission in the cavity by constant pumping; thus energy is stored. At the moment that the Q-factor is suddenly switched to a high level and the desired amount of energy is stored, spontaneous emission grows into lasing and a laser pulse starts to build up in the laser cavity. The pulse grows stronger until the gain equals the losses. When the pulse peak power is reached and depletes the gain completely, the laser is no longer able to oscillate. The Q-switched is open again (low Q), and the process starts from the beginning to build up more inversion for the next consecutive pulse. It is useful to have a long upper state lifetime

of a gain medium in order to store gain, therefore it does not disappear as fluorescence emission before the Q-switched is opened (Digonnet, 2002).

Q-switched fiber lasers can be achieved by either active or passive approaches. In active Q-switching, an external modulator is employed to modulate the losses in the laser cavity and thus control the output characteristics of the generated pulsed. (El-Sherif & King, 2003; Kee et al., 1998; Riesbeck & Lux, 2009; Shang et al., 2012). In passive Q-switching, no external modulator is required where the cavity loss is modulated by saturable absorber (SA). Various types of SA such as transition metal doped crystals (Pan et al., 2007; Philippov et al., 2004) SESAMs (Huang et al., 2009; Paschotta et al., 1999) single-walled carbon nanotubes (SWCNTs) (Dong et al., 2011; Harun et al., 2012; Liu et al., 2013; Song, 2012) graphene (Wei et al., 2012; Zhang et al., 2012), graphene oxide (GO) (Ahmad et al., 2012; Yap et al., 2013) and reduced graphene oxide (rGO) (Jiang et al., 2011; Sobon et al., 2012; Yap et al., 2012) can be used to realize a passively Q-switched fiber laser. The SA transmission or reflection depends on the light intensity where the low light intensity will be absorbed by the material and the high light intensity will be released depending on the material recovery time. SA can also be exhibited artificially by polarization effect such as nonlinear polarization rotation (NPR) (Liu et al., 2011; Wang et al., 2011; Zhang et al., 2008). Compared to mode-locking, Q-switching requires less control of cavity parameter and thus it is normally more efficient in term of cost, operation and implementation (Popa et al., 2010).

2.6   Mode-locking

Another method to obtain ultra-short pulses from a fiber laser is by mode-locking technique. The mode-locked laser is achieved when the longitudinal modes are locked in a fixed relationship through constructive interference and destructive

interference at other points generating coherence to form pulses of light. Figure 2.5 shows three longitudinal waves that interfere constructively to produce a total field amplitude and intensity output that has characteristic of repetitive pulse nature and the laser is considered to be mode-locked. When more modes are locked together, narrower pulse width is produced. When a single pulse is circulating a ring cavity, superposition of longitudinal modes produces a pulse with a period, *T*, which is given by:

$$T = \frac{nL}{c} \tag{2.4}$$

where *n* is the refractive index, *L* is the length of the cavity and *c* is the speed of light.
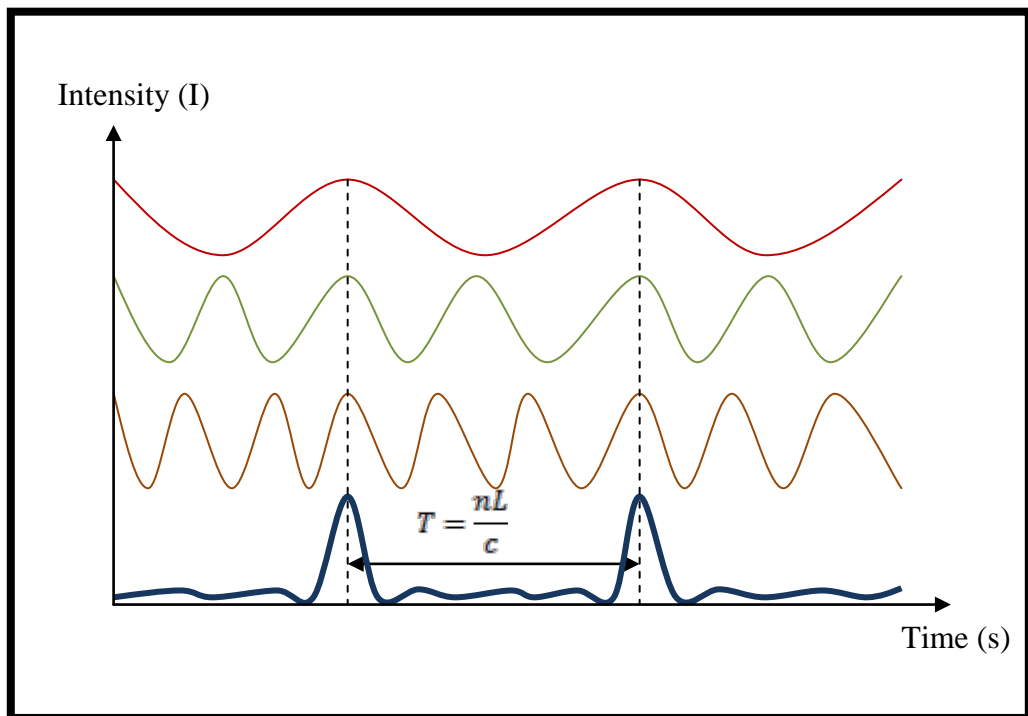
Figure 2.5: Superposition of three longitudinal modes leading to repetitive pulse generation

The cavity arrangement for a mode-locked laser is usually much more complicated than Q-switched laser because the ultra-short pulse generation involves dispersion, self-phase modulation (SPM), cross phase modulation (XPM) and etc (Agrawal, 2001). The repetition rate of the generated pulse train is determined by the

cavity length of the laser, and for laser with ring cavity the relation is given by (Hasan et al., 2011).

$$\Delta f = \frac{1}{T} = \frac{c}{nL} \tag{2.5}$$

Typically the repetition rate of a mode-locked laser is in the range of Megahertz and the pulse width is ranging from nanosecond to femtosecond. Mode locked fiber lasers can be realized by two approaches: active and passive. Active mode locking involves the periodic modulation of the resonator losses or of the round-trip phase change. In practice, it is achieved by using an external modulator as shown in Figure 2.6. The major disadvantage of the active mode-locking is that it has a complicated setup and very bulky.
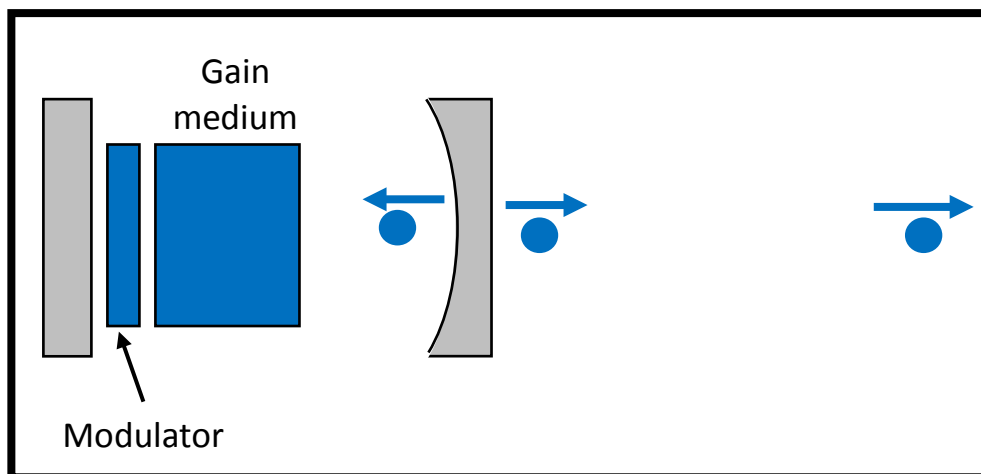
Figure 2.6: Schematic setup of an actively mode-locked laser

Passive mode-locking techniques do not require an external source to produce pulses. They use the light in the cavity to cause a change in some intra-cavity element, which will then itself produce a change in the intra-cavity light. It is commonly achieved by using a passive SA (Bao et al., 2009) such as SESAMs, SWCNTs, graphene and GO. The passive mode-locked fiber laser is capable to generate a much shorter pulses than that of the active technique. This is due to the employment of SA, which can modulate the resonator losses much faster than an electronic modulator: the

shorter the pulse becomes, the faster the loss modulation, provided that the absorber has a sufficiently short recovery time. Figure 2.7 shows a schematic setup of a passively mode-locked laser, which uses a SESAM. In this thesis, the major interest is to demonstrate Q-switched and mode-locked fiber lasers by employing various passive SAs such as multi-walled carbon nanotubes, graphene oxide paper, NPR and solid state thulium fiber.
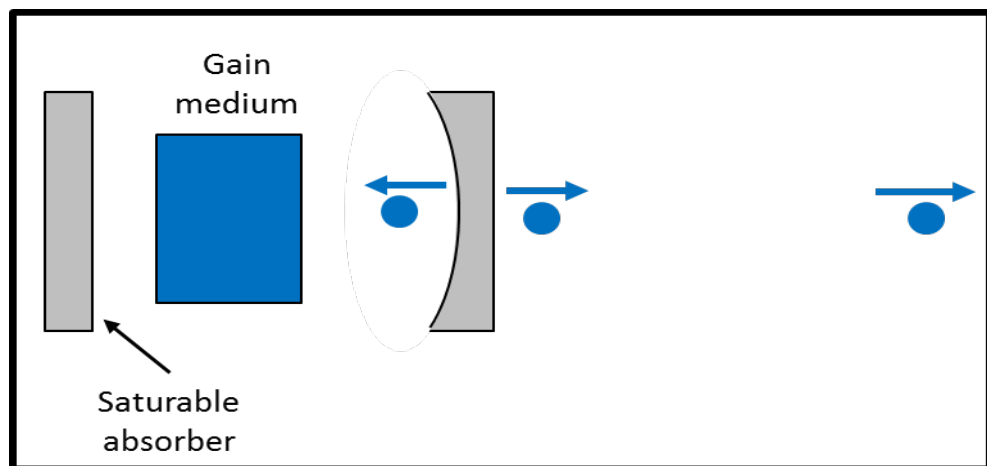
Figure 2.7: Schematic setup of a passively mode-locked laser.

2.7   Saturable Absorber (SA)

A saturable absorber (SA) is an intensity dependent material which possesses saturable absorption behavior. Saturable absorption refers to the condition where high intensity light bleaches a material and reduces the absorption (Yamashita, 2012). In other word, the SA absorbs any low intensity light while allowing higher intensity light to pass through with less attenuation. Consider a simplified 2 level energy system of a material, which consists of ground state and upper state. When the incident optical intensity is low, the material absorbs the incoming light, resulting in transition of atom from ground state to upper state. However, majority of the atoms are still in the ground level. When the incident intensity is high, a large number of atoms will be excited into the upper level such that there is inadequate time for them to decay back to the ground

state before the ground state becomes depleted. Eventually, the absorption finally saturates and ceased.

The absorption coefficient is given by the following equation (Yamashita, 2012):

$$\alpha = \frac{\alpha_o}{1 + \dfrac{I}{I_s}} + \alpha_{us} \qquad (2.6)$$

where $\alpha_o \left/ \left(1 + \dfrac{I}{I_s}\right)\right.$ and α_{us} are the saturable and unsaturable absorption, respectively. α_o is the linear absorption coefficient. I and I_s are the optical intensity and saturation intensity respectively. Saturation intensity is defined as the optical intensity required in a steady state to reduce the absorption to half of its unbleached value. We describe the saturation intensity I_s as:

$$I_s = \frac{h\nu}{\sigma\tau} \qquad (2.7)$$

where $h\nu$ is the photon energy, σ is the absorption cross section from ground state to upper state and τ is the recovery time. Recovery time is the return of the atom population to the ground state.

The main application of the SA is in generating short pulses through Q-switching and mode-locking processes. The important parameters of a SA are such as saturable and non-saturable absorption, modulation depth, saturation intensity, saturation fluence, recovery time and damage threshold (Jung et al., 1997). Popular SAs in the past were dyes. (Bradley & O'neill, 1969). But, they often had high toxicity and degradation problem under high power of laser pulses. The commonly used saturable absorbers now are semiconductor saturable absorber (SESAM) (Chen et al., 2009; Moghaddam et al., 2011), graphene (Sotor et al., 2012) and carbon nanotubes (CNTs) (Going et al., 2012; Set et al., 2004). In this PhD work, we introduce and demonstrate a

pulse generation using a low cost and simple SA based on multi-walled carbon nanotubes (MWCNTs) and graphene oxide paper.

2.8   Carbon nanotubes

Carbon nanotubes (CNTs) are an allotrope of carbon, which takes the form of cylindrical carbon molecules. They have novel properties that make them potentially useful in a wide variety of applications in nanotechnology, electronics, optics and other fields of materials science. There are basically two main types of carbon nanotubes as shown in Figure 2.8, according to the numbers of graphene cylinders in their structure: single-walled carbon nanotubes (SWCNTs) and multi-walled carbon nanotubes (MWCNTs).
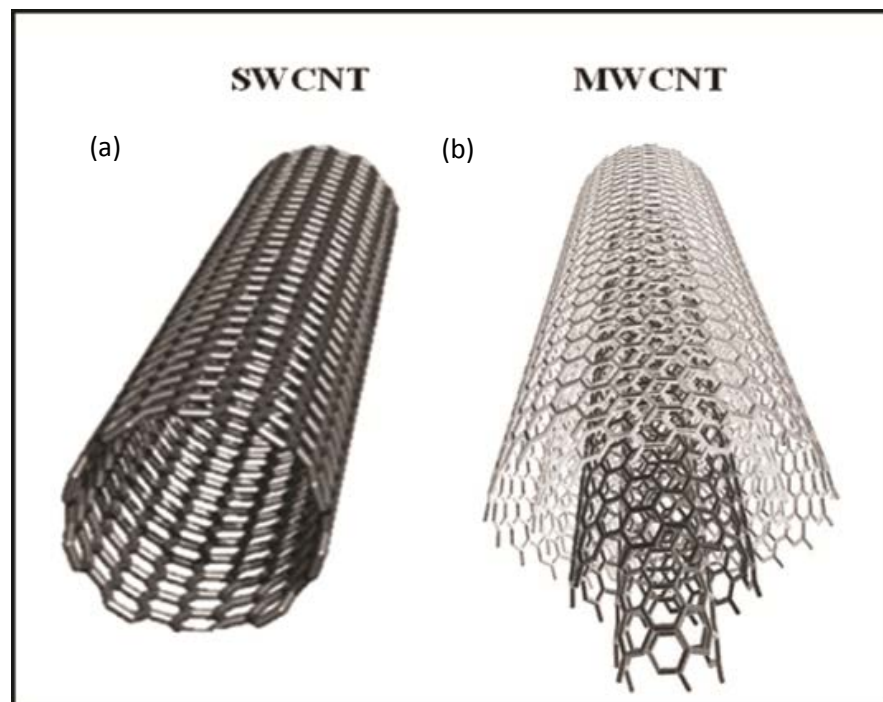
Figure 2.8: Schematic of a (a) SWCNT and (b) MWCNT (Lacerda et al., 2007)

SWCNTs can be viewed as a graphene sheet rolled into a cylinder which is terminated by two half-fullerene caps. The diameter of these species typically ranges from 0.7 nm to 2.5 nm, and their aspect ratio can be as high as 10^4–10^5. These very strong confinements along their circumference make them behave like 1-D materials (Dresselhaus et al., 2001; Jorio et al., 2007; Léonard, 2009). On the other hand, MWCNTs are elongated hollow cylindrical nano objects made of sp^2 carbon (Andrews et al., 2002; Forro & Schoenenberger, 2001; Lehman et al., 2011). Their diameter is 3–30 nm and they can grow several cm long, thus their aspect ratio can vary between 10 and ten million. The wall thickness of a MWCNTs is fairly constant along the axis, and therefore the inner channel is straight. MWCNTs can be distinguished clearly from SWCNTs on the basis of (i) their larger diameter and (ii) their Raman spectrum. A major difference between MWCNTs and SWCNTs is that the former are stiff, rigid, rod-like structures whereas single-walled carbon nanotubes are flexible.

2.8.1 Synthesis of SWCNTs and MWCNTs

SWCNTs and MWCNTs can be prepared using a broad variety of synthesis methods such as arc discharge (Colbert et al., 1994; Jong Lee et al., 2002) laser ablation (Guo et al., 1995; Iijima et al., 1996; Thess et al., 1996; Wakabayashi et al., 1997), chemical vapour deposition (CVD) methods (Fan et al., 1999; Kind et al., 1999) and catalytic chemical vapour deposition (CCVD) methods (Bajwa et al., 2008; Ivanov et al., 1994). In this work, the MWCNTs are purchased from cheap tubes Inc. in form of dry powder synthesis by catalytic chemical vapour deposition CCVD technique. The tubes have an outer diameter and a length distribution in a range of 10–20 nm and 1-2 μm, respectively. The purity of the MWCNTs is >99 wt%. The sample was used as per received without any further purification process.

2.8.2 Spectroscopic properties of carbon nanotubes

Raman spectroscopy has rapidly become a pivotal technique for studying carbon nanotubes (Bommeli et al., 1997; Jishi et al., 1993; Kastner et al., 1994; Tanaka et al., 1994). Figure 2.9 shows the typical Raman spectrum of SWCNTs sample, which indicates various Raman-active vibrational modes. The lowest frequency mode ($\approx$ 100–400 cm^{-1}) is known as the radial breathing mode (RBM), which is obtained due to an isotropic stretching vibration that occurring in the radial direction perpendicular to the tube axis. (Jorio et al., 2007; Rao et al., 1997). The RBM frequency varies inversely with nanotubes diameter (Rao et al., 1997) and thus it can be used to optically determine the size of the SWCNTs. The energy at which the RBM Raman intensity reaches a maximum corresponds to the incident and scattered photon resonances with the SWCNT optical transition. Thus, the optical transition energy of the SWCNTs structure could also be determined from the RBM spectrum (Doorn et al., 2004; Fantini et al., 2004; Maultzsch et al., 2005; Telg et al., 2004).
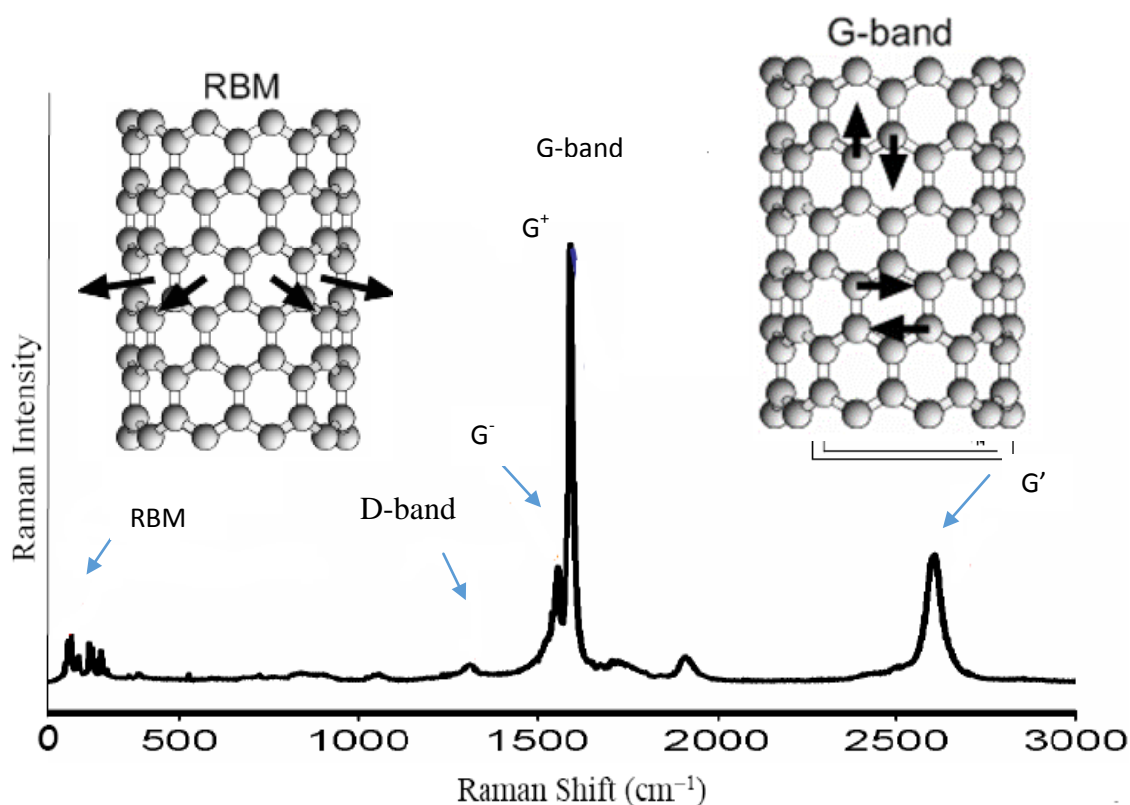
Figure 2.9: Typical Raman spectrum of a SWCNTs sample (Jorio et al., 2003)

The G-band vibration is shown at around 1550–1600 cm^{-1}. This intense vibration is common to all sp^2-hybridized carbon. It is isotropic in graphene but anisotropic in carbon nanotubes due to the curvature induced inequality of the two bond-displacement directions which causes the phonon to split into two, the G^+ and G^- peaks. Because of the splitting of the G-band into two separate but related modes, the overall line shape and intensity of the G-band can identify whether the tubes undergoing resonance with the excitation laser are metallic or semiconducting (Brown et al., 2001; Hároz et al., 2011; Piscanec et al., 2007; Wu et al., 2007). Another important mode is the D-band phonon, an out-of-plane bending mode with frequency at around 1300 cm^{-1} (Jorio et al., 2007). This mode is normally Raman-inactive in pristine or perfect sp^2-carbon due to symmetry considerations. It becomes Raman active when the translational symmetry of the extended structure of graphite, graphene or carbon nanotube is broken by some sort of disorder. The intensity of D-band generally increases with the degree of disorder. The G'-band is also observed in the Raman spectrum at frequency of 2600–2700 cm^{-1} region. This band is common to all sp^2-hybridized carbon. It is a dispersive, second-order Raman mode which highly sensitive to small changes in electronic and vibrational structure (Jorio et al., 2007).

Figure 2.10 shows the Raman spectra for three different MWCNTs samples. The primary differences of Raman spectroscopy of SWCNTs and MWCNTs are the lack of RBM modes in MWCNTs and a much more prominent D band in MWCNTs. The RBM modes are not present because the outer tubes restrict the breathing mode. The more prominent D band in MWCNTs is to be expected to a certain extent given the multilayer configuration and indicates more disorder in the structure. The Raman spectrum of MWCNTs is dominated by two peaks: the G-band at 1590 cm^{-1} and D-band at 1350 cm^{-1}. The G-band corresponds to tangential stretching C−C (carbon-carbon) vibrations in the nanotube wall plane while the D band originates from a double resonance

process, which is caused by the presence of amorphous disordered carbon (Kürti et al., 2002; Saito et al., 2001). It should be emphasized that the D band is not a good measure of nanotube wall defects; rather, its intensity is proportional to the amount of amorphous carbon in the system (Bose et al., 2005; Osswald et al., 2005). Nevertheless, measuring the intensity ratio of the D and G bands is a widely accepted method of assessing the general purity of a MWCNTs sample (DiLeo et al., 2007).
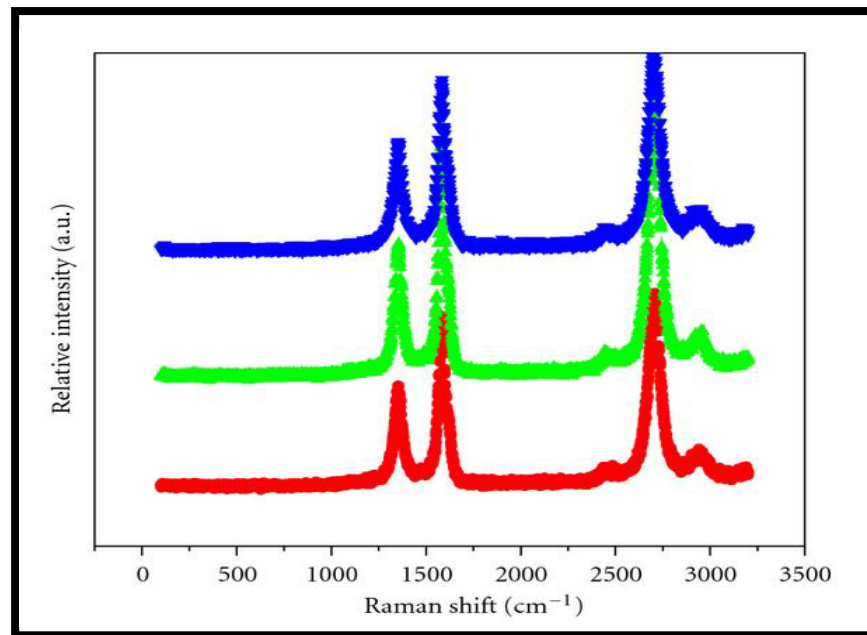
Figure 2.10: Typical Raman spectra for various MWCNTs samples.

2.8.3   Linear Absorption of SWCNTs and MWCNTs

Figure 2.11 shows an absorption spectrum of the SWCNT embedded in polyvinyl alcohol (PVA), which was used to demonstrate an ultra-short pulse generation in L-band region (Sun et al., 2008). SWCNTs are a folded graphene and exist as a 1-D structure. This leads to a restriction on the energy states resulting in the several absorption regions (Wang et al., 2008). SWCNTs will absorb photons strongly at these energy levels while being almost transparent at other energy levels. The positioning and magnitude of these absorption peaks is strongly dependent on both the radius of the

individual tubes and their chirality (Tan et al., 2007). Smaller diameter tubes will have their peaks shifted to higher energy levels, while absorption peaks of larger diameter tubes will shift to lower energies. This characteristic of SWNT's allows for the tailoring of optical absorption spectra using different SWCNT growth parameters and techniques, allowing for the engineering of CNT based SA's across a broad range of frequencies (Kataura et al., 1999).
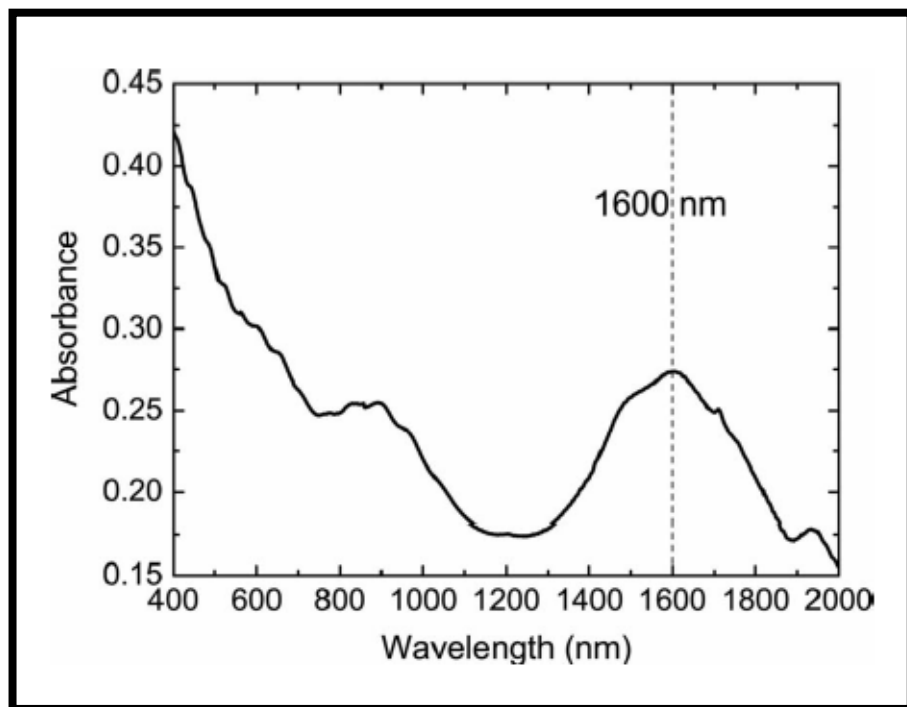
Figure 2.11: Absorption spectrum of the SWCNT-PVA film (Sun et al., 2008)

(Zhang et al., 2011) reported an absorption spectrum of the MWCNTs based SA which was used to generate ultrafast laser in solid state laser system. The absorption spectrum is shown in Figure 2.12. The authors claim the MWCNTs SA has an ultra-broad absorption compared to SWCNTs which is diameter and chirality dependence.
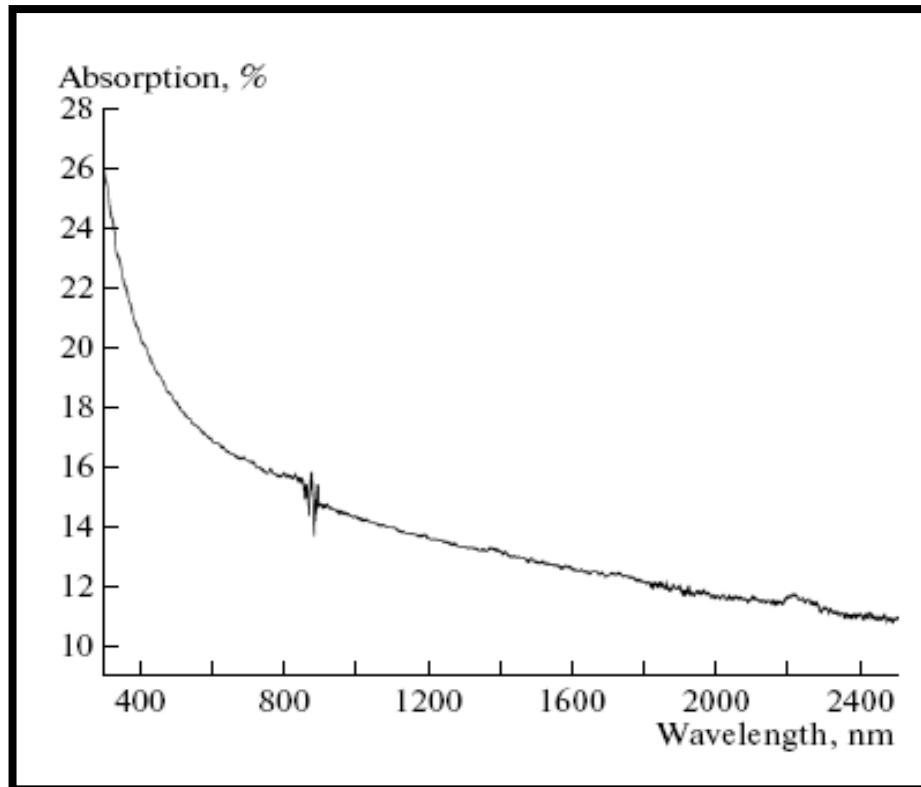
Figure 2.12: Linear Absorption of MWCNTs based saturable absorber (Zhang et al., 2011).

2.8.4 Recovery time of SWCNTs and MWCNTs

The SWCNTs' ultrafast recovery time (~1 ps) was measured through a pump-probe experiment (Chen et al., 2002; Schmidt et al., 2009) as shown in Figure 2.13. If the laser wavelength is tuned to the near-infrared absorption band, a large optical nonlinear effect, especially a saturable absorption effect will occur. So the SWCNTs are promising for all optical switching applications. For pulse generation, slower recovery time could facilitate laser self-starting while the fast recovery time is to stabilize the pulse oscillation. Most SWCNTs samples consist of a mix of semiconducting and metallic species with different chirality, thus this could have ultrafast recovery time and wider absorption band. Different chirality of SWCNTs provides a different region of absorption. The recovery time of a semiconducting SWCNTs is around 30 ps. Bundles and/or entanglements of semiconducting and metallic SWCNTs will determine the

recovery time of a mixture of carbon nanotubes. Fast recovery time of semiconducting SWCNTs is due to coupling of electrons from photon exited semiconducting SWCNTs to metallic SWCNTs (Kashiwagi & Yamashita, 2010). Therefore, the mixture of Semiconducting and metallic SWCNTs inherently have ultrafast recovery time shorter than 1 ps (Kashiwagi & Yamashita, 2010).
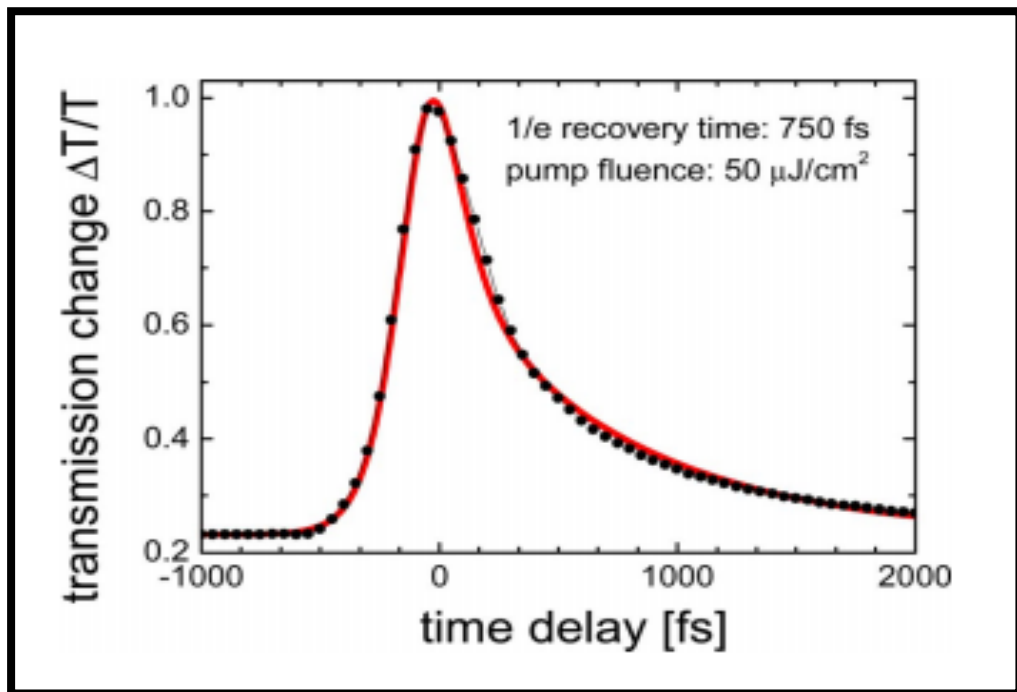
Figure 2.13: Recovery time of SWNT (Schmidt et al., 2009)

The MWCNTs' recovery time was measured through a pump-probe experiment and the reported recovery time is around 230 fs (Zhang et al., 2011). The recovery time is shown in Fig. 2.14. The recovery time of the MWCNTs is longer than that of SWCNTs, but they manage to generate mode-locked solid state laser using the MWCNTs. The reported works for passive saturable absorber using MWCNTs based saturable absorber is not extensively reported as compared to the SWCNTs based SA. This is maybe due to longer recovery time, but the SA could be investigated for pulse

laser regimes which not require fast recovery time such as Q-switched regime. Furthermore, the reported pulse laser is using solid state laser, which using bulky component and need precise alignment, this create a new interest to integrate a MWCNTs SA in fiber laser to generate pulsed laser.
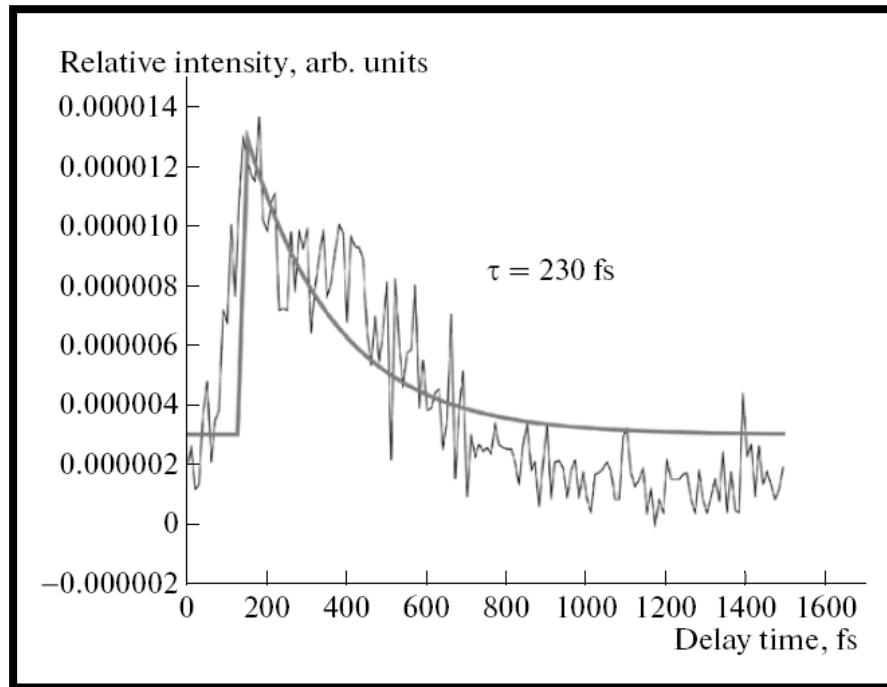
Figure 2.14: The recovery time of 230 fs for MWCNTs based SA (Zhang et al., 2011)

2.8.5   Modulation depth of SWCNTs and MWCNTs

Wang et al., 2008 reported modulation depth of SWCNTs-PVA composite based thin film is around 6% in transmission mode as shown on Figure 2.15. They also reported a saturable absorption (α_s) of 16.9%, non-saturable absorption (α_{ns}) of 82.5%, and a saturation fluence of $\sim$18.9 MW/cm^2 using a 50 µm ticked SWCNTs-PVA thin film. Using the same film, the group reported a stretched-pulse fiber lasers, incorporating segments of normal and anomalous dispersion fibers (Sun et al., 2010). It is found that the modulation depth of around 16% is sufficient to provide strong pulse shaping, reliable self-starting and stabilized pulse generation (Keller, 2004).
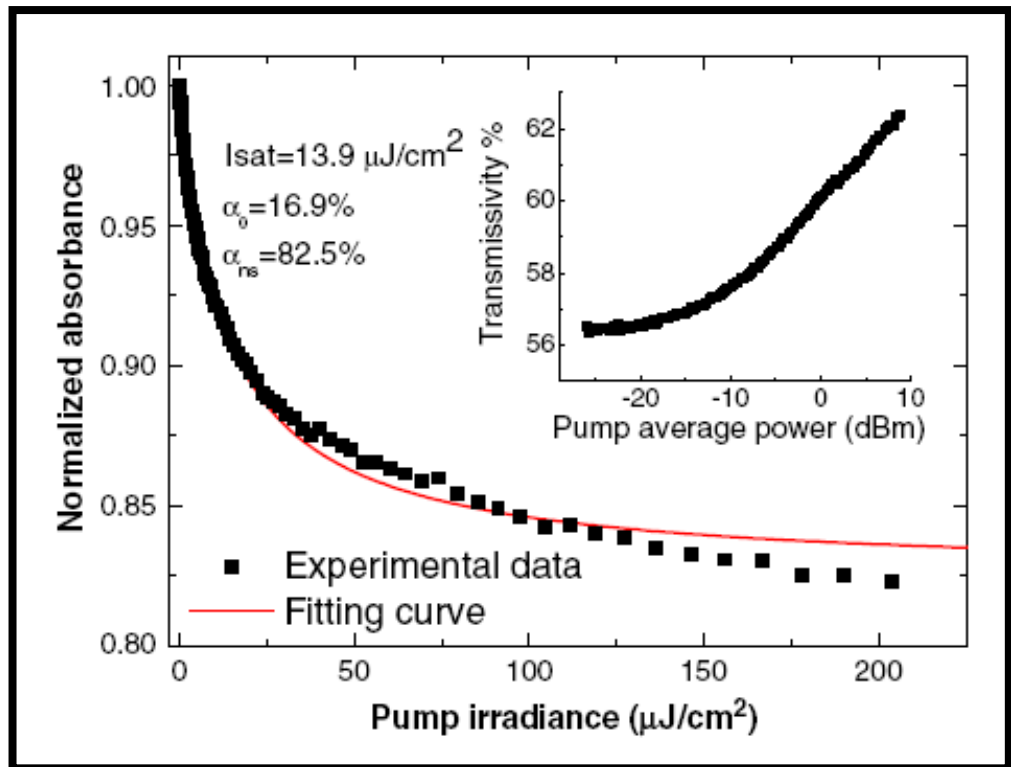
Figure 2.15: Modulation depth of SWCNTs-PVA film (Wang et al., 2008)

Although (Zhang et al., 2011) reported a passive mode locked solid state laser using the MWCNTs based SA, but they didn't characterized the SA parameters such as modulation depth or saturation fluence of the SA. Recently, (Lin et al., 2013) had characterized the layer of MWCNTs in a quartz substrate as shown in Figure 2.16. As shown in the figure, the MWCNTs have a modulation depth of 4.7 % and a saturation fluence of 90 $\mu J/cm^2$. The reported modulation depth is lower than SWCNTs based SA in polymer composite which is around 16% with saturation fluence of 13.9 $\mu J/cm^2$ (Wang et al., 2008).
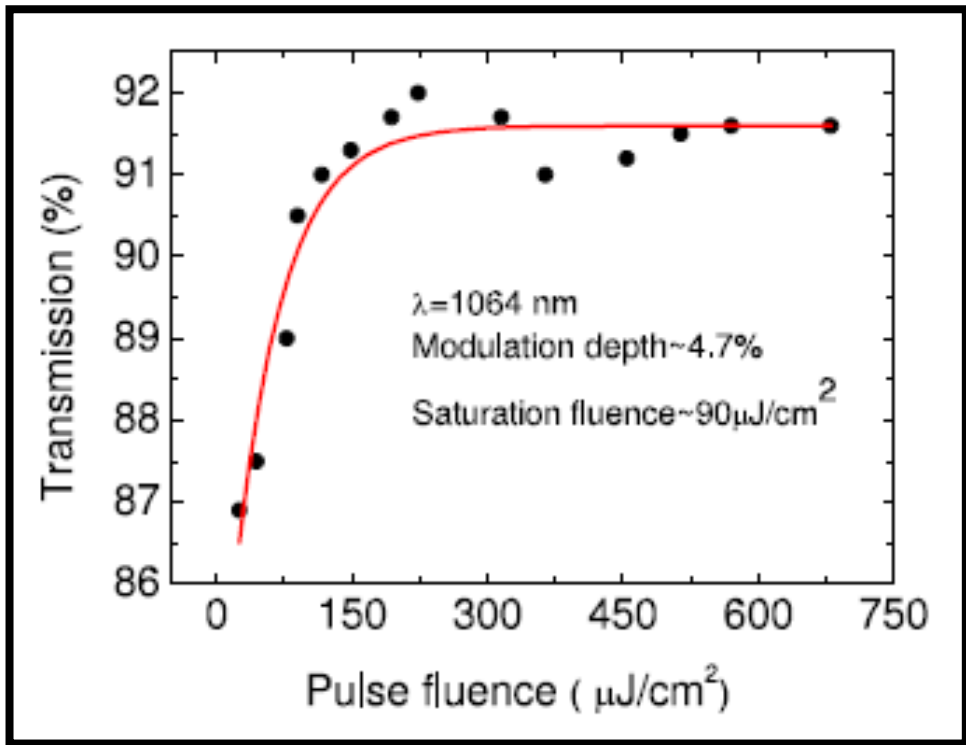
Figure 2.16: Modulation depth and saturation fluence of MWCNTs (Lin et al., 2013)

2.9 Graphene

Graphene is a planar allotrope of carbon where all the carbon atoms form covalent bonds in a single plane. The sp^2 interactions in graphene result in three bonds called σ-bonds, which are the strongest type of covalent bond. The σ-bonds have the electrons localized along the plane connecting carbon atoms and are responsible for the great strength and mechanical properties of graphene. Figure 2.17 shows the planar honeycomb structure of graphene.
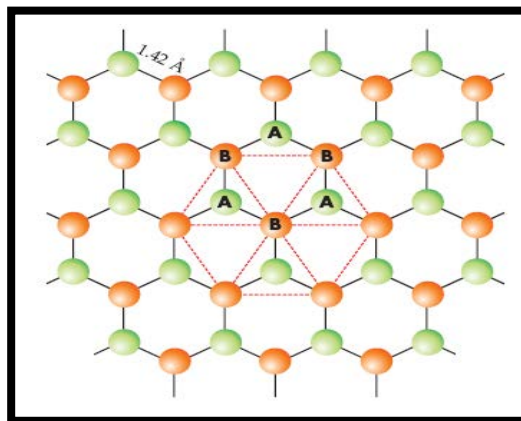
Figure 2.17: Structure of graphene (Geim & MacDonald, 2007)

There are mainly four approaches to synthesize graphene and its derivatives. The first approach is called as the mechanical exfoliation of graphite, which is also known as the "Scotch tape" or peel-off method (Novoselov et al., 2004). This approach gives the best samples in terms of electronic properties, but the yield is quite low, only suitable for fundamental studies. The second method is based on epitaxial growth on electrically insulating surfaces such as SiC (Berger et al., 2006). The third was CVD on metals such as Ni (Kim et al., 2009) and Cu (Li et al., 2009). This method can produce large area uniform graphene film, which can be used for making optoelectronic devices (Bae et al., 2010). The fourth approach was the creation of colloidal suspensions or liquid-phase exfoliation, which includes the production of graphene and chemically modified graphene from colloidal suspensions made from graphite, derivatives of graphite (such as graphite oxide), and graphite intercalation compounds. This approach is both scalable, affording the possibility of high-volume production, and versatile in terms of being well suited to chemical functionalization. These advantages mean that graphene and its derivatives produced by the colloidal suspension method are good nanofillers to incorporate into polymer to form functional composites.

The three significant Raman spectral features in graphene are the G peak at $\approx$ 1580 cm^{-1}, the D peak at $\approx$ 1350 cm^{-1}, and the 2D peak at $\approx$ 2700 cm^{-1}, as shown in Figure 2.18. The G peak is due to the E_{2g} mode, i. e., in-plane vibrations of the carbon atoms. The D peak and 2D peak are strongly dispersive, with excitation energy due to the Kohn anomaly at the K-point, while the G peak is not. The 2D peak is the second order of the zone boundary phonons and therefore does not require defects. For monolayer and few-layer graphene, the 2D peak serves as a fingerprint for identification (Ferrari et al., 2006).
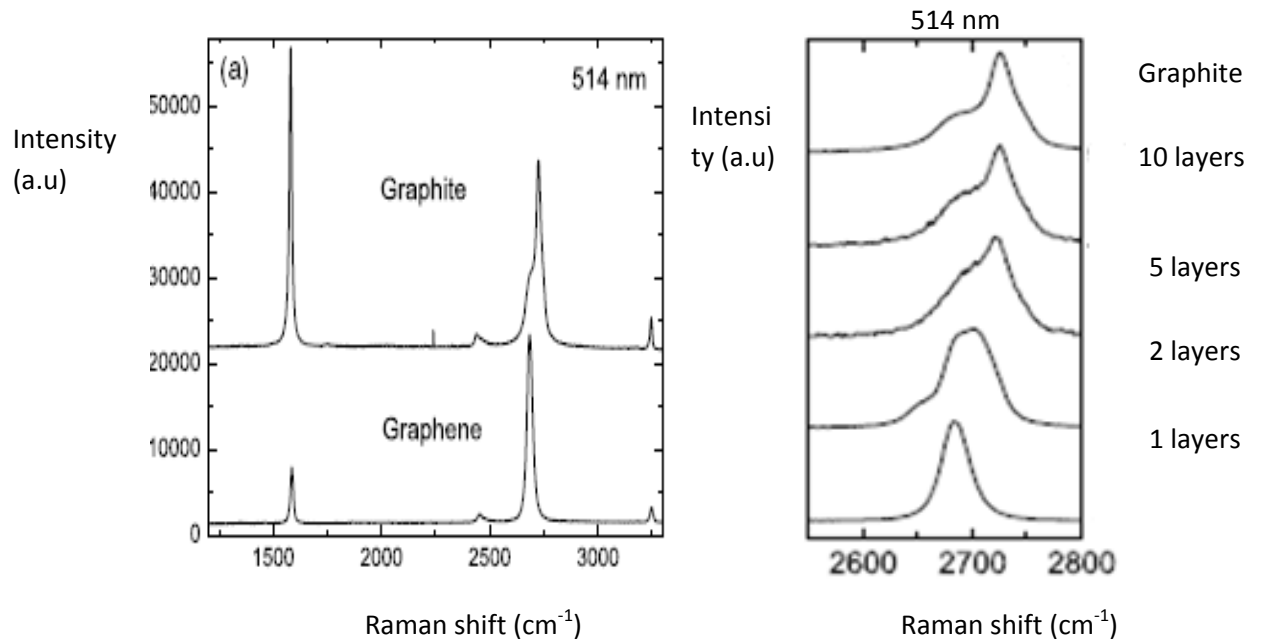
Figure 2.18: Raman spectra of (a) graphite and graphene (b) 2D peak of different number of graphene layers

Monolayer graphene has a single sharp 2D peak while the 2D peak appears up-shifted and broader in bilayer graphene. As the number of layers further increases, the 2D peaks reduce in intensity, and beyond five layers, it resembles the 2D peak of bulk graphite. A similar observation can also be made for the D peak (Ferrari et al., 2006). The D peak of monolayer graphene is a single sharp peak, while in bulk graphite it can be resolved into two peaks, D1 and D2. The D peak is observed in defective graphene, and prominently at the edges of graphene flakes.(Das et al., 2008) demonstrated the number of layer in the graphene could be estimated by calculating the ratio of I(G)/I(2D) from the Raman spectrum. For bulk HPOG, the ratio is larger around 3.1 compared to monolayer graphene with the ratio of 0.2. Basically, if the ratio of I(G)/I(2D) is greater than 0.5, we can conclude that the graphene is consisting of multi-layer graphene.

The saturable absorption is achieved in graphene due to a *Pauli blocking* process (Zitter, 1969). The experimental observation of saturable absorption in graphene was demonstrated in many literatures. For instance, (Bao et al., 2009) reported that a monolayer graphene has a remarkable large modulation depth of 65.9%. In another work (Huang et al., 2012) reported that a modulation depth of graphene with 21 layers was around 2.93 %. Similar saturable absorption phenomenon was also obtained using graphene–PVA polymer composites (Popa et al., 2010), graphene oxide (GO) and reduced graphene oxide (rGO) (Sobon et al., 2012), where the reported modulation depths are 2%, 21% and 18%, respectively. The large modulation depth and the high ratio of saturable to nonsaturable absorption indicate stronger noise suppression and pulse shaping ability (Sakakibara et al., 2005). Nonsaturable loss generally arises from scattering losses by defects or aggregates, nonsaturable absorption from the polymer host and coupling loss in fibers.

2.10   Cladding pumping

The early fiber lasers and amplifiers had only one effective wave-guiding component: the core. Since both the signal and pump light are guided in the core, for the fiber lasers to achieve efficient and robust laser operation, the pump light emitted from laser diodes needs to be coupled into the small core area with high efficiency and stability. This requires the laser diodes to be single-mode and have high brightness. However, high-power single-mode laser diodes remain to be a technique challenge up to date and the output powers from the core-pumped fiber lasers are still limited to ~1 W due to the pump power availability. To break this stringent pump source requirement and take advantage of the available high-power multimode laser diodes of relative low brightness, cladding-pumped fiber devices were introduced in late 80s (Snitzer et al., 1988).

Double-cladding fibers are designed for the cladding-pumping scheme, as shown in Figure 2.19, a second (outer) cladding with lower index than that of the first (inner) cladding is added. The pump light is injected into the inner cladding and is confined there, because the total internal reflection condition is satisfied at the inner-outer cladding interface. At the same time, since only the core is doped and the signal light is generated and confined inside the core, the signal will still have a high brightness regardless of the properties of the pump light. It should be noted that in this figure the outer cladding (or polymer coating) must have a lower index of refraction than the inner cladding and the core must have higher index than the inner cladding.
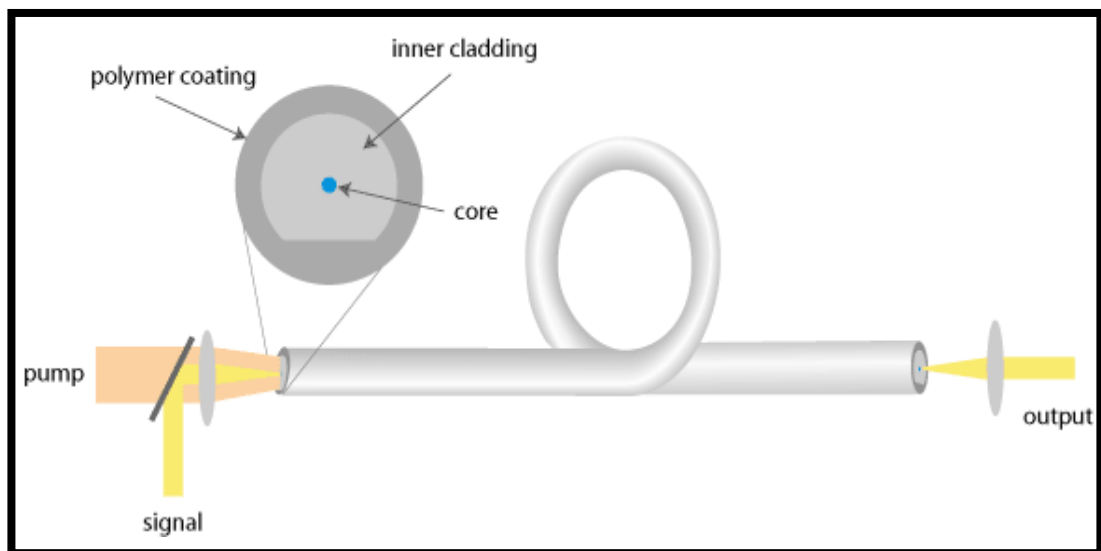
Figure 2.19: Cladding pumping technique using a double clad fiber

Often the inner cladding is not round as shown in Fig. 2.19, but otherwise shaped (D-shape) to improve pump absorption. This innovation led to a period of extremely rapid increase in fiber laser output power that was largely only limited by power levels of pump diodes. Another major advantage of the cladding-pumping scheme is that these fiber lasers have high thermal tolerance for high-power CW laser

operation. Though the pump power fills out the inner cladding during its propagation along the fiber, only the core region absorbs the pump light. The pump absorption coefficient of the fiber is thus proportional to the ratio of core area over the inner cladding area, if the pump power is evenly distributed across the cross-section of the inner cladding. Therefore, one can always lower the core doping level and increase the inner cladding size to effectively reduce the pump absorption coefficient, at the same time, elongate the fiber length to ensure sufficient pump absorption. Another thermal concern is that as laser diode arrays of very high CW power are available, the output power of the fiber laser can be limited by the breakdown of the active core region, due to the high optical power density at the single mode core center. To reduce the intensity at the core center, large and slightly multimode cores can be used instead of the small single-mode cores. Though large cores may allow a few transverse modes, careful designs and special techniques, such as bending, can be used to strip out the high order modes so that the large cores can still be under fundamental mode operation. Large core size will also help overcome yet another power scaling limitation factor: the nonlinear effects such as stimulated Raman and Brillouin scatterings. Since the threshold powers of these nonlinear effects are proportional to the effective modal area, large cores will enhance the threshold powers and postpone the output power rollover caused by nonlinear effects to a later stage in power scaling.

.

2.11   Dual wavelength fiber lasers (DWFL)

Dual wavelength fiber lasers (DWFL) research has increased considerably in recent years due to the potential applications of these optical devices in diverse investigation areas. Interest of use of DWFL includes areas such as fiber sensors, wavelength division multiplexing, optical communications systems, optical instrumentation and recently in microwaves generation (Liu et al., 2007; Mao & Lit, 2002; Talaverano et al., 2001). DWFL are considered profitable optical sources because of their advantages such as low cost, easy and affordable optical structures, low losses insertion and space optimization.

Principal issue to generate two simultaneous laser lines resides in the cavity losses adjustment. In DWFL designed with Erbium-doped fiber (EDF) as a gain medium there is a strong competition between the generated laser lines due to the EDF's homogeneous gain medium behavior at room temperature. To reduce the competition between the wavelengths, several techniques have been reported aiming to achieve stable multi-wavelength laser oscillations (Liu et al., 2007). Moreover, fiber Bragg gratings (FBG) have been extensively used in DWFL cavities design due to their advantages as optical devices including easy manufacture, fiber compatibility, low cost and wavelength selection among others. FBG's wavelength selection property is commonly used as a narrow band reflector inside the laser cavity to generate a laser line at a specific wavelength. Several DWFL experimental setups using FBG's have been reported including use of a FBG written in a high birefringence or in a multimode fiber (Latif et al., 2011).

In a large majority of DWFL using EDF and FBG's, the laser cavity losses correspond to different generated laser lines at a specific wavelength position over the gain medium spectrum. The generated wavelength should be balanced to achieve two simultaneous laser lines. Consequently, both oscillation lines have the same pump

threshold. Commonly the wavelengths adjustment is realized through arbitrary methods as use of polarization controllers (Rao et al.) and variable optical attenuators (VOA) (Han & Lee, 2007). With the progress on DWFL research studies have been followed two different pathways in order to enhance stability of the simultaneously generated laser lines by improving the cavity losses adjustment methods.

On the one hand, the research focuses on incorporating of cutting-edge devices in an effort to obtain more stable and efficient dual laser emissions. In such a way that these researching works reports the use of newly developed optical fibers such as photonic crystal fibers, leading to use optical devices that allow the exploit of nonlinear optics (Parvizi et al., 2011). Most of the reported works on this area tend to have more complex designs and non-straightforward settings. By the other hand, a second pathway is in function of simplicity and optimization of laser cavity length, taking into account that a reduced cavity length implies a decrease of laser modes within the cavity, allowing, in a first instance analysis, a dual laser emission with lower instability, a simple adjustment of the competition between laser lines with a substantial reduction of implementation space that can improve the results repeatability (Liu et al., 2009).

In recent years, obtaining of dual-wavelength laser emission does not represent an advance by itself in DWFL progress because the increasing need to analyze the behavior of the competition between the generated laser lines obtained by the cavity losses adjustment methods. Using arbitrary methods like adjustment by polarization controllers and variable optical attenuators do not allow a behavioral analysis of the competition between generated wavelengths because these methods do not have a measurable physical variable to characterize the adjustment and difficultly can provide repeatability in results.

The spectral selectivity of the interferometer is caused by birefringence that has to be introduced to the loop. A lot of effort has been made to suggest and investigate a

variety of Fiber optic loop mirror (FOLM) designs (Harun et al., 2005; Lim et al., 2009; Liu et al., 2004). The transmittance spectrum of the FOLM presents a periodic behavior with maxima and minima depending on the Hi-Bi fiber length and birefringence. For dual-wavelength lasers, low contrast offers the advantage of smoother cavity loss adjustment for the generated wavelengths where the principal mechanism of the adjustment of the cavity loss is the shift of the wavelength of the reflection maxima of the FOLM. The wavelength shift is achieved by the change of the temperature of the Hi-Bi fiber. This method allows generating two wavelengths with a well-controlled ratio between their powers (Álvarez-Tamayo et al., 2011).

Moreover, the tuning of the laser generated wavelengths promises to be an advantage for DWFL microwave generation application making it possible through the tuning of separation between wavelengths. A simple method of wavelength tuning is related to the Bragg period modification of a FBG. Wavelength tunable DWFL were reported. (Álvarez-Tamayo et al., 2011). In most configurations the FBG's are used with Bragg wavelength shift by temperature change (Li et al., 2004), compression or stretch. (Moore et al., 2009). Most of the techniques reported before as a matter of fact realize an adjustment of the losses between the two wavelengths to achieve stable dual-wavelength generation.

In this work proposes the application of multi-mode fiber (MMF), tapered fiber and mismatch effect as a spectral filter to adjust finely the laser cavity losses, to generate dual-wavelength in 2 micron fiber by using thulium doped fiber as gain medium.

CHAPTER 3

All-fiber Dual-Wavelength Fiber Laser Operating at 2 Micron Region

3.1   Introduction

In the recent years 2 μm laser sources have drawn a great interest in the research area of photonics since it offers a possibility for combining high efficiency and high output power with eyesafe operation. In addition, it suggests a number of specific applications associated exclusively with its infrared wavelength, e.g., in the fields of remote sensing and biomedicine (Fried & Murray, 2005; Szlauer et al., 2009; Taccheo et al., 1996; Zeller et al., 2010). The wavelength overlaps with many absorption lines of several molecules, e.g. carbon dioxide (CO_2) or hydrogen bromide (HBr) (Zeller et al., 2010), which creates the possibility of constructing cost-effective trace-gas sensing platforms. Strong water absorption in this range makes the light source extremely desirable in biomedical applications. It has been shown, that 2 μm laser outperform 1 μm and 1.55 μm sources in dermatology and surgery, serving as precise and efficient optical scalpels (Fried & Murray, 2005; Szlauer et al., 2009). The light source operating in the range of 1.8 to 2.0 μm can be realized using Thulium-doped fiber laser (TDFL).

The lasing near 2 μm is initiated by the transition of thulium ions from $^3H_6$ to $^3F_4$ because of the so-called cross-relaxation energy transfer process between Thulium ions. During this process, two ground-level Thulium ions are excited to the upper lasing level of $^3F_4$ by absorbing only one pump photon near 790 nm. This suggests that one excited Tm^{3+} ion at the $^3H_4$ level generates two Tm^{3+} ions at the $^3F_4$ upper laser level. However, commercial high power diodes required for the excitation in this wavelength range are difficult to obtain as well as very costly. Pumping Thulium-doped fibers at another pumping wavelength of 1200 nm or 1600 nm is complicated because semiconductor laser diodes with sufficient power are not commercially available. An alternative

approach is to co-dope the Thulium fiber with Yb^{3+} so that it can be pumped by a commercial 905−980 nm laser diode. This is due to the $^3H_5$ level of Tm^{3+}, which is (quasi-) resonant with the excited Yb^{3+} level ($^2F_{5/2}$) and thus allows the sensitization of Tm^{3+} doped fibers with Yb^{3+}, similar to the case of Yb^{3+} sensitized Er^{3+}-doped fibers (Pal et al., 2010). The up-conversion system has long been proposed based on Tm^{3+}-Yb^{3+} co-doped glass and fibers (Halder et al., 2012), but only more recently the concept is used for the 2-μm fiber laser application (Harun et al., 2012). A cheap and stable low power fiber laser operating near 2 μm region is useful for many potential applications like toxic gas sensing and component characterization.

Recently, many works on all-fiber dual-wavelength fiber lasers have been reported due to interests in their potentials in applications such as optical instrument testing, optical signal processing, fiber sensing systems and microwave photonics (Ahmad et al., 2009; Harun et al., 2012; Jeon et al., 2010). Different strategies have been adopted to generate a dual-wavelength lasing for example by using a twin-peak reflection grating and dual-cavity configuration. But, most of the lasers that have been demonstrated operate at 1.00 and 1.55 μm band. For the longer wavelength region of 2 μm, fiber components are not as readily available as those at the shorter wavelengths of 1.00 and 1.55μm. Very recently, 2041.3 nm/2054.6 nm simultaneous dual wavelength Tm, Ho: YVO4 solid state microchip laser was demonstrated (Chan, 1997). However, 2 μm band all-fiber laser is urgently expected in practical use due to its compact and robust property.

In this chapter, new all-fiber dual-wavelength 2 μm fiber lasers are proposed and demonstrated based on three different approaches; spatial filtering effect, inline microfiber Mach Zehnder Interferometer and multimode interference effect.

3.2 Dual wavelength TDFL based on spatial filtering effect

In an earlier work, Zhou et al. (Zhou et al., 2011) have demonstrated a room-temperature all-fiber dualwavelength TDFL based on a cascaded fiber Bragg grating array. However, the FBG structure requires an expensive UV laser to be fabricated and the conventional FBG cannot operate at a temperature higher than 300°C. In this section, we develop a room-temperature all-fiber dual-wavelength TDFL operating near 1900 nm, which uses a simpler approach based on a spatial filter generated due to mismatch at the splicing points of a Thulium doped fiber (TDF). A scheme of our dual-wavelength TDFL is shown in Figure 3.1. The laser is constructed using a simple ring cavity, in which a 2 m long TDF is used as an active medium. The TDF used by us has the core and cladding diameters of 9 µm and 125 µm respectively, the cut-off wavelength of 1750 nm, and the numerical aperture of 0.15. The absorption of Thulium ions in this fiber has a peak at 793 nm (27 dB/m). The TDF is pumped by an 800 nm laser diode via an 800/2000 nm wavelength division multiplexer. The operating wavelength of our TDFL is determined by a spatial filter, which is formed by controlling the phase mismatch at the splicing points of the TDF. The mismatch creates oscillations within the TDF. The output of the dual-wavelength laser is tapped from a 10 dB output coupler, allowing for 90 per cent of the light to remain in the cavity. The output spectrum and the power of the laser are measured with an optical spectrum analyser.
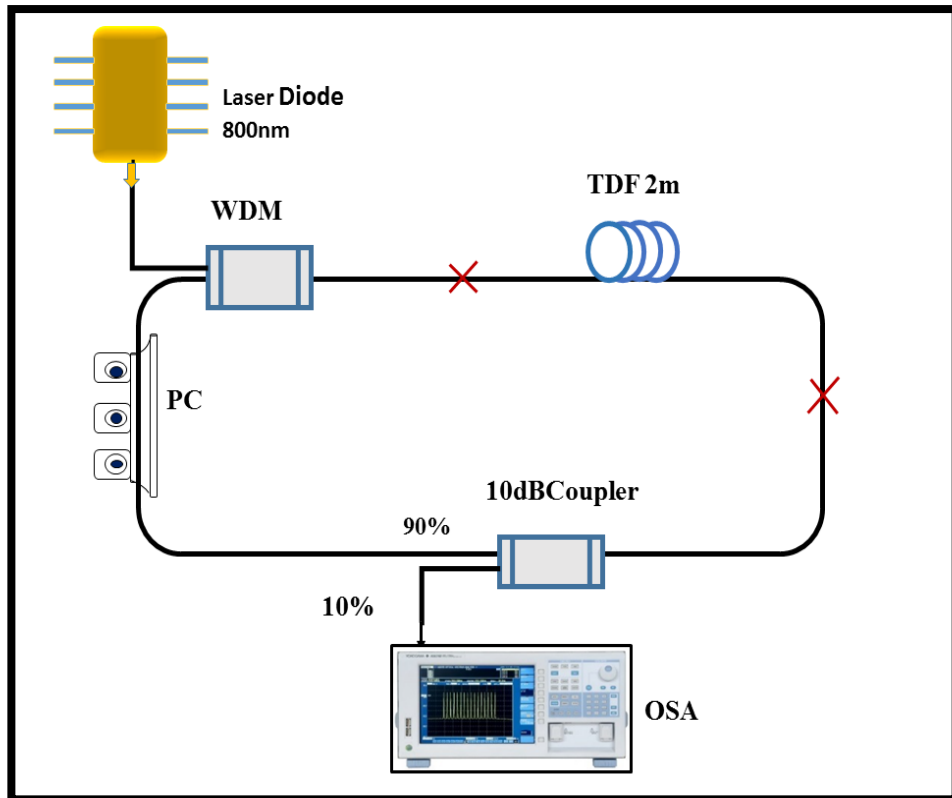
Figure 3.1: Experimental setup of our dual-wavelength TDFL: crosses correspond to splicing points of the TDF

Figure 3.2 shows the transmission spectrum of the spatial filter. In our experiments, a broadband 1550 nm source of amplified spontaneous emission is launched into the setup from the input port of the wavelength division multiplexer coupler, and the output spectrum is measured after a 10 dB coupler, using an optical spectrum analyser. As we control precise details of the splicing between the single-mode fiber and the TDF, the power oscillations occur within the TDF, thus producing some wavelength-dependent losses. As a result of specific transmission function of the spatial mode-beating filter, the spectrum at the output signal has a comb-type characteristic as shown in Figure 3.2. From Figure 3.2, the spacing between the two neighbouring peaks is measured to be approximatly 1.8 nm.
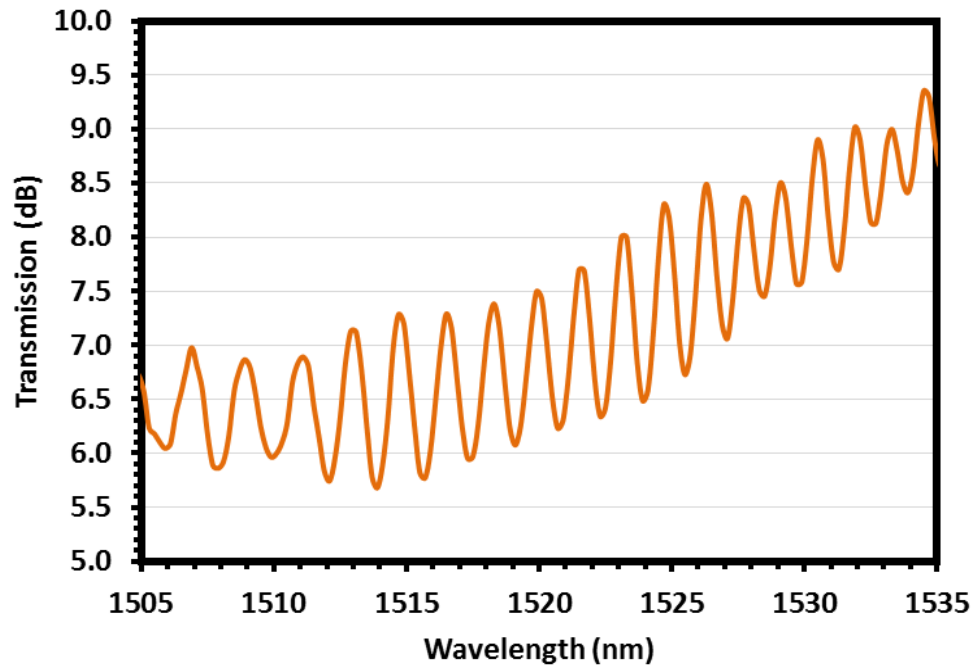
Figure 3.2: Comb-type spectral structure of signal produced by our spatial mode beating filter.

As the TDF is pumped, an amplified spontaneous emission is generated in the vicinity of 1900 nm via both spontaneous and stimulated emission processes. The Thulium ions are excited to level as they absorb the pumping photons to create the population inversion between the levels. Then they drop to the ground state ($^{3}H_{6}$) and emit light at 1.9 µm. The amplified spontaneous emission oscillates in the ring cavity, resulting in a laser that operates according to the transmission characteristic of the spatial mode-beating filter. Since the filter has a wide bandwidth, the regime of dual-wavelength laser output can easily be implemented. Due to the transmission characteristic of the filter, the signals at two different wavelengths can oscillate in the cavity whenever the difference of the cavity losses for them are somewhat reduced. By adjusting the polarization state of the light propagating in the laser cavity, one can tune the cavity losses for these two wavelengths to seek dual-wavelength oscillations with the aid of the TDF, whose gain broadening behaves inhomogeneously. Figure 3.3 shows the output spectrum of the TDFL recorded by the optical spectrum analyser at different

pump powers. As seen from Figure 3.3, the dual-wavelength output lines are obtained at 1844.8 and 1852.0 nm, so that their spacing is equal to 7.2 nm. This spacing is four times larger than that associated with the spatial filter at 1550 nm. At the pump power as low as 124.5 mW, the signal-to-noise ratios for the 1844.8 and 1852.0 nm lines are respectively equal to 30 and 21 dB, with the 3 dB bandwidth being approximately equal to 2.0 **nm.**
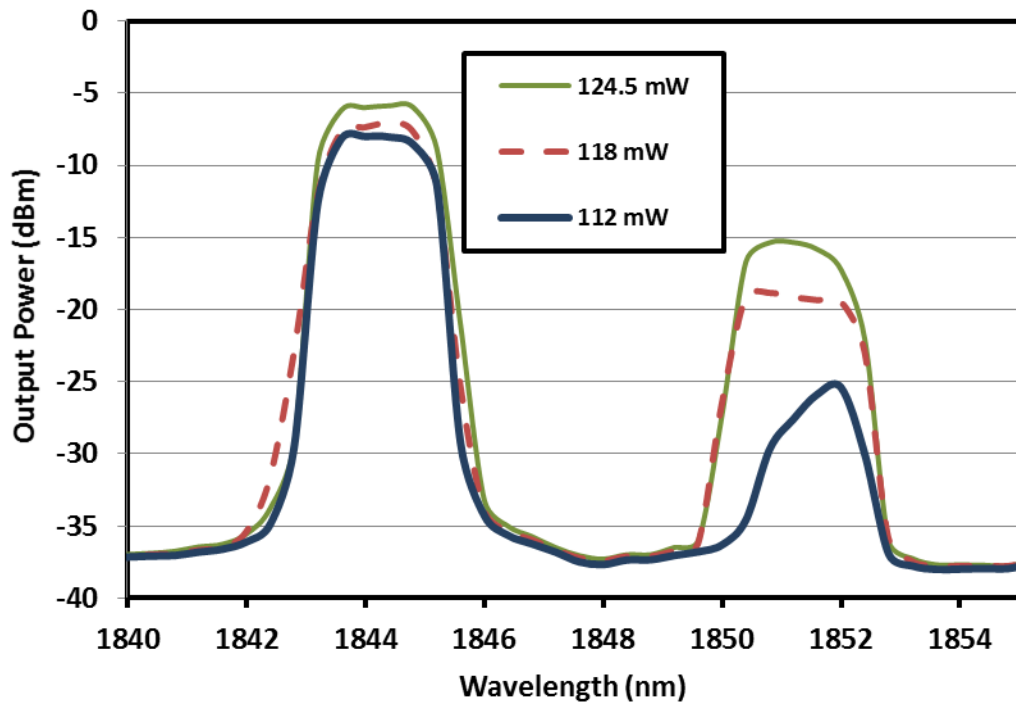
Figure 3.3:output spectrum of our TBFL at three different pump power as indicated in the legend.

The relationships between the pump power and the peak powers of the dual-wavelength output lines located at 1844.8 nm and 1852.0 nm are shown in Figure 3.4. The dual-wavelength laser starts to lase above the threshold pump power of 109.3 mW. Then both output-peak powers increase linearly with increasing pump power. At the maximum pump power of 131.7 mW dealt with in the present experiments, the 1844.8 and 1852.0 nm laser lines have the maximum output powers of 0.297 and 0.038 mW, respectively. Figure 3.5 shows the output optical spectrum of our dual-wavelength laser for the case when the scanning interval is 10 min. In our experiments, the dual-

wavelength operation can be stable for more than two hours if only the temperature variations and the mechanical vibrations are kept reasonably small, as with standard laboratory facilities. As seen from Figure 3.4, the corresponding difference for each laser wavelength is less than 1 dB, thus pointing to enough stability of the output. No other lasing modes have been observed inside the Thulium gain band. Since the operating laser wavelengths are determined only by the spatial filter, they can be tuned by controlling the mismatch between the fiber associated with the wavelength division multiplexer and the TDF, or by using some other techniques.
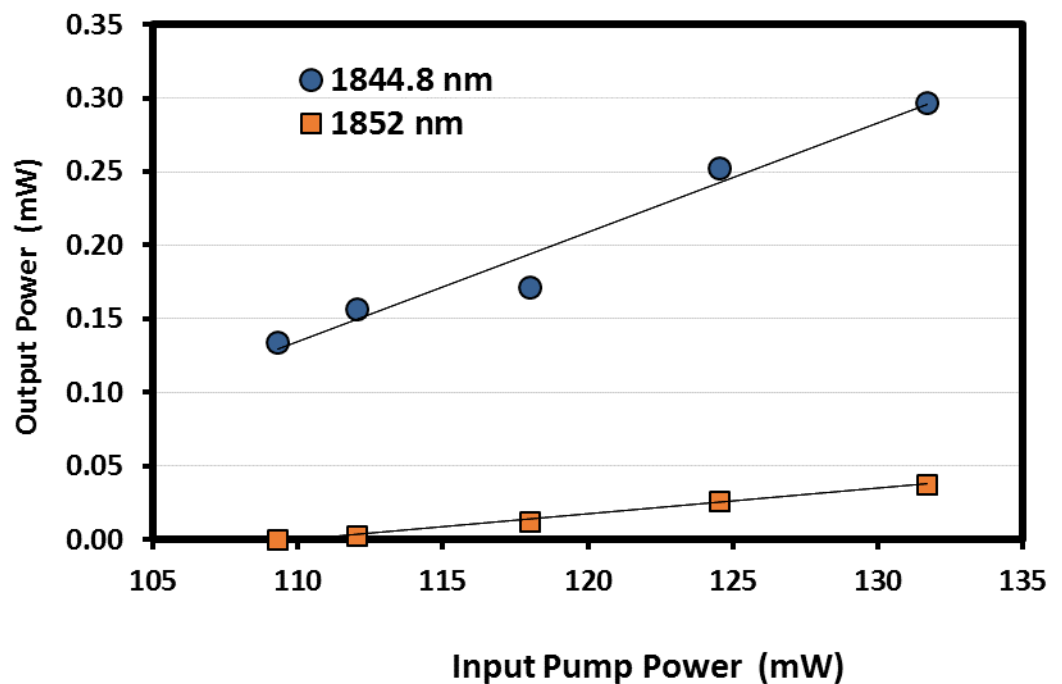
Figure 3.4: Dependences of peak output powers of the two laser lines on the input pump power.
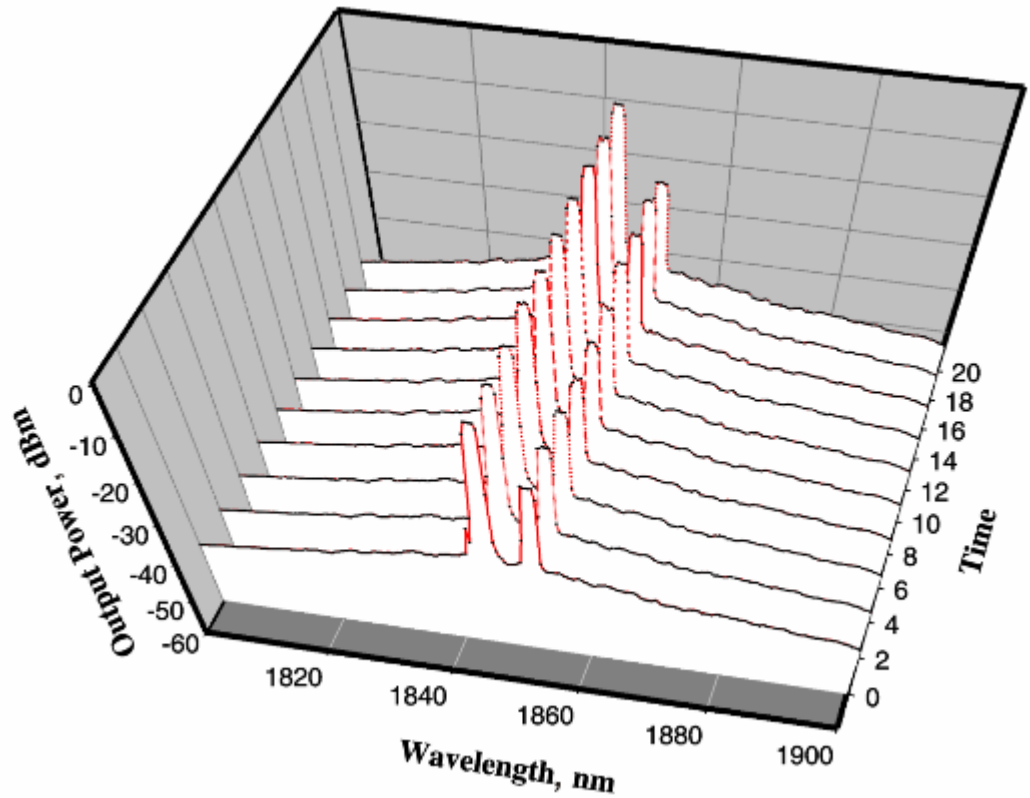
Figure 3.5: Output power spectra of our TDFL taken with 10 min periods between

frames to illustrate stability of the laser.

3.3 Dual-Wavelength 2 μm Fiber Laser Based on Inline Microfiber Mach-Zehnder Interferometer:

In this section, a room temperature all-fiber dual-wavelength fiber laser operating in 1955 nm region is demonstrated using an inline microfiber Mach Zehnder Interferometer (MMZI). The MMZI is incorporated in the laser cavity to act as a comb filter. The proposed laser uses a cascaded commercial Thulium-doped fiber (TDF) and laboratory made double-clad Thulium-Ytterbium co-doped fiber (TYDF) as a gain medium, which is forward pumped by a single-mode 800 nm and a multimode 905 nm pumps respectively,

3.3.1 Fabrication and characteristic of inline MMZI

An inline MMZI is constructed from a low loss microfiber, which was drawn from a standard SMF using flame brushing technique. The microfiber is firstly fabricated by heating a portion of the unjacketed fiber to its softening temperature, and then pulling one of the ends apart to reduce the fiber's diameter down to 46 μm. The torch is then moved to the left and right for further tapering the transition part to a smaller diameter of 12 μm and 6.4 μm, respectively. The middle part of the structure acts as an interference region for the inline MMZI structure. Figure 3.6 (a) shows the schematic diagram of the fabricated MMZI. The total length of the fabricated structure is approximately 50 mm where the length of the first tapered region, second tapered region and the interferometer region was 25mm, 4mm and 8mm respectively. The microscopic images of these regions are shown in Figure 3.6(b). During the tapering process, a broadband amplified spontaneous emission light is launched into the microfiber to monitor the loss and spectral response using an optical spectrum analyzer at the output end of the microfiber. In principle, the inline MMZI works as follows; the input modes of light split into two types of modes defined as guided and unguided modes at the interference region. The guided mode keeps travelling in the core and the unguided mode propagates through the cladding.

(a)

(b)
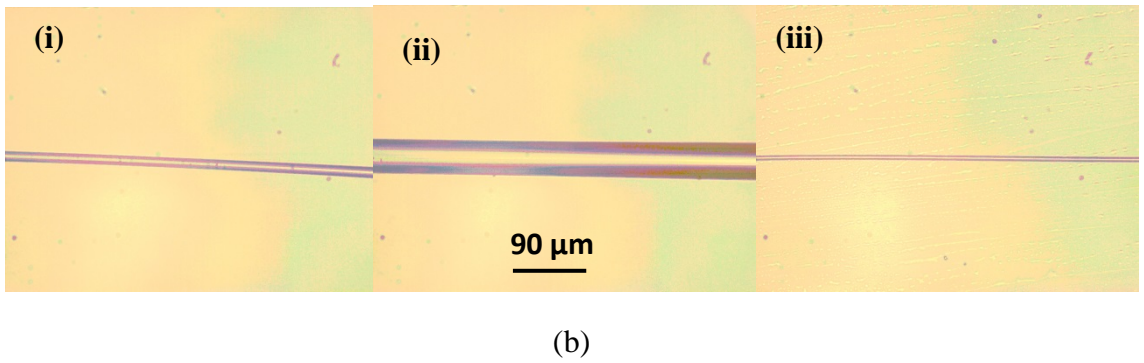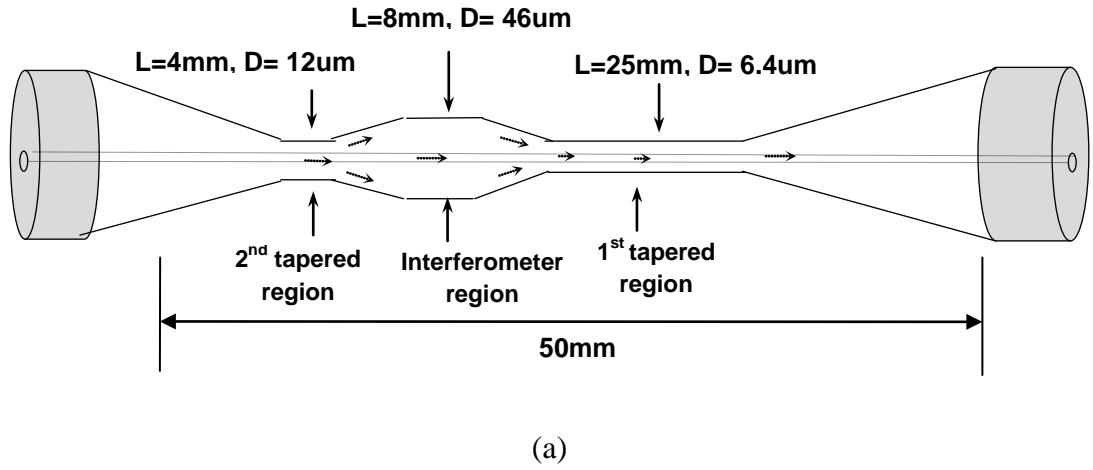
Figure 3.6: (a) Schematic diagram of the fabricated inline MMZI and (b) microscopic images for the three tapered regions of inline MMZI, where the images (i), (ii) and (iii) represent the 2nd tapered region, interferometer region and 1st tapered region respectively.

The phase difference between the core and cladding modes can be expressed as:

$$\varphi = \frac{2\pi \left(\Delta n_{eff} \right) L}{\lambda} \qquad (3.1)$$

Where Δn_{eff} is defined as ($n_c^{eff} - n_{cl}^{eff}$) which is the difference of the effective refractive indices of the core and the cladding modes, L is the length of the interferometer region and λ is the input wavelength. Interference occurs due to the phase difference φ, and the transmission dip wavelength λ_m of the interference and can be expressed as:

$$\lambda_m = \frac{2\pi(\Delta n_{eff})L}{2m+1} \qquad (3.2)$$

Where *m* is the interference order.

Figure 3.7 shows the transmission spectra of the inline MMZI at 1550 nm region, where the spectra is showing the interference fringes with a spacing of around 3.7 nm and extinction ratio of approximately 15 dB. The insertion loss of fabrication inline MMZI is observed to be approximately 9 dB at 1550 nm region.
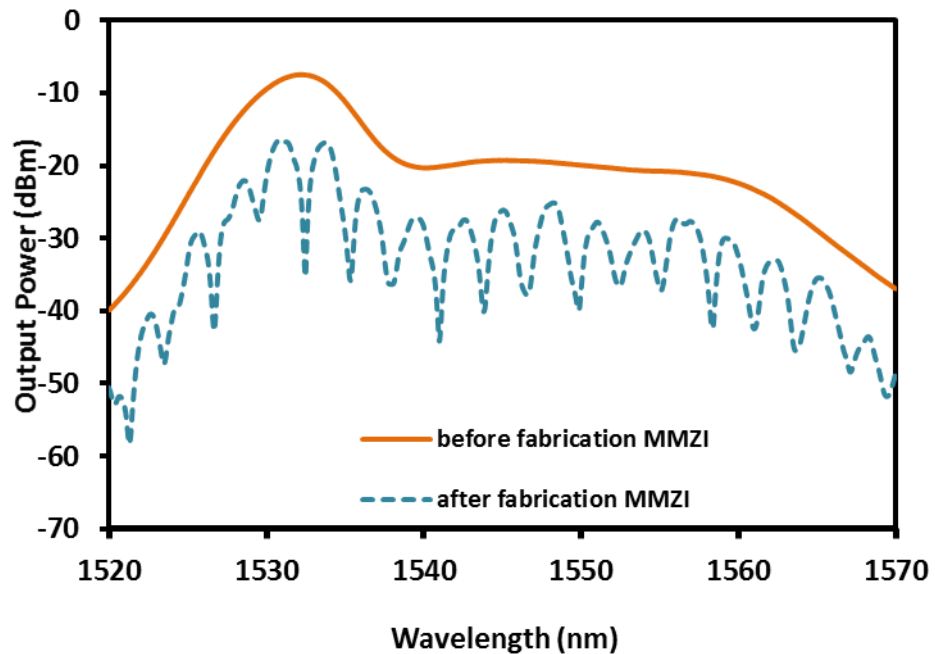
Figure 3.7: Transmission spectrum of the inline MMZI

3.3.2 Configuration of the proposed MMZI based dual-wavelength laser

The schematic diagram of the proposed dual-wavelength fiber laser operating at 1955 nm region is shown in Figure 3.8. The fiber laser is constructed using a simple ring cavity, in which a 2 m long commercial TDF and 15 long laboratory made TYDF are cascaded to produce the ASE at 1955 nm region. The TDF is pumped by a 800 nm

laser diode via an 800/2000 nm wavelength division multiplexer (WDM) while the TYDF is pumped by a 905 nm multimode laser diode via a multimode combiner (MMC). The TDF has a core and cladding diameters of 9 µm and 125 µm respectively, a loss of less than 0.2 dB/km at 1900 nm and Tm ion absorption of 27 dB/m at 793 nm. The laboratory made TYDF has an octagonal shaped double-clad structure, which was drawn from a lithium-alumino-germano-silicate (LAGS) core glass optical preform. The preform was fabricated via the modified chemical vapour deposition (MCVD) process, followed by solution doping technique. The preform consists of an Al_2O_3, Y_2O_3, Tm_2O_3 and Yb_2O_3 dopants with average weight percentage of 5.5, 3.30, 0.70 and 4.0, respectively. Such octagonal geometry of the cladding improves the pump absorption efficiency. The doping levels of Tm^{3+} and Yb^{3+} ions of the fabricated TYDF are measured to be around 4.85 ions/cc and 27.3 ions/cc, respectively using an electron probe micro-analyser (EPMA). NA and core diameter of the fabricated TYDF are measured to be 0.23, and 5.96 µm, respectively. The cascaded gain media is used to reduce the threshold pump power for the Thulium fiber laser so that the laser can be realized using an available pump power.

The operating wavelength of the proposed TDFL is determined by the filtering characteristic of the fabricated inline MMZI. A polarization controller is used to adjust the polarization state of the oscillating light in the laser cavity. The output dual-wavelength laser is tapped from a 10 dB output coupler while allowing 90 % of the light to remain in the cavity. The output spectrum and power of the laser are measured by using an OSA

Figure 3.8: Experimental setup for the proposed dual wavelength fiber laser using a cascaded TDF and double-clad TYDF as the gain medium and an inline MMZI as a wavelength selective filter.

3.3.3   Performance of the MMZI based dual-wavelength laser

At first, we investigate the transmission spectrum of the inline MMZI filter by launching a broadband amplified spontaneous emission light centred at 1950 nm and measure the output spectrum using an OSA. Due to the phase difference between the core and cladding modes inside the MMZI structure, interference occurs to form a comb-like spectrum at the output as shown as a dashed line in Figure 3.9. Compared to the output interference at 1550 nm region, at least two oscillations are observed at 1955 nm region. This is most probably due to the higher number of modes travelling in the cladding as the system is operating at a longer wavelength. As shown in the figure, the

dominant wavelength separation is around 3.76 nm is obtained at around 1955 nm with a signal to noise ratio is approximatly 10 dB.

Figure 3.9: Comparison between the transmission spectrum of the inline MMZI filter and the laser output spectrum.

As the TDF is pumped, an ASE is generated at 1900 nm region via spontaneous and stimulated emission process. Thulium ions are excited to $^3F_4$ level as they absorb the pump photon to create a population inversion between $^3H_6$ and this energy level. Then they drop to the ground state ($^3H_6$) while emitting at 1.9 µm. The ASE is then amplified by the forward pumped double-clad TYDF. The amplified ASE centered at relatively longer wavelength region of 1955 nm due to the use of Thulium Ytterbium co-doped fiber, which provides a higher gain at longer wavelength due to energy transfer from Ytterbium to Thulium ions. The ASE oscillates in the ring cavity to generate laser that operates within the transmission characteristic of the MMZI filter. Due to the transmission characteristic of the filter, it is possible to have the oscillation of two wavelengths in the cavity if the difference of the cavity loss between them can be reduced. By adjusting the polarization state of the propagating light in the laser cavity,

the cavity loss of the two wavelengths can be tuned to seek dual-wavelength oscillation with the help of both TDF and TYDF, whose gain broadening behaves inhomogeneously.

The output spectrum of the proposed laser as recorded by an OSA is shown as a solid line in Figure 3.9, when the single mode 800 nm and multimode 905 nm pump are fixed at 110 mW and 2.0 W, respectively. As seen in the figure, a dual-wavelength output lines are obtained at 1952.93 and 1956.68 nm, which coincided to two of the transmission peaks of the MMZI filter. The 1952.93 and 1956.68 nm lasers peak at -18.5 and -17.4 dBm with a signal to noise ratio of more than 35 dB. The 3 dB bandwidth of both lasers is measured to be less than 0.2 nm. The relation between the peak power of the dual-wavelength output lines of 1952.93 and 1956.68 nm against the pump power is shown in Figure 3.10. In the experiment, the 800 nm pump is fixed at 110 mW while the multimode 905 nm is varied from 0 to 2.0 W. The dual-wavelength laser starts to lase at threshold power of 1.6 W before both output peak power increase linearly with the increment of multimode pump power. At the maximum multimode pump power of 2.0 W, the 1956.68 nm laser line produces the maximum output power of 18.1 μW while the output power of the 1952.93 nm line reduces due to the saturation effect. \the output power is relatively low due to high cavity loss.

Figure 3.10: The peak power of the dual-wavelength laser lines against the input 905 nm pump power when the 800 nm pump is fixed at 143 mW.

Figure 3.11 shows the output optical spectrum of the dual-wavelength laser with a scanning time interval of 10 minutes. In our experiment, the dual-wavelength operation can be stable for more than two hour if the temperature variation and mechanical vibration are reasonably small. As seen in Figure 3.11, the difference in each laser wavelength is less than 1.0 dB, which indicates the stability of the output. No other lasing modes are observed in the thulium gain band. Since the laser wavelength is only determined by the function of the MMZI filter, the operating wavelength could be tuned by controlling the number of unguided modes inside the cladding and their phase difference.
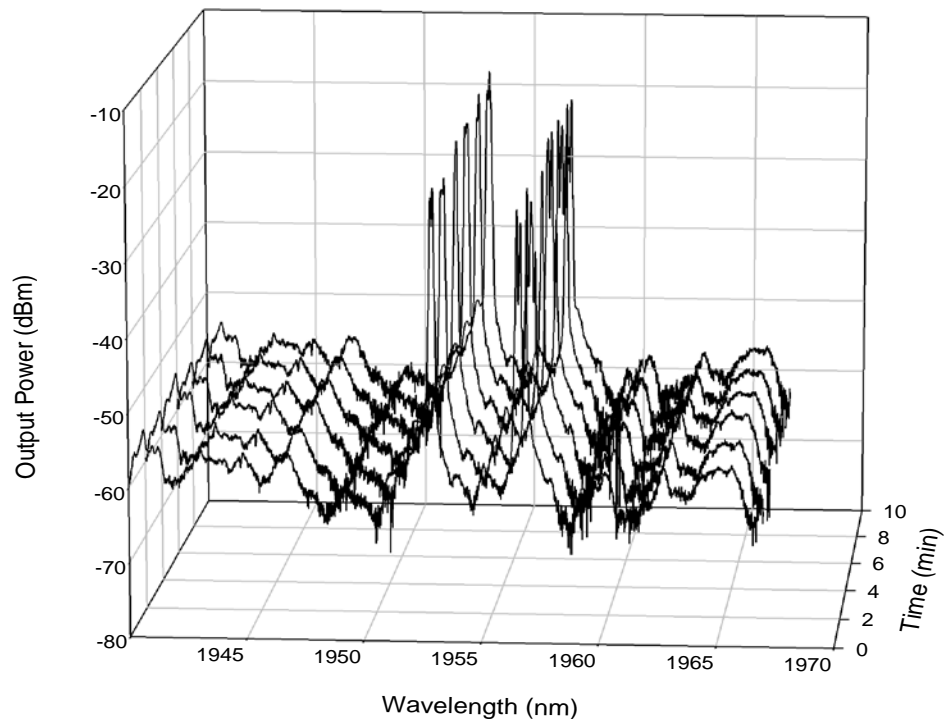
Figure 3.11: The stability graph of the proposed dual-wavelength laser with 10 minutes

period for each frame

3.4 Dual-wavelength fiber laser operating in 1950 nm region based on multimode Interference filter

In this section, a new all-fiber dual-wavelength fiber laser operating in 1950 nm

region is proposed using a simpler approach based on an incorporation of a short length

of multimode fiber (MMF) in the laser cavity to act as a multimode interference filter.

The configuration of the proposed laser is almost similar with the previous section,

which uses a commercial TDF and laboratory made double-clad Thulium-Ytterbium co-

doped fiber (TYDF) as a cascaded gain medium. The schematic diagram of the

proposed dual-wavelength fiber laser based on MMI filter is shown in Figure 3.12. The

fiber laser uses a ring cavity consisting of a 2 m long commercial TDF and 15 long

laboratory made TYDF a gain medium, which are forward pumped by a single-mode

800 nm and a multimode 905 nm pumps respectively as. The characteristics of both

gain media are the same with the previous laser. The operating wavelength of the proposed 2 µm laser is determined by the MMI filter, which is obtained by splicing a 13.5 cm long MMF between two single-mode fibers (SMFs) inside the laser. A polarization controller is used to control the polarization state of light in the laser cavity. The 10dB output coupler is used to tap 10% of the laser out while the OSA is used to measure the output spectrum and the power of the laser.
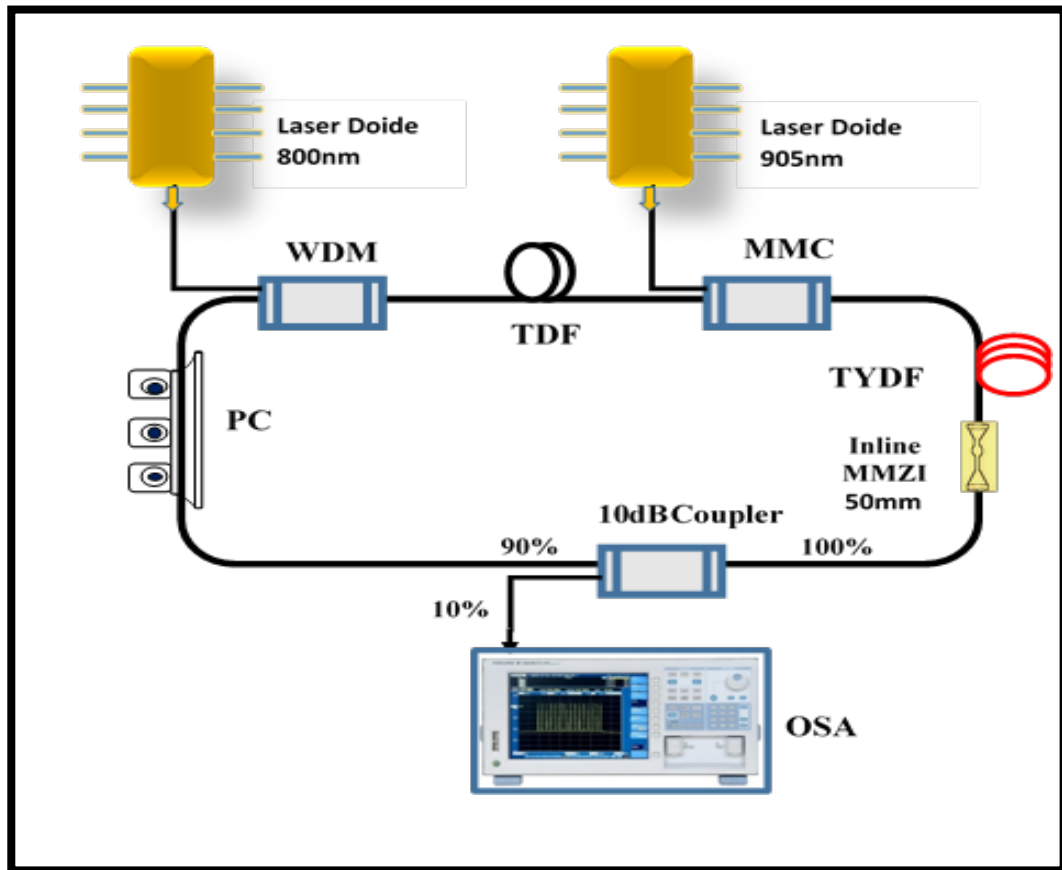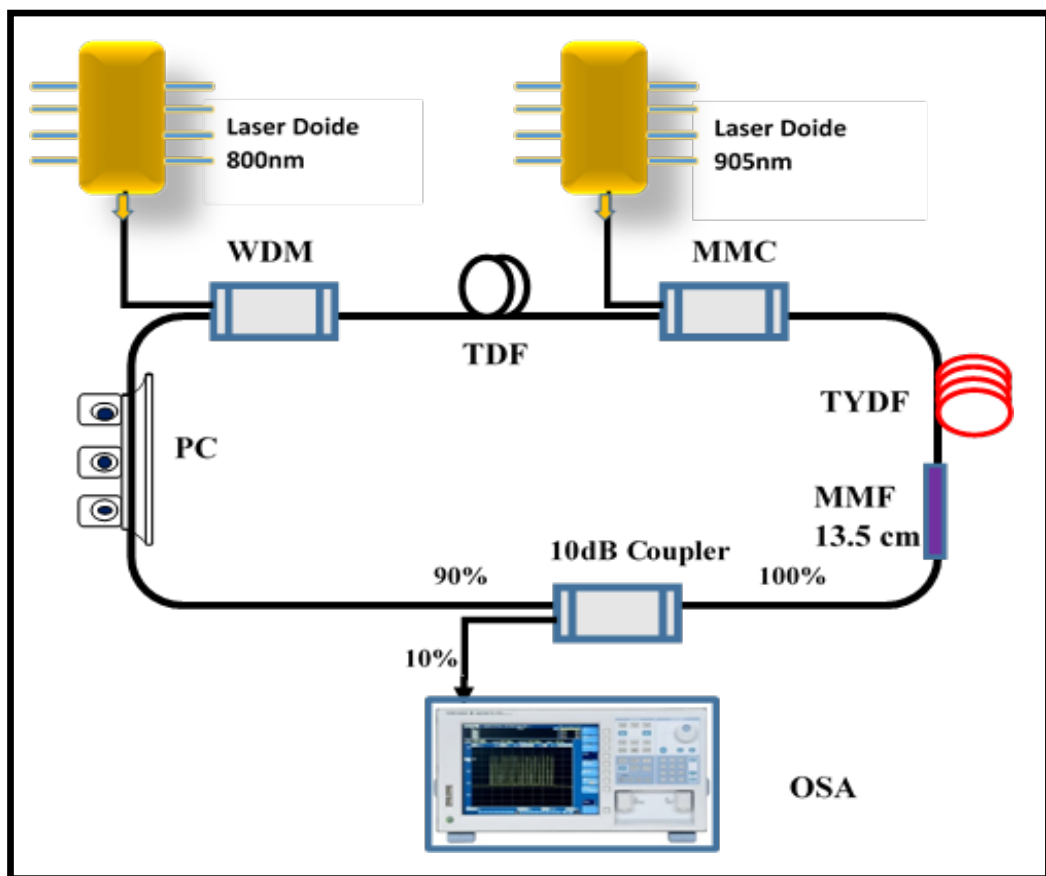

Figure 3.12: Schematic diagram of the setup for the proposed dual wavelength fiber laser using a cascaded TDF and double-clad TYDF as the gain medium and an inline MMI as a wavelength selective filter.

At first, we investigate the transmission spectrum of the MMI filter, which consists of a 13.5 cm long MMF axially spliced at both its ends to identical SMFs. In

the experiment, broadband amplified spontaneous emission light centred at 1950 nm is launched into the MMF section through the lead-in SMF at the first splice. Generally, the spot size of the fundamental mode of the MMF is different than that of the SMF. This leads to the excitation of a number of guided modes in the MMF at the input splice. Due to their different propagation constants, the guided modes of the MMF develop a certain phase difference as they propagate along the MMF length. At the lead-out splice the MMF modal fields are then coupled to the fundamental mode of the lead-out SMF. This forms a comb-type structure at the output as a result of the transmission function of the MMI filter, as shown as a dashed line in Figure 3.13. It can be seen that the maximum transmission dip is obtained at 1951.0 nm. \this is attributed to the characteristic of the filter, where the transmission dip is determined by the phase difference in the path lengths. Two peaks at 1939.68 and 1959.60 nm have the maximum extinction ratio with the transmission losses of around 4 and 5 dB, respectively.
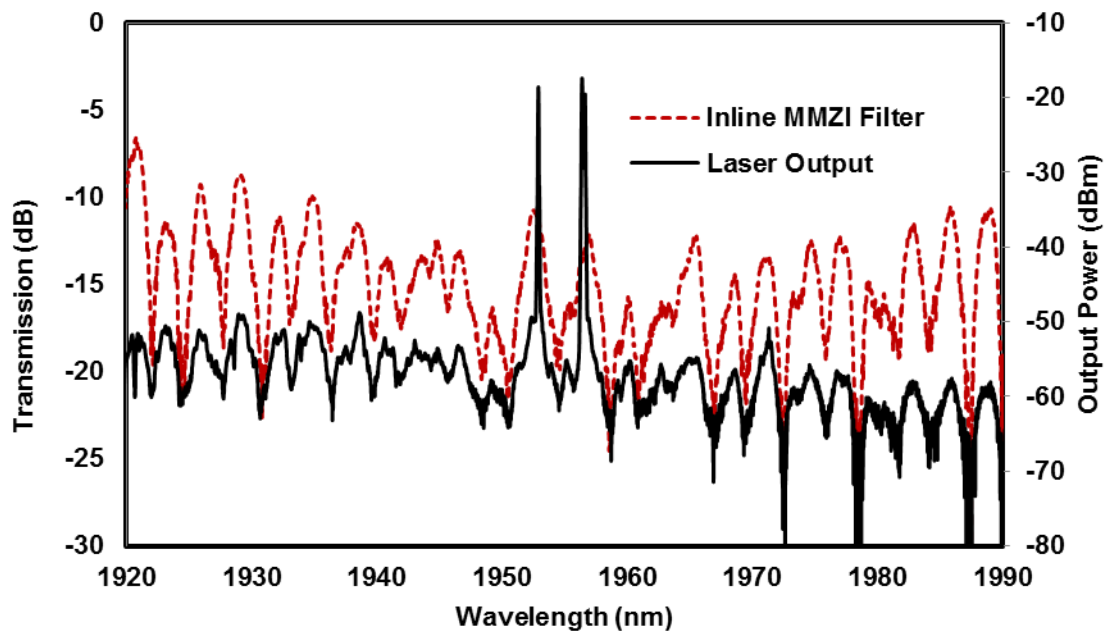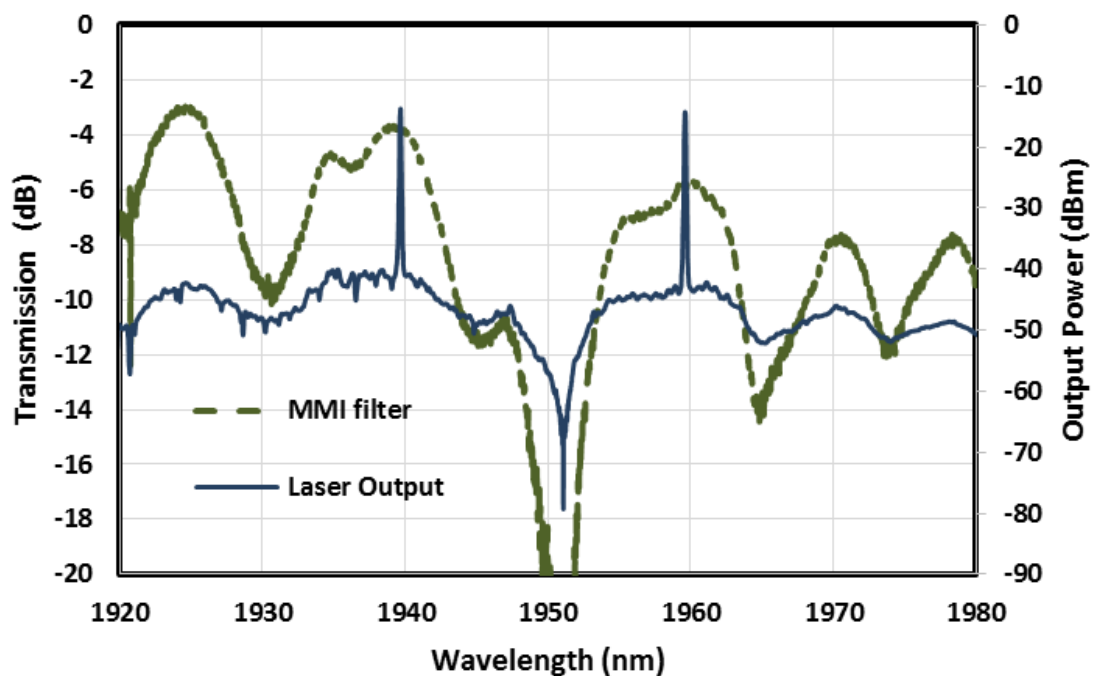

Figure 3.13: Comparison between the transmission spectrum of the MMI filter and the laser output spectrum.

As both gain media are pumped, an ASE centered at 1951 nm region is generated in both directions via spontaneous and stimulated emission processes. The ASE oscillates in the ring cavity to produce laser for which the operating wavelength is determined by the transmission characteristic of the MMI filter. By adjusting the polarization state of the oscillating light in the ring cavity, it is possible to have the oscillation of two wavelengths in the cavity. The output spectrum of the laser is depicted as a solid line in Figure 3.13 when the single mode 800 nm and multimode 905 nm pump are fixed at 143 mW and 1.5 W, respectively. As shown in the figure, a dual-wavelength output lines are located at 1939.68 and 1959.60 nm, which coincide to two of the transmission peaks of the MMI filter. The 1939.68 and 1959.60 nm lasers peak at -13.8 and -15.2 dBm with a signal to noise ratio of about 27 and 28 dB, respectively. The 3 dB bandwidth of both laser lines are measured to be less than 0.2 nm.

The relation between the peak power of the dual-wavelength output lines of 1939.68 and 1959.60 nm against the pump power is shown in Figure 3.14. In the experiment, the 800 nm pump power is fixed at 143 mW while the 905 nm multimode pump power is varied from 0 to 2.0 W. The dual-wavelength laser starts to lase at threshold power of 1.5 W before both output peak powers increase linearly with the increment of multimode pump power. At the maximum multimode pump power of 2.0 W, the 1939.68 and 1959.60 nm laser lines produce the maximum output powers of 0.21 and 0.20 mW, respectively. The output spectrum of the dual-wavelength laser is scanned every 20 minute interval as shown in Figure 3.15. In this experiment, the dual-wavelength operation is observed to be stable for more than two hours provided that the temperature variation and mechanical vibration are reasonably small (i.e., in a laboratory). The stability of the output is indicated by the small difference in each laser wavelength which is less than 0.2 dB. As expected, no other lasing modes are observed in the Thulium gain band. Since the laser wavelength is only determined by the function

of the MMI filter, the operating wavelength could be tuned by controlling the number of
guided modes inside the core and their phase difference. The inexpensive and stable low
power fiber laser has tremendous potential for many applications such as in sensing toxic
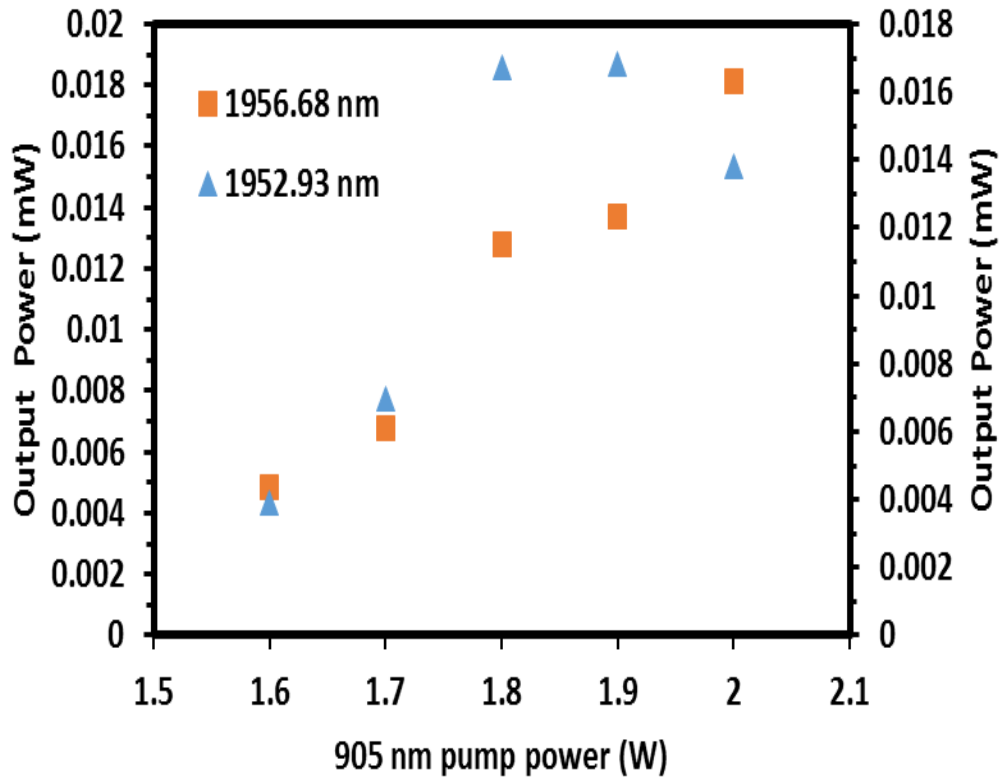gases due to their specific infrared region (IR) absorption.
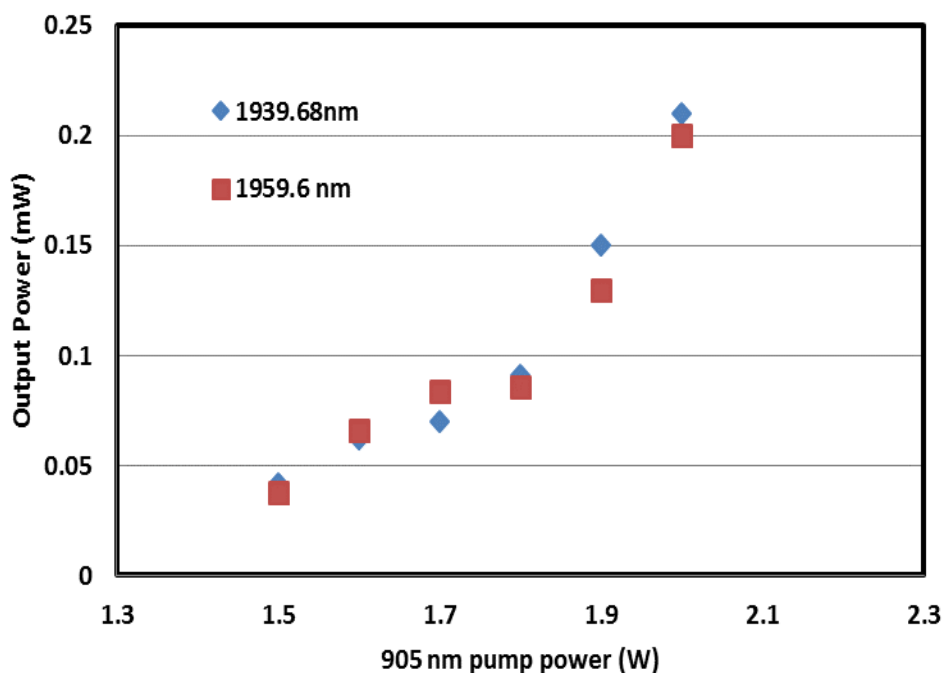
Figure 3.14: The peak power of the dual-wavelength laser lines against the input 905 nm
pump power when the 800 nm pump is fixed at 143 mW.
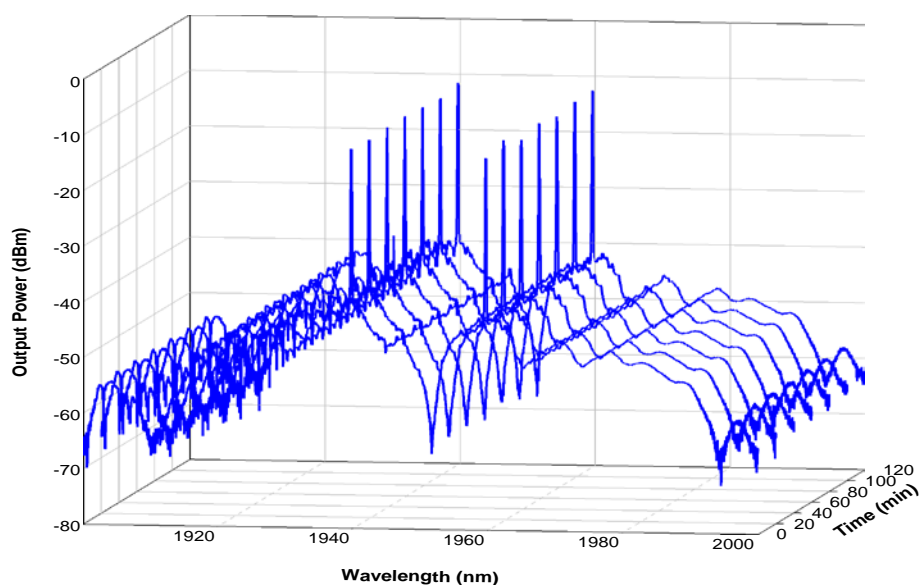
Figure 3.15: The stability graph of the proposed dual-wavelength laser with 20 minutes

period for each frame

3.5   Summary

Let us summarize the main results of this chapter. An all-fiber dual-wavelength fiber laser operating near 1900 nm is developed. It functions at the room temperature and uses a filter to suppress the mode competition in the cavity. The performance of the laser is compared for three different filters; a spatial filter, inline MMZI and MMI filter. The spatial filter is designed for controlling the phase mismatch at the splicing points of the TDF. The laser developed by us generates the dual-wavelength output lines at 1844.8 and 1852.0 nm, with the wavelength spacing amounts to 7.2 nm. The corresponding optical signal-to-noise ratios are 30 and 21 dB, respectively. The device starts to lase at both of the lines above the threshold pump power of 109.3 mW. When the pump power reaches the maximum value of 131.7 mW as observed in our experiments, the output powers of the laser lines correspond to 1844.8 and 1852.0 nm and are equal to 0.297 and 0.038 mW, respectively.

All-fiber dual-wavelength fiber laser operating in 1955 nm region is then demonstrated using an MMZI filter in conjunction with a cascaded gain medium, which consists of 2 m long TDF and 15 m long laboratory made double-clad TYDF. The inline MMZI filter is fabricated using a flame brushing technique to realize comb filter with a spacing of 3.7 nm based on modal interference. The proposed laser generates dual-wavelength output lines at 1952.93 and 1956.68 nm with the optical signal to noise ratio of more than 35 dB. Both lines start to laser at threshold pump powers of 110 mW and 1.6 W for 800 nm and 905 nm pumps, respectively and the output laser power increases with the pump power.

Finally, all-fiber dual-wavelength is demonstrated using a MMI filter in conjunction with the cascaded gain medium. The MMI filter is designed by splicing a

13.5 cm long MMF inside a ring cavity so that two transmission peaks at 1939.68 and 1959.60 nm with the maximum extinction ratio can be realized based on modal interference. The proposed laser generates dual-wavelength output lines at 1939.68 and 1959.60 nm with the corresponding optical signal to noise ratio of 27 dB and 28 dB, respectively. Both lines start to laser at threshold pump powers of 143 mW and 1.5 W for 800 nm and 905 nm pumps, respectively and the output laser power increases with the pump power. The laser was stable for more than two hours and the dual wavelength operation could be tuned by adjusting the parameters of the MMI filter.

CHAPTER 4

Pulsed Fiber Lasers Operating at 2 Micron Region

4.1   Introduction

Pulsed fiber lasers operating in the "eye-safe" wavelength region ($\lambda > 1.4$ μm) are promising for various applications such as metrology, remote sensing, free-space communication, time-resolved molecular spectroscopy, and mid-IR super-continuum generation. In the past several years, many studies on passively mode-locked or Q-switched Thulium-doped pulse fiber lasers have been reported based on either active or passive methods (El-Sherif & King, 2003; Jiang et al., 2013; Wang et al., 2011). These lasers have been demonstrated based on various host media such as Silica, Tellurite, Germanate and Fluoride fibers (El-Sherif & King, 2003; Jiang et al., 2013; Wang et al., 2011). For instance, Fang et. al. reported an actively Q-switched 2 μm fiber laser based on Thulium-doped Germanate fiber laser that produced 15 ns pulses with peak power greater than 33 kW (Fang et al., 2012). In another work, Q-switched pulse laser based on 2.1 μm $Tm^{3+}/Ho^{3+}/Yb^{3+}$-triply-doped tellurite fiber was demonstrated using a mechanical chopper operating at 19.4 kHz with an average power of 26 mW, pulse energy of 0.65 μJ and pulse width in the range 100-160 ns (Richards et al., 2008). Wang et al. reported an SESAM-based mode-locked fiber laser operating in the anomalous dispersion regime at 1980 nm with pulse duration of 1.5 ps and energy of 0.76 nJ (Wang et al., 2009). Among the host materials used, silica is preferable because of its compatibility with standard optical components.

Compared with the active ones, passively mode-locked or Q-switched fiber lasers feature flexibility of configuration and do not require additional switching electronics. These lasers have been successfully demonstrated using different kinds of saturable absorbers (SAs), such as semiconductor saturable absorber mirrors (SESAMs)

(Kivistö et al., 2008), carbon nanotubes (CNTs) (Ahmad et al., 2014; Kieu & Wise, 2009) and graphene (Sotor et al., 2012). However, SESAMs are still expensive and complex to be fabricated and consequently only one or two companies can supply 2 µm SESAMs.

In this chapter, various Q-switched and mode-locked fiber lasers operating in 2 micron region are demonstrated using either commercial Thulium-doped fiber (TDF) or a newly developed Thulium-Ytterbium co-doped fiber (TYDF) as the gain medium. The performance of these lasers is investigated for both artificial and passive saturable absorbers. In this work. Multi-walled carbon nanotubes (MWCNT) film and graphene oxide paper are used as a passive saturable absorber.

4.2   Q-switched fiber laser operating in 2 micron region based on nonlinear Polarization rotation approach.

There are growing interests in compact 2 micron Q-switched laser sources mainly driven by applications in spectroscopy, sensing, medicine and nonlinear optical research (Baudelet et al., 2010; Lu et al., 2013; Theisen-Kunde et al., 2007; Wang et al., 2012).Unlike active Q-switching (El-Sherif & King, 2003) passive Q-switching is a more convenient and cost-effective way to achieve high energy pulses because it does not require additional switching electronics (Anyi et al., 2013; Harun et al., 2012). Compared with lasers based on bulk gain media, a fiber format offers distinct advantages including small footprint, robust beam confinement and environmental stability . Thulium (Tm)-doped silica fiber (TDF) is a promising two-micron gain material. It exhibits high quantum efficiency as well as a broad gain spectrum extending from 1.8 to 2.1 µm. Passive Q-switching of Tm fiber lasers has so far been realized by a number of techniques including multiple quantum wells (Kivistö et al., 2008), Cr:ZnS or Cr:ZnSe crystals (Qamar & King, 2005; Tang et al., 2008). However, all of these implementations require the use of additional bulk components such as mirrors or lens

pairs, thus compromising the key benefits of fiber lasers, in their compactness and alignment-free operation .

Nonlinear polarisation rotation (NPR) effect in a fiber laser cavity is also widely used to initiate and shape the pulses especially in mode-locked fiber laser. In fact, the NPR technique can produce the intensity-dependent transmission by self-phase modulation mechanism to provide an artificial SA effect in a fiber ring laser (Hamzah et al., 2013). The saturable absorption strength can be adjusted by simply rotating the polarization controller. In this section, we reported for the first time a passively Q-switched all fiber ring laser operating at near 2 micron region based on NPR technique.

4.2.1   Configuration of the Q-switched laser

The schematic of the proposed Q-switched 2 micron fiber laser is shown in Figure 4.1. It was constructed using a simple ring cavity, in which a 2 m long commercial TDF and a 15 m long laboratory made Thulium Ytterbium co-doped fiber (TYDF) was used as the active medium. The TDF is pumped by 800 nm laser diode via an 800/2000 nm wavelength division multiplexer (WDM) while the TYDF is pumped by 905 nm multimode laser diode via a multimode combiner (MMC). The TDF has a core and cladding diameters of 9 µm and 125 µm respectively, a loss of less than 0.2 dB/km at 1900 nm and Tm ion absorption of 27 dB/m at 793 nm. The laboratory made TYDF has an octagonal shaped double-clad structure, which was drawn from a lithium-alumino-germano-silicate (LAGS) core glass optical preform, which was fabricated via the MCVD process, followed by solution doping technique. The preform consists of an Al_2O_3, Y_2O_3, Tm_2O_3 and Yb_2O_3 dopants with average weight percentage of 5.5, 3.30, 0.70 and 4.0, respectively. Such octagonal geometry of the cladding improves the pump absorption efficiency. The doping levels of Tm^{3+} and Yb^{3+} ions of the fabricated TYDF are measured to be around 4.85 x 1019 ions/cc and 27.3 x 1019 ions/cc,

respectively using an electron probe micro-analyser (EPMA). The NA and core diameter of the fabricated TYDF are measured to be 0.23, and 5.96 µm, respectively.

Both gain media are cascaded to produce amplified spontaneous emission at 1950 nm region. The pigtails of the optical components were spliced by using a commercially available fusion splicer. A PC is employed in the laser cavity to adjust the polarization state of the circulating light. The laser output is taken by a 10% port of the output coupler. An optical spectrum analyser and an oscilloscope behind the output coupler are used to study the pulse spectrum and the output pulse train, respectively. The output power is also measured by an optical power meter. In order to avoid the passive mode-locking in our fiber laser, it is worth noting that we intentionally employ a cascaded gain medium while imposing large splicing loss in the laser cavity.
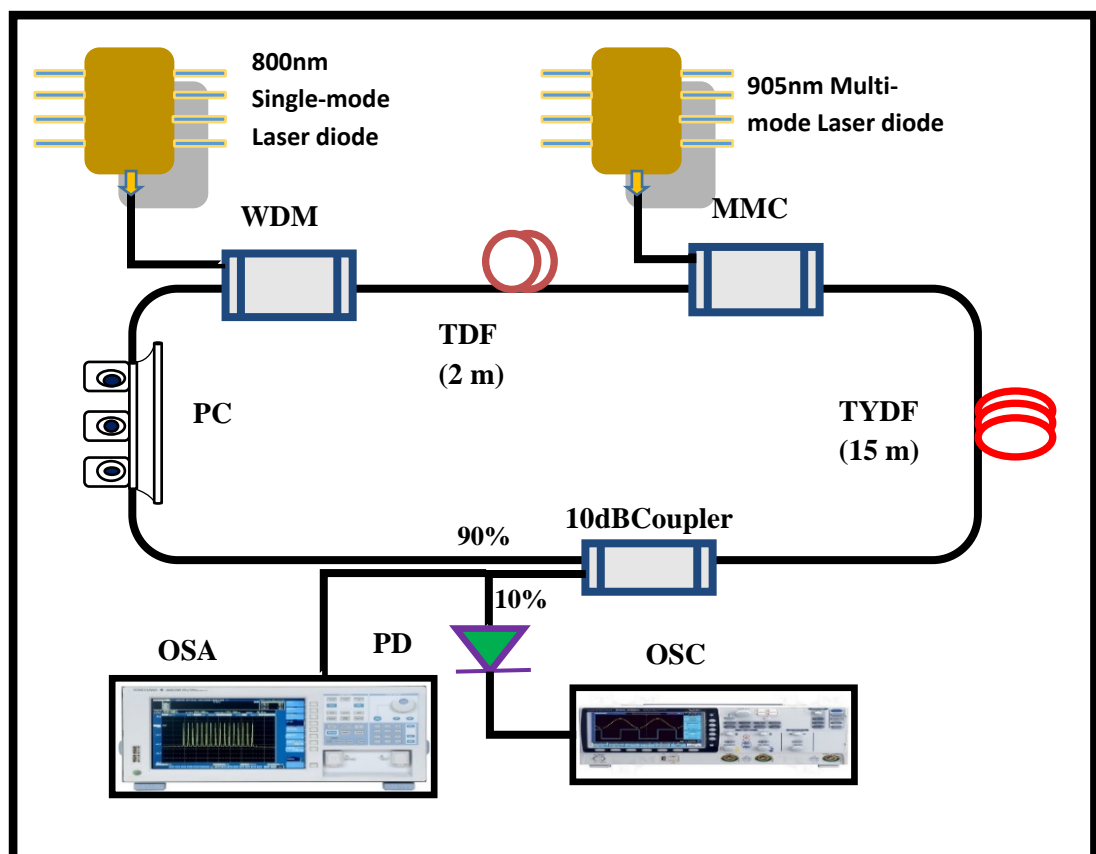
Figure 4.1: Configuration of the proposed NPR based Q-switched fiber laser operating at 1950 nm region

4.2.2   Performance of the Q-switched laser

The NPR technique is used for achieving the passively Q-switched operation in our fiber laser. Adjusting the PC, due to the NPR the MMC becomes an artificial saturable absorber with the intensity-dependent transmission such that the intensive wave can transmit the MMC and the weak wave is reflected. In the experiment, the 800 nm pump power is always fixed at 110.4 mW. When the 905 nm multimode pump power was increased to about 2 W, the Q-switched pulses were always observed by properly rotating the PC. A stable Q-switched operation commences from the modulation of population inversion induced by the phase modulation of laser cavity, which consists of a PC, MMC and highly birefringence gain media.A Q-switched pulse is initiated when the PC is regulated so that the cavity loss is high. In this condition, the lasing radiation is weak whereby it encountered very small nonlinear effects. This weak radiation could not pass through the MMC and is blocked from circulating in the cavity. Concurrently, inversion population will take place as the pumping continues and the gain of the cavity builds up. After a certain time duration, optical amplification due to stimulated emission begins. At this time, the radiation becomes strong enough to pass through the polarizer where the loss of the cavity decreases abruptly and the population inversion depletes quickly. Hence, the Q-switched pulse is formed. The Q-switching operation is maintained when the pump power is further increased up to 2.5 W. However, the pulse train disappears as the multimode pump power is increased above 2.5 W.

Figure 4.2 shows the optical spectrum of the Q-switched laser at 905 nm pump power of 2.3 W. It operates at 1949.0 nm with a signal to noise ratio of more than 36 dB. Correspondingly, the typical Q-switched pulse train is presented in Figure 4.3. The repetition rate is 13.49 kHz. The pulse duration, which was measured directly from an oscillograph, is about 3.089 µs. In order to further investigate the characteristics of the

output Q-switched pulses, we fixed the orientation of the PC and only changed the 905 nm pump power from 2.0 to 2.5 W while maintaining the 800 nm pump power at 110.4 mW. Figure 4.4 presents the pulse repetition rate of the Q-switched operation and the pulse width as a function of the pump power. Like typical Q-switched fiber lasers, the pulse repetition rate increases from 6.36 to 16.45 kHz with increasing pump power from 2.0 to 2.5 W. On the other hand, the pulse width decreases from 7.82 to 2.93 µs as the 905 nm pump power is increased within the same range. This effect is due to gain compression in the Q-switched fiber laser (Herda et al., 2008).
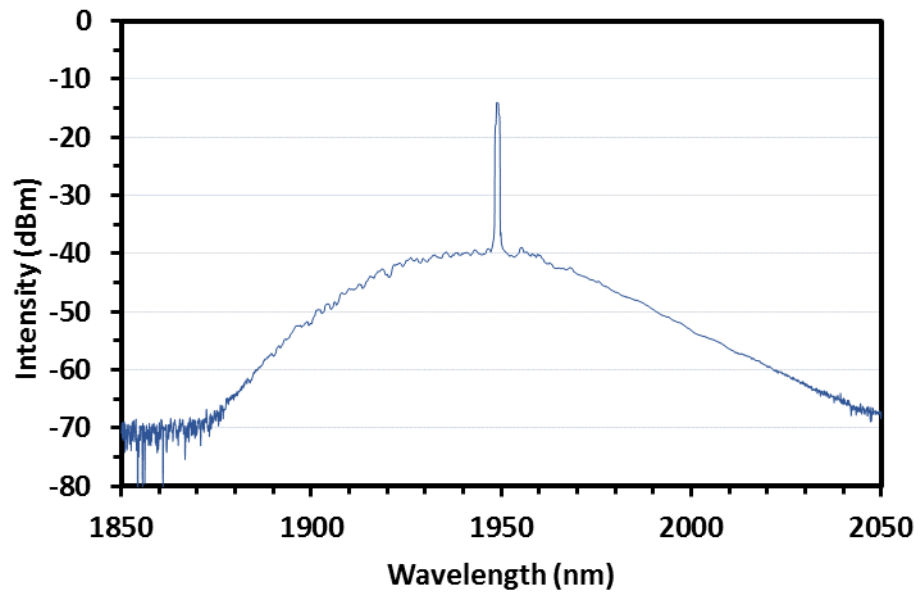
Figure 4.2: Output spectrum of the proposed NPR-based Q-switched fiber laser.
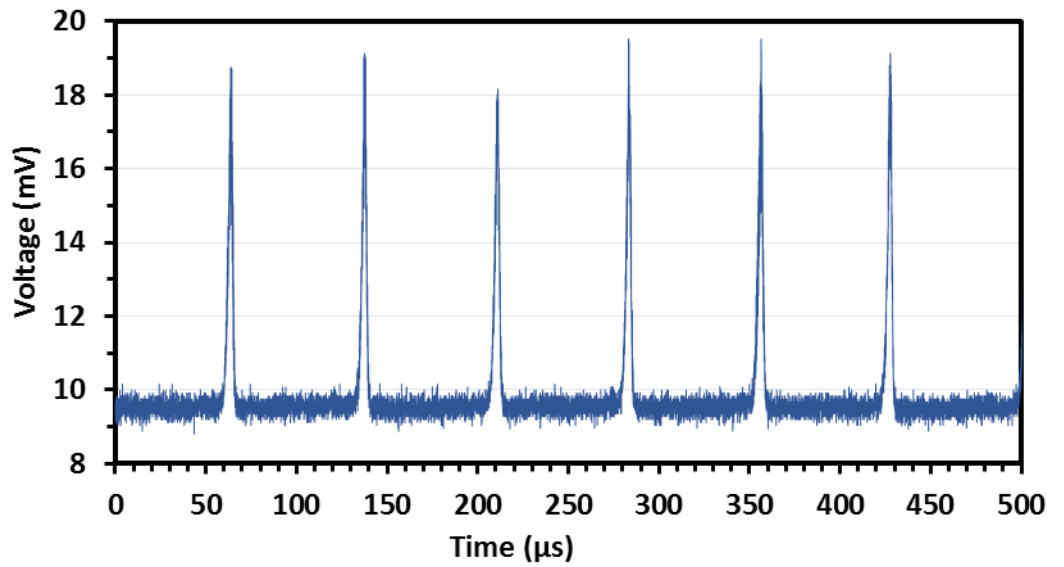
Figure 4.3: Typical pulse train of the proposed NPR-based Q-switched fiber laser at 800

nm and 905 nm pump powers of 110.4 mW and 2.3 W, respectively.
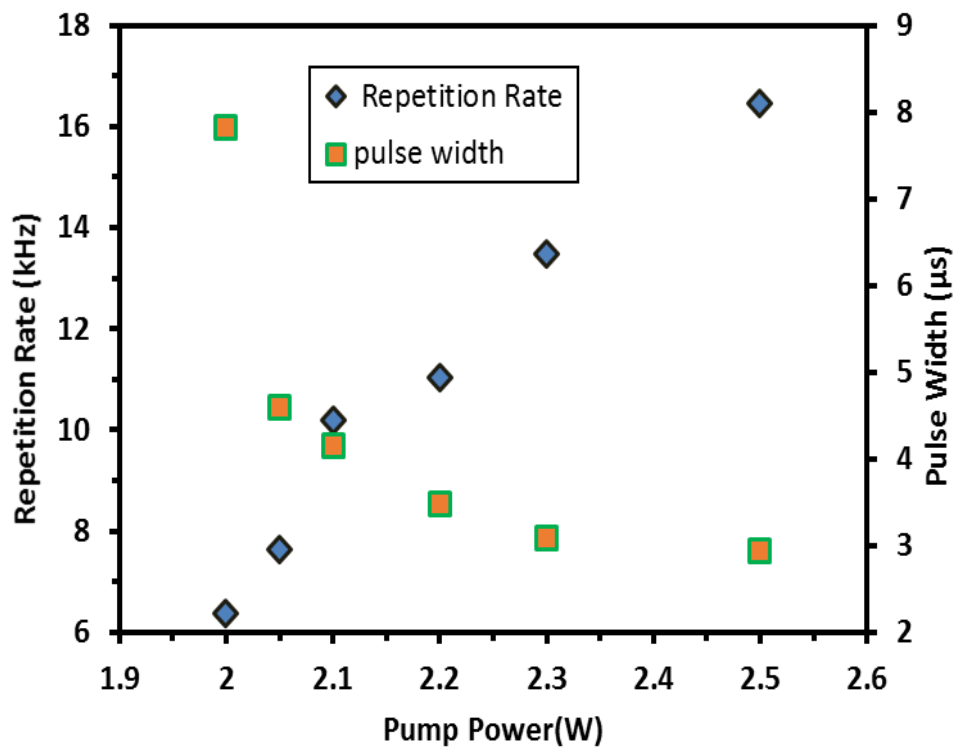
Figure 4.4: Repetition rate and pulse width of Q-switched pulses versus pump power.

Figure 4.5 shows the relation between average output power and pulse energy of the Q-switched laser and 905 nm pump power. In the experiment, the 800 nm pump power is fixed at 110.4 mW. Both output power and pulse energy increase almost linearly with the pump power. The maximum pulse energy of 11 nJ is obtained at 800 nm single mode and 905 nm multimode pump powers of 110.4 mW and 2.5 W, respectively. We believe that a further optimization of the cavity parameters should significantly enhance the Q-switching performance.
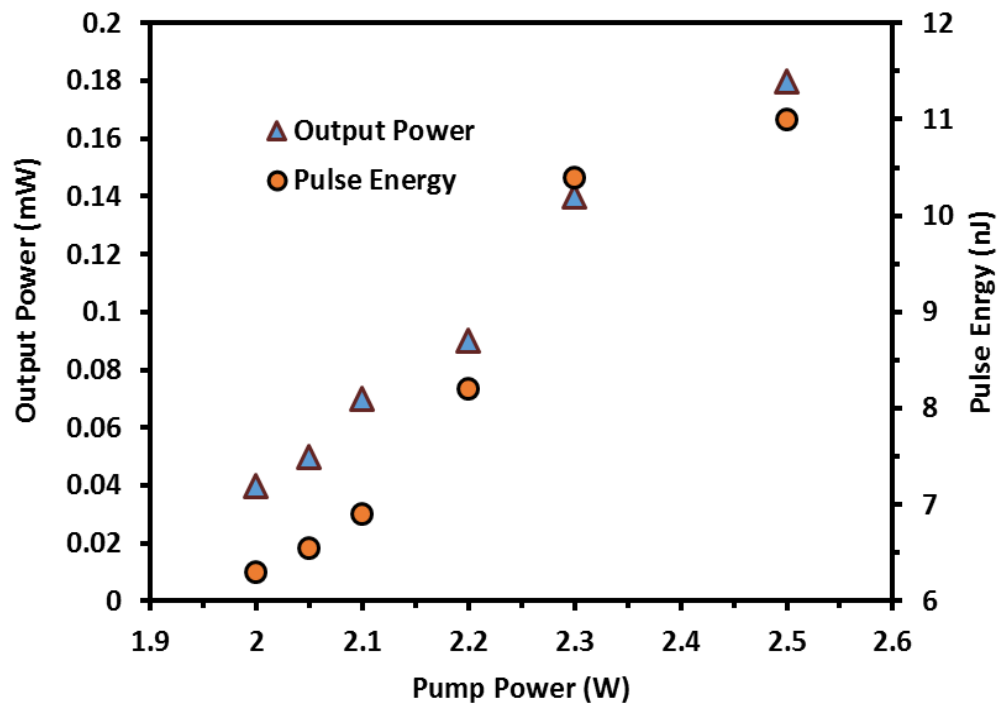
Figure 4.5: Average output power and pulse energy variation as a function of pump power

4.3 Mode-locked fiber laser operating in 2 micron region based on nonlinear Polarization rotation approach.

Mode-locking techniques can also be used for generating ultra short pulse fiber lasers which may extend the applications of the 2 micron fiber lasers. A number of passively mode-locked TDF lasers have been reported (Sharp et al., 1996). They can be roughly divided

independently of the operation wavelength into two major categories depending on the mode-locking mechanism. The first group can be defined as material saturable absorber (SA) based laser, in which the real absorbing media, e.g., semiconductor saturable absorber mirror (SESAM), single-wall carbon nanotube saturable absorber (SWCNTSA) and graphene, are employed to initiate and shape the pulses. The second is referred to as nonlinear switching based laser, in which the transmission or reflectivity property is dependent on the nonlinear phase shift induced by nonlinear polarization rotation (NPR) effect in a laser cavity. The NPR technique exhibits the capability of pulse self-shaping that is equivalent to a real saturable absorber (SA).

Up to date, many NPR-based mode-locked fibers laser have been demonstrated operating in the 1.0 and 1.5 µm regions (Liu et al., 2008; Tu et al., 2007). However, there is still a lack of research work on 2 micron mode-locked fiber lasers. In this section, we demonstrated a 2.0-µm all-fiber mode-locked double-clad TYDF laser (TYDFL) using a NPR technique.

4.3.1 Configuration of the mode-locked laser

The experimental arrangement for the all-fiber mode-locked double-clad TYDFL based on NPR technique is shown in Figure 4.6. The ring oscillator consists of a MMC, a 15 m long TYDF, a 10 dB output coupler and a PC. The active fiber in the ring oscillator is a laboratory made double-clad TYDF with an octagonal shaped pump inner cladding with a core diameter of 5.96 µm and a NA of 0.23. The selected fiber length of 15 m provides > 90% pump absorption. A 905 nm multimode laser diode was used to pump the TYDF through a MMC. The pulses are coupled out of the oscillator using a 10 dB coupler, which allows 90% of the light to oscillate in the ring cavity. A PC was placed in between the MMC and the output coupler to induce the nonlinear phase shift through the NPR effect and initiate mode-locking in the cavity. The length of total cavity is about 24.4 m including 15 m TYDF, 9.4 m SMF-28 pigtail fiber from the pump combiner, PC and coupler. For the measurements of the laser output, an InGaAs photodetector (EOT ET-5000F, USA) with a response time of approximately

28 ps connected to a 500 GHz digital oscilloscope was used to measure the pulse train and pulse waveforms. The spectrum of pulse was measured by an OSA (Yokogawa AQ6375, Japan). The total cavity length is estimated to be around 24.4 m.
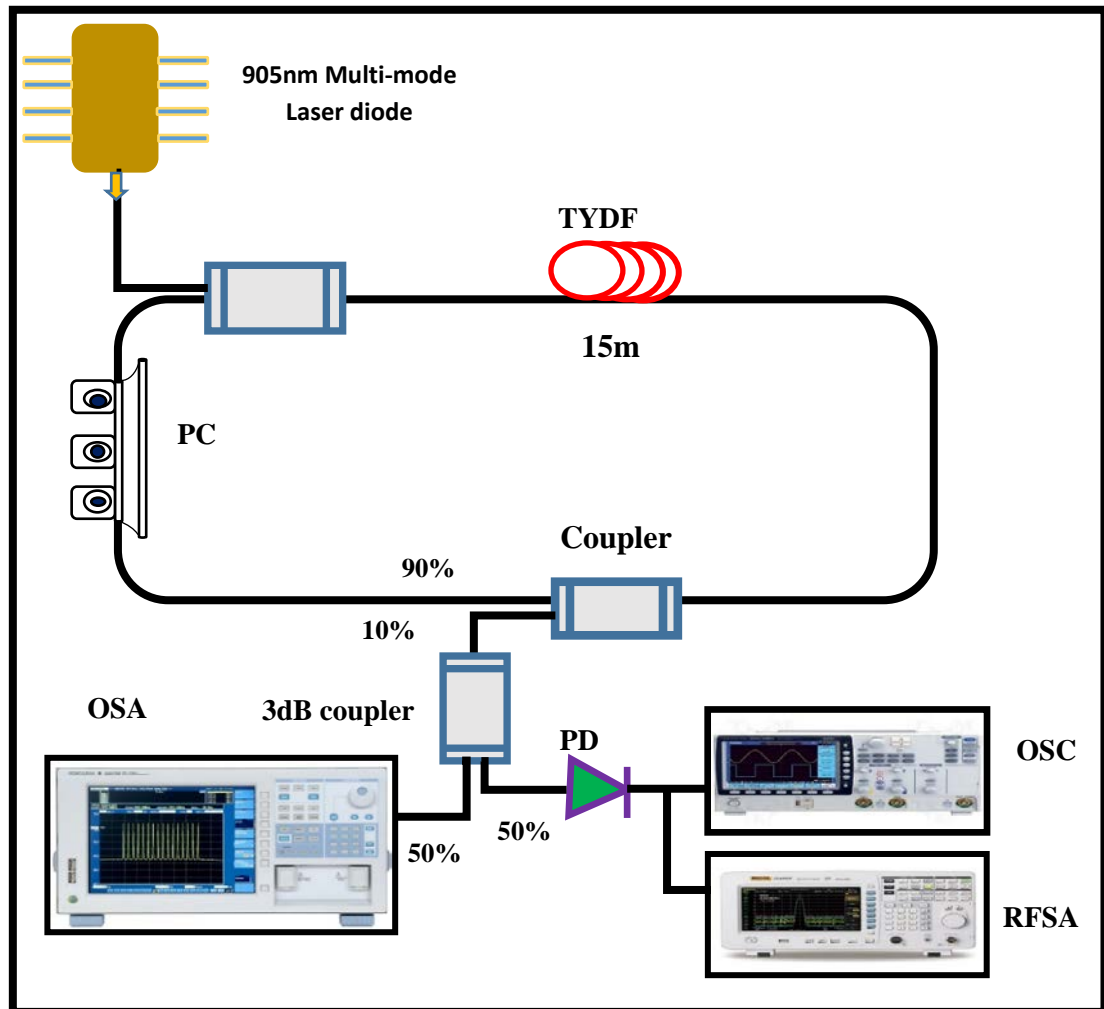
Figure 4.6: The experimental setup of the proposed all-fiber mode-locked double-clad TYDFL based on NPR technique

4.3.2 Performance of the mode-locked laser

The oscillator started to operate at continuous wave (CW) regime after reaching the launched pump power of 1.6 W. Operation in this regime occurred with a small pump power range. Stable self-starting mode-locked pulses were observed as shown in Figure 4.7 by carefully adjusting the PC when the launched pump power was increased to 2.7 W. As shown in the figure, the time interval is measured to be around 30.2 ns,

which corresponds to a repetition rate of 33.1 MHz. Multiple pulses are generated as identified in the pulse train, which is due to the energy quantization. The high repetition rate obtained is due to the multiple pulses circulating inside the cavity that generate harmonics mode-locked fiber laser. The major factors that create this phenomenon are inter-related with the peak-power limiting effect of the laser cavity besides the gain competition between the multiple pulses. Based on cavity length dependent theoretical value, the generated mode locked laser operates in the 4th harmonic mode. This proves that the mode-locked laser in double-clad TYDFL is able to operate without any isolator in the ring cavity. At 2.7 W pump power, the average output power was measured to be 1.55 mW and the pulse energy was calculated to be 46.9 nJ. It is worth mentioning that the performance of the proposed mode-locking laser was significantly sensitive to the PC orientation. Slight adjustment of the PC from their optimized position would lead to CW breakthrough because of the existence of CW path in the oscillator induced by the 10 dB coupler. Fortunately, the PC enabled polarization dependent loss of the coupler to close the CW path.
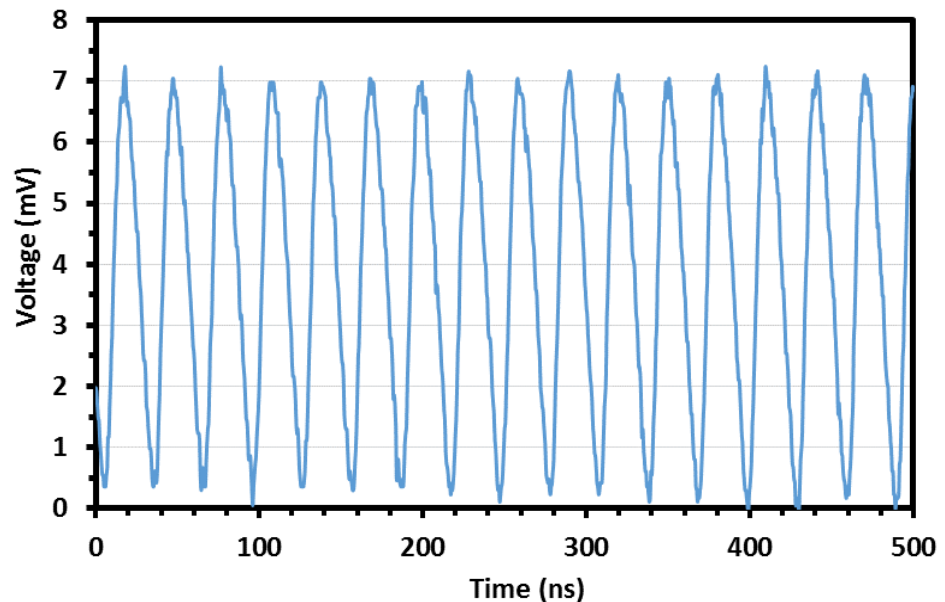
Figure 4.7: Oscilloscope trace of the laser output at pump power of 2.7 W showing a pulse train with a repetition rate of 33.1 MHz.

The optical spectrum of the passively mode-locked laser is shown in Figure 4.8. It operates at the center wavelength of 1953.5 nm without any observation of Kelly sidebands. A slight spectral broadening is also observed with full-width half maximum (FWHM)of around 0.4 nm, which is most probably due to self-phase modulation effect. We estimate the minimum attainable pulse width according to the 3 dB bandwidth of the output pulses, which is around 0.4 nm. Assuming that the output pulses possess a transform-limited, secant hyperbolic temporal shape, their temporal width must be ~10 ps at a wavelength of 1953.5 nm. If the pulses have a frequency chirp, their temporal width must be larger than that of the transform limited pulses. The radio frequency (RF) spectrum measured with 30 MHz frequency span is depicted in Figure 4.9. The repetition rate of the laser is 33.1 MHz, which corresponds to the fourth order harmonic pulse with an approximately 22.4 m long cavity. A signal-to-noise ratio of about 12 dB is observed, highlighting the moderate-amplitude fluctuation of the laser.
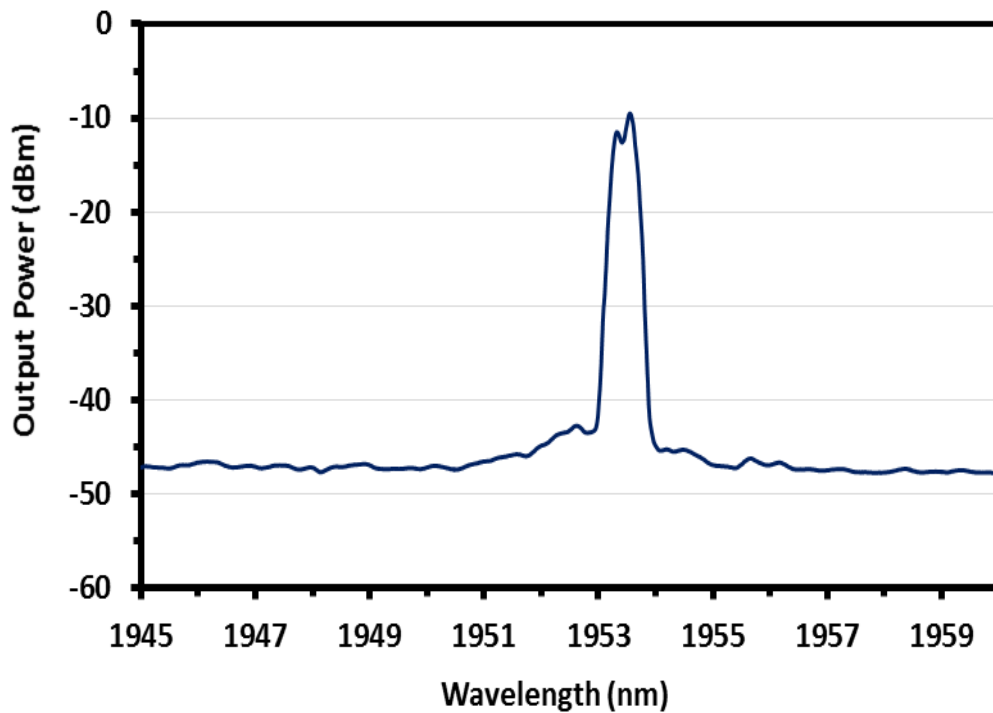
Figure 4.8: Output spectrum of the proposed mode locked TYDFL at pump power of 2.7W.
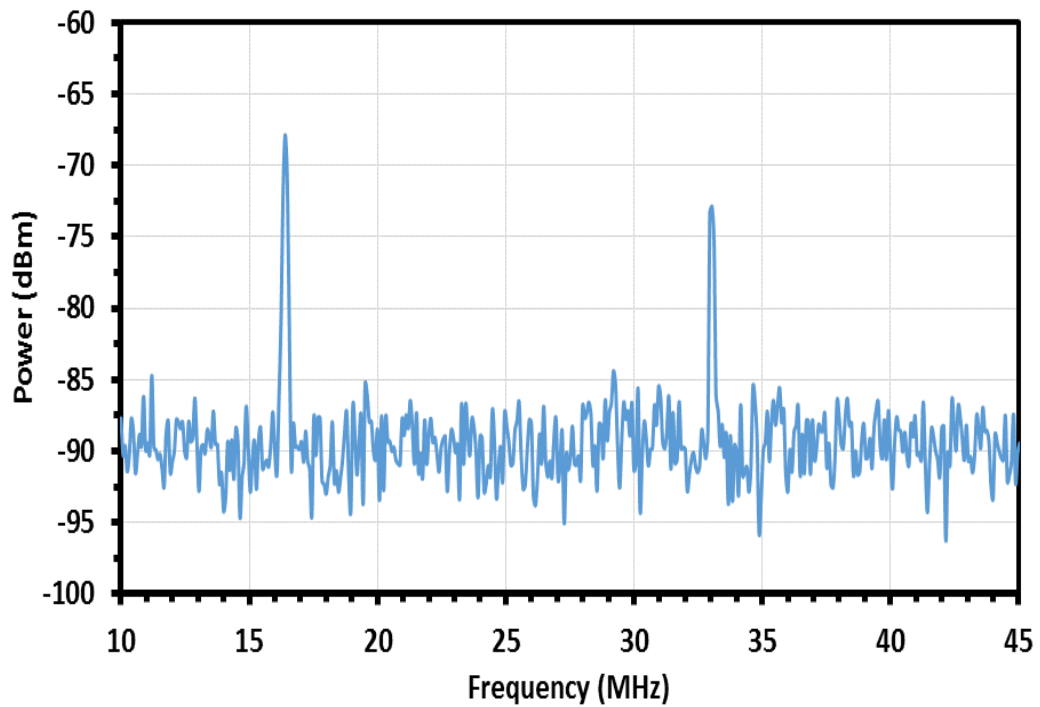
Figure 4.9: RF spectrum of the mode-locking pulse from the TYDFL

4.4 Multi-walled carbon nanotubes based Q-switched 2 micron fiber lasers

Recently, a new member of carbon nanotubes (CNT) family, multi-walled carbon nanotubes (MWCNTs) (Iijima, 1991; Su et al., 2012), have also attracted many attentions because they possesses many advantages in nonlinear optics. The growth of the MWCNT material does not need complicated techniques or special growing conditions so that its production yield is high for each growth. Therefore the production cost of MWCNT material is about 50% - 20% of that of single-walled CNT material (Zhang et al., 2011). Additionally, MWCNT material has good thermal characteristics, which is of great importance for high power ultrafast laser development. The Young modulus of MWCNT is around 1000 GPa (Schadler et al., 1998),and the thermal conductivity of MWCNT, 3000 Wm K, is very high (Kim et al., 2001). Compared with

SWCNTs, the MWCNTs have higher mechanical strength, better thermal stability as well as can absorb more photons per nanotube due to its higher mass density of the multi-walls. These favorable features are due to the structure of MWCNTs which takes the form of a stack of concentrically rolled graphene sheets. The outer walls can protect the inner walls from damage or oxidation so that the thermal or laser damage threshold of MWCNT is higher than that of the single-walled CNTs (Banhart, 1999; Ramadurai et al., 2008).

To date, there are only a few reported works on application of MWCNTs material as a saturable absorber (SA). For instance, Lin et. al. Employs multi-walled MWCNTs based SA for mode locking of a Nd:YVO$_4$ laser (Lin et al., 2013). In another work, Q-switched Nd-YAG laser is demonstrated using the MWCNTs based saturable absorber as a Q-switcher. In this section, Q-switched Thulium-doped fiber laser (TDFL) is demonstrated using a new developed MWCNTs-based SA. To the best of our knowledge, this is the first demonstration using MWCNTs as the Q-switcher in the all-fiber laser. The SA is constructed by sandwiching a multi-walled CNT- polyvinyl alcohol (MWCNT-PVA) film between two fiber connectors. The proposed Q-switched TDFL operating at 1846.4 nm region has potential applications in optical communication, fiber sensor, laser processing, laser marking, etc.

4.4.1 Preparation and Raman characterisation of the saturable absorber

The SA was fabricated using MWCNTs powder with a diameter 10-20 nm and the length distribution of 1-2 µm as a raw material. The MWCNTs was functionalized with sodium dodecyl sulphate (SDS) so that it can be dissolved in water. 4 g of SDS was mixed with 400 ml of deionized water before 250 mg MWCNT was added to the solution. The mixture was sonicated for 60 minutes at 50 W to obtain a homogeneous dispersion of MWCNTs that was then centrifuged at 1000 rpm to remove large particles of undispersed MWCNTs. This

dispersed suspension is expected to be stable for a few weeks. The dispersed MWCNTs suspension was mixed with a PVA solution at three to two ratio to obtain MWCNTs-PVA composite. In our experiment, the PVA solution was prepared by dissolving 1 g of PVA (Mw = 89×103 g/mol) in 120 ml of deionized water. The composite was sonificated for more than one hour to realize a homogeneous MWCNTs-PVA precursor before it was casted onto a glass petri dish and left to dry at room temperature for about one week to produce a film. The film has a thickness of around 50 μm. The SA was fabricated by sandwiching a small cutting of the film between two FC/PC fiber connectors. Index-matching gel was applied onto the fiber ends of the connectors before matching to reduce insertion loss. The insertion loss of the SA was approximately 3.3 dB at 1900 nm.

Raman spectroscopy was performed on the MWCNT-PVA film using laser excitation at 532 nm to confirm the presence of MWCNT. Figure 4.10 shows the Raman spectrum, which indicates the distinct feature of the MWCNT. It is shown that the Raman spectrum bears much similarity to graphene, which is not too surprising as it is simply a rolled up sheet of graphene. MWCNT has many layers of graphene wrapped around the core tube. We can see well defined G (1580 cm^{-1}) and G' (2705 cm^{-1}) bands in the figure as there were in graphene and graphite. The G band originates from in-plane tangential stretching of the carbon-carbon bonds in graphene sheet. We also see a prominent band around 1350 cm^{-1}, which is known as the D band. The D band originates from a hybridized vibrational mode associated with graphene edges and it indicates the presence of some disorder to the graphene structure. This band is often referred to as the disorder band or the defect band and its intensity relative to that of the G band is often used as a measure of the quality with nanotubes. There is another series of bands appearing at the low frequency end of the spectrum known as Radial Breathing Mode or RBM bands. The RBM bands correspond to the expansion and contraction of the tubes. The RBM modes are not clearly present in the MWCNT because the outer

tubes restrict the breathing mode. As expected, the prominent D band is observed in Fig. 4.10, which indicates that the carbon nanotubes are a multi-walled type, which has multi-layer configuration and disorder structure. The D' band which is a weak shoulder of the G-band is also observed at 1613 cm^{-1} due to double resonance feature induced by disorder and defect. In addition, others distinguishable features like G + B band (2920 cm^{-1}), a small peak at 854 cm^{-1} and Si were also observed as depicted in Figure 4.10. The nonlinear characteristic of the MWCNT was also investigated where the modulation depth was measured at around 4.7%.
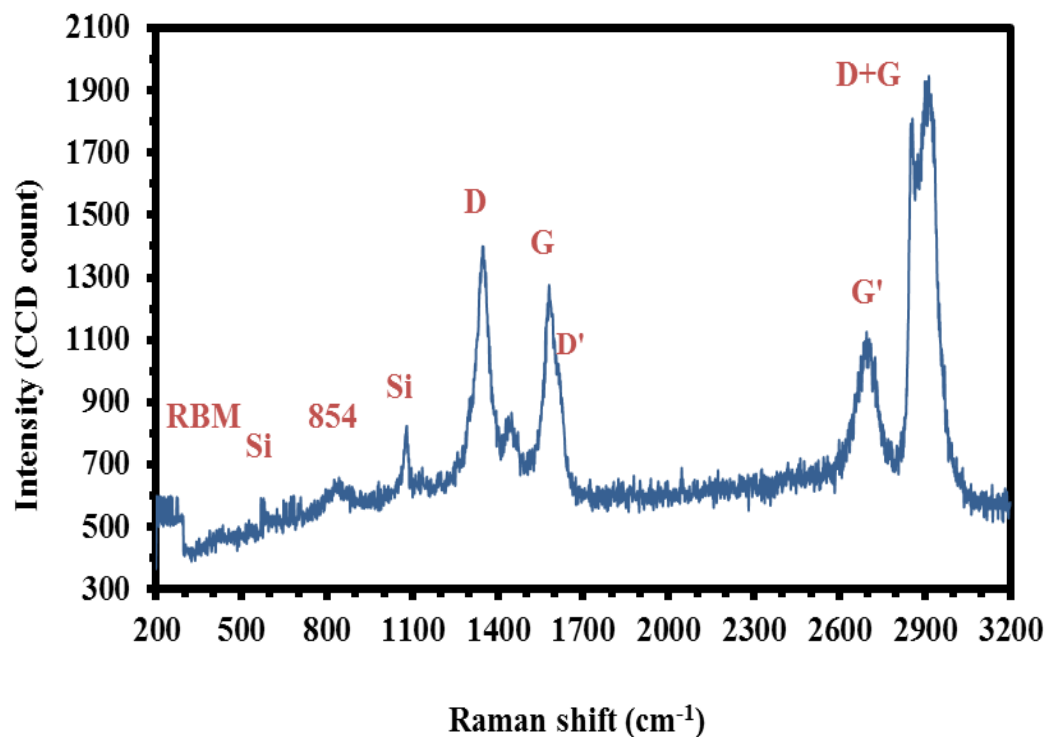
Figure 4.10: Raman spectrum obtained from the MWCNT-PVA film

4.4.2 Configuration of the MWCNTs based Q-switched TDFL

The configuration of the proposed Q-switched TDFL is shown in Figure 4.11. The resonator consists of a 2 m long commercial TDF, which is forward pumped by a 800 nm laser diode via a 800/2000 nm WDM, a MWCNT-PVA film based SA, and 10 dB output coupler. The TDF has a core and cladding diameters of 9 µm and 125 µm respectively, a loss of less than 0.2 dB/km at 1900 nm and Tm ion absorptions of 27 dB/m and 21 dB/m, at 800 nm and 1210 nm, respectively. The high absorption allows the use of short active gain medium. The output of the laser is tapped from the cavity through a 10 % port of the 10 dB coupler. The optical spectrum analyser (OSA, Yokogawa, AQ6370B) is used for the spectral analysis of the Q-switched TDFL with a spectral resolution of 0.02 nm whereas the oscilloscope (OSC, Tektronix,TDS 3052C) is used to observe the output pulse train of the Q-switched operation via a 460 kHz bandwidth photo-detector (Thor lab, PDA50B-EC). The total cavity length of the ring resonator is measured to be around 5 m. Figure 4.12 shows the output spectrum of the laser at pump power of 121.1 mW. It operates at 1846.4 nm with side-mode suppresion ratio of more than 10 dB.
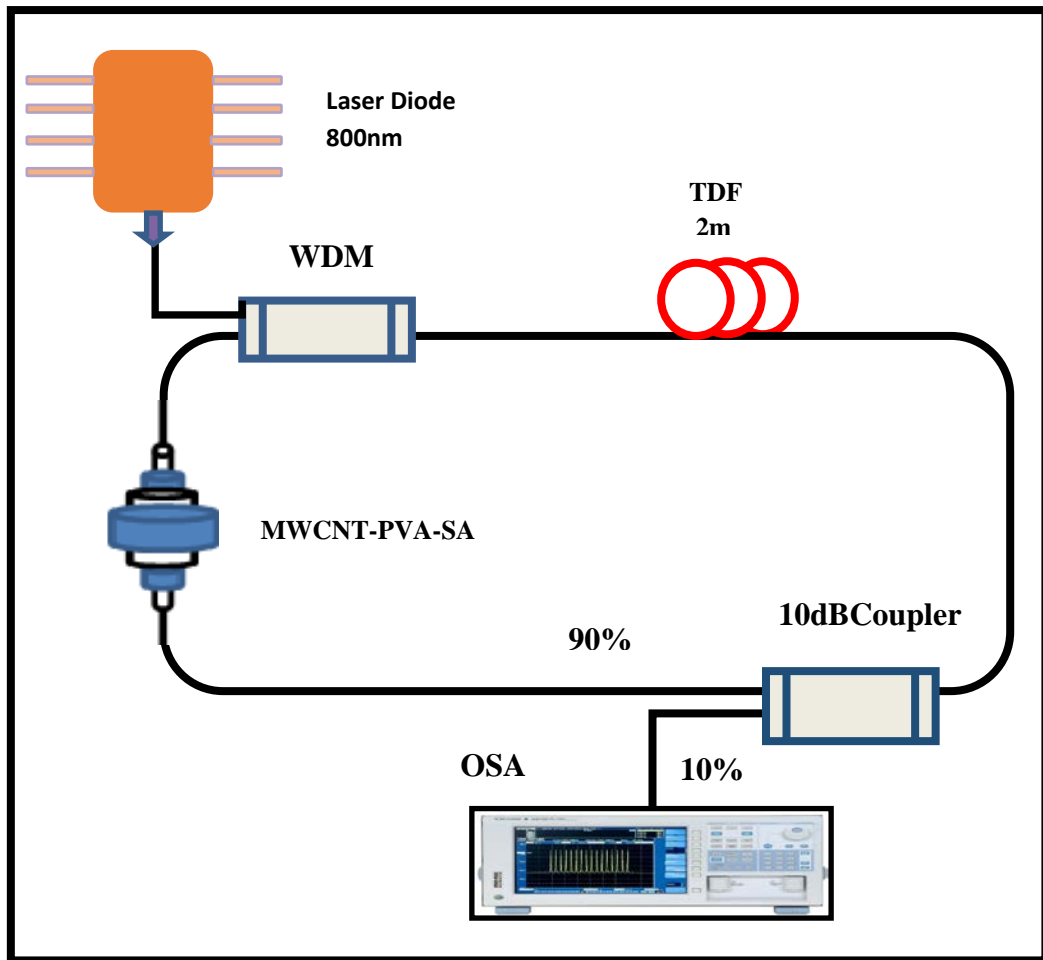
Figure 4.11: Configuration of the Q-switched TDFL.
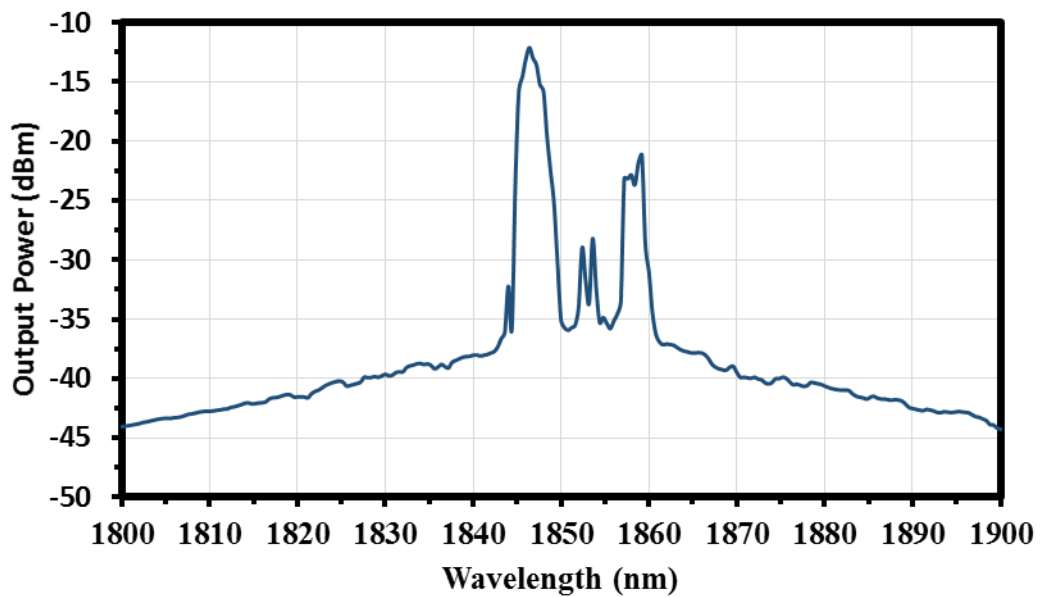
Figure 4.12: The output spectrum of the Q-switched TDFL operating at 1846.4 nm.

4.4.3   Performance of the Q-switched TDFL

Initially, the continuous wave (CW) TDFL was investigated without putting the MWCNT-PVA SA and the laser threshold was found to be at the pump power of 89.7 mW. It should be noted that no Q-switched operation occurs without the MWCNT-SA connected in the laser cavity. It is clear that the Q-switched operation is mainly induced by the SA. However, a stable and self-starting Q-switched operation was only observed at the pump power of 121.1 mW. Figure 4.13 shows the oscilloscope traces of the Q-switched pulse train, which shows no distinct amplitude modulation in each Q-switched envelop spectrum. This indicates that the self-mode locking effect on the Q-switching is weak for the proposed laser. At 121.1 mW pump power, a stable passively Q-switching operation is obtained with an average output power of 0.12 mW and a repetition rate of 10.38 kHz. The pulse energy is calculated to be around 11.34 nJ. The pulse energy could be improved by reducing the insertion loss of the graphene saturable absorber and optimizing the laser cavity. Figure 4.14 shows the typical oscilloscope trace of the pulse envelop at the pump power of 121.1 mW. As seen in the figure, the full-width at half maximum or pulse width is approximately 17.52 μs, which corresponds to peak power of 0.62 mW. Further reduction in pulse width is expected by shortening the cavity length using a higher dopant fiber.
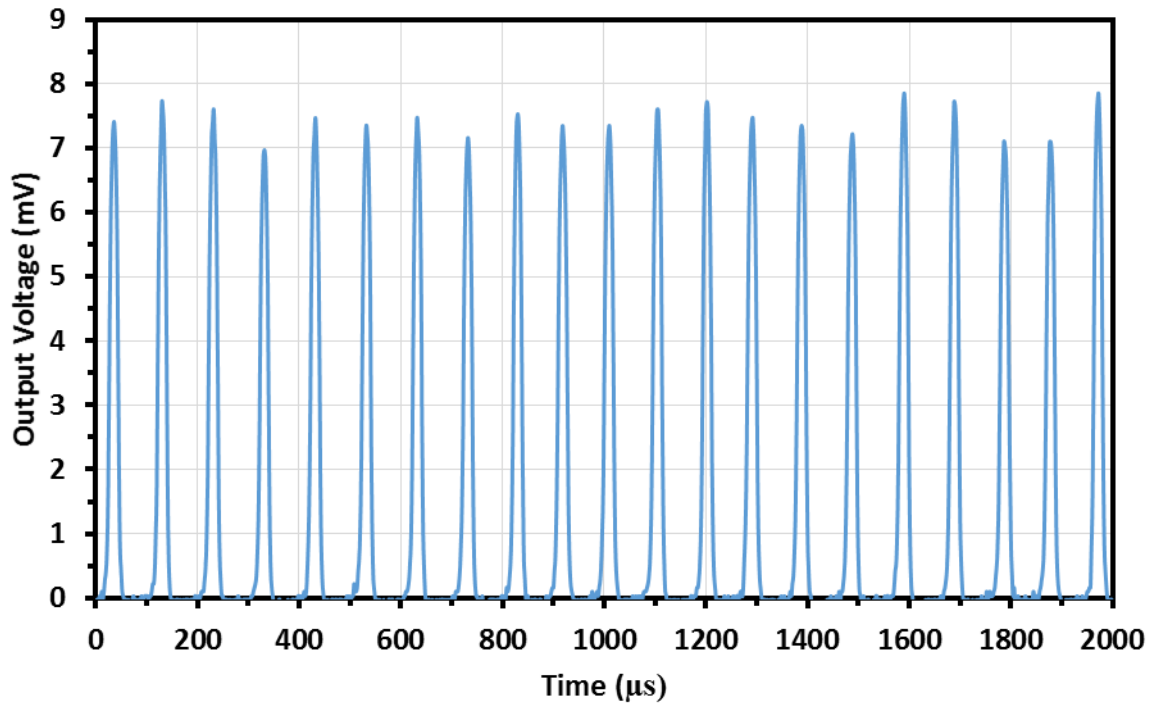
Figure 4.13: The pulse train for the proposed TDFL with MWCNT-PVA SA at 121.1

mW pump power with the repetition rate of 10.38 kHz.
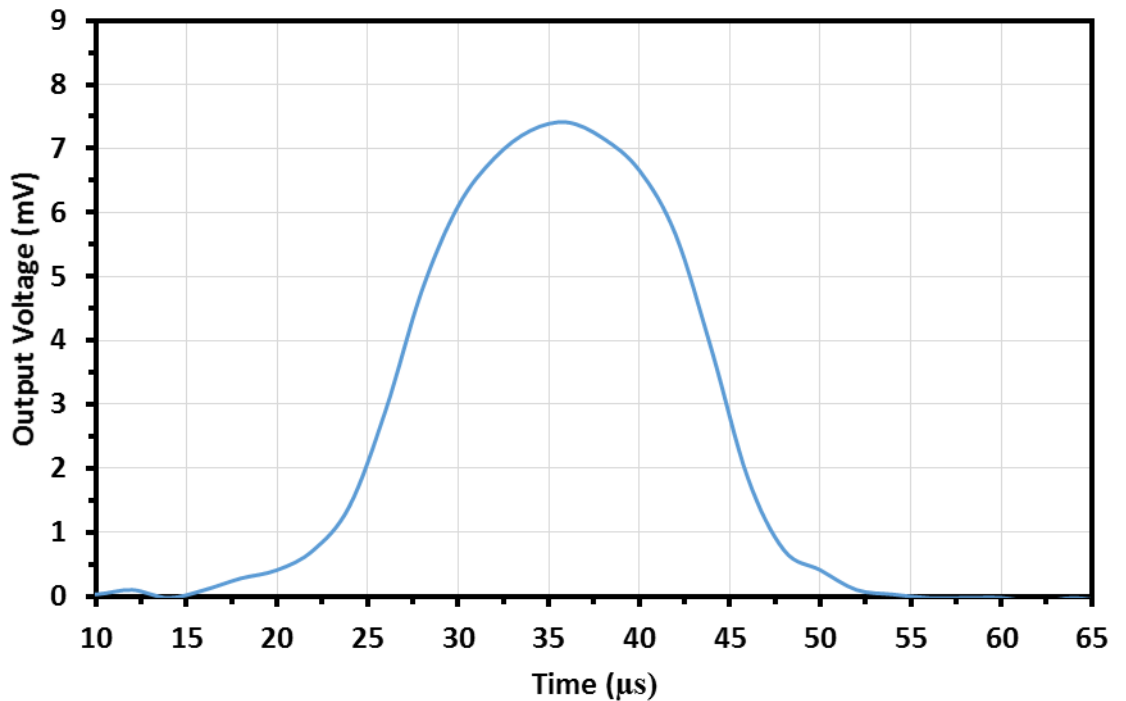
Figure 4.14: Pulse spectrum envelop at pump power of 121.1 mW with pulse width of

17.52 μs.

These results indicate that MWCNTs has a big potential for superior Q-switching and saturable absorption in 1900 nm region compared to conventional light absorbing components when carefully employed in an appropriate laser system. The fabrication of the SA is also simple and thus the cost of the laser should be low. Further refinement of the fabrication process is required to obtain mode locking operation in both regions. The simple and low cost laser is suitable for applications in metrology, environmental sensing and biomedical diagnostics.

4.5   Mode-locked 2 micron fiber laser with MWCNTs-PVA SA

In section 4.3, mode locked Thulium Ytterbium co-doped fiber laser (TYDFL) operating at 1953.5 nm was achieved using nonlinear polarization rotation (NPR) technique and Thulium Ytterbium co-doped fiber as the gain media. . Although the NPR technqiue is well established in 1.5 μm region, NPR induced lasers tend to be environmentally unstable. In this section, a mode-locked 2 μm fiber laser is demonstrated using a simpler and low cost MWCNTs-PVA based SA. In this work, a commercial Thulium-doped fiber and homemade double-clad TYDF are used as the gain media.

4.5.1   Experimental arrangement and Raman spectrum

Figure 4.15 shows the experimental setup of the proposed mode-locked 2 micron fiber laser using the fabricated MWCNTs-PVA film as a SA. A 2 m long TDF is employed as a gain medium pumped by a 800 nm laser diode via an 800/2000 nm WDM and 15 m long homemade TYDF, which is pumped by 905 nm multimode laser diode via a MMC as gain media. The TDF and TYDF have same specifications with the previous sections. The output laser is tapped via a 10 dB coupler which keeps 90% of the light oscillating in the ring cavity. The cavity length is measured to be approximately 23.5 m. A PC is utilized to tune the polarization state of light in the laser cavity. The OSA with a spectral resolution of 0.05 nm is used for the spectral analysis of the mode-locked laser and an oscilloscope is used to analyze the

output pulse train of the mode-locking operation via a photo-detector. The SA was fabricated using the same MWCNTs raw material with the similar process as described in section 4.4. The only difference is on the mixing ratio of MWCNTs with PVA. In this work, the dispersed MWCNTs suspension was mixed with a PVA solution at one to four ratio to reduce the film's loss for mode-locking operation.

Figure 4.16 shows the Raman spectrum, which was obtained by exciting the MWCNTs-PVA film using a 352 nm laser. It shows a well-defined G (1585 cm^{-1}) and D (1433 cm^{-1}) bands as normally observed in the spectra of graphite or graphene. The existence of prominent D-band in Raman spectrum shows that the carbon nanotubes are a multi-walled type with multi-layer configuration and disordered structure. The D band which is less intense than the G peak is reported to be upshifted to 1275 cm^{-1} in MWNTs-PMMA composite, while in this work we observed a downshift of D band for MWNTs-PVA polymer composites. The absence of Radial Breathing Mode (RBM) at ~250 cm^{-1} band in the Raman spectrum confirms the multi-walled type of CNT used in our experiment. This is due to the diameter of the wrapped CNT which consist of too many walls or the inner wall diameter is too big as discussed in the previous section. Furthermore, other prominent features like D+G band (2900 cm^{-1}) and a small peak at 845 cm^{-1} can also be observed in the Raman spectrum of Figure 4.16.
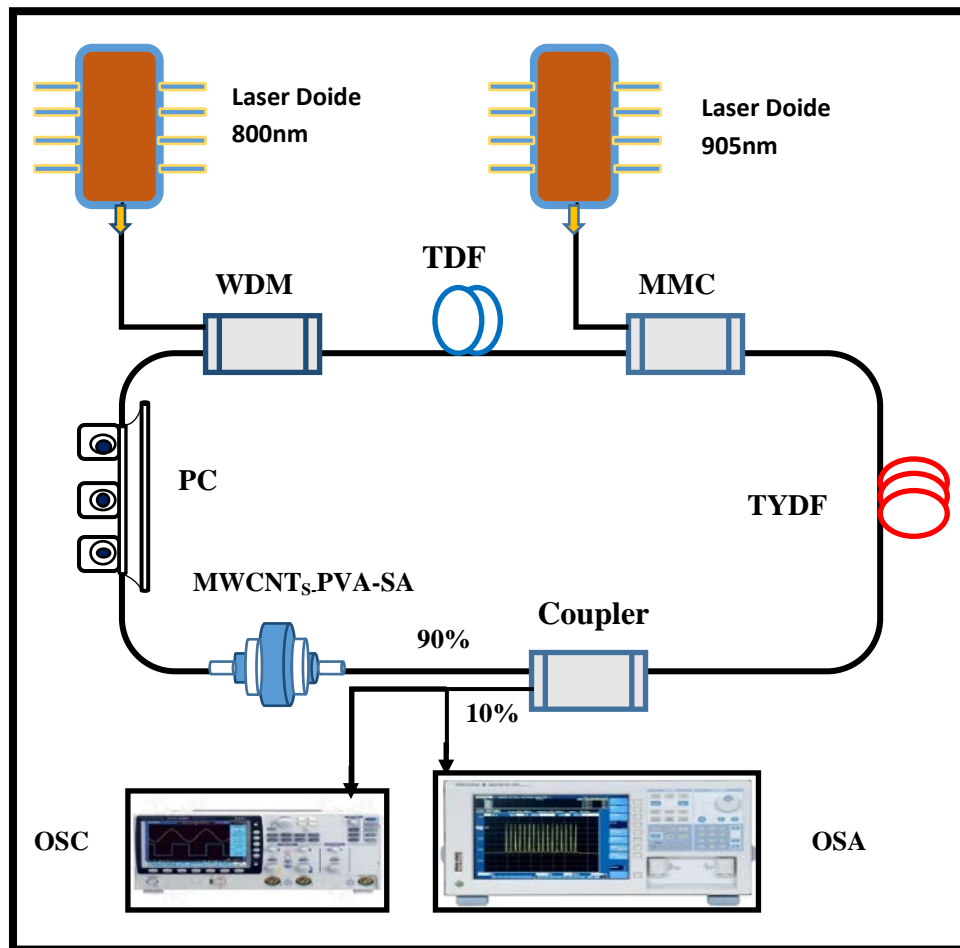
Figure 4.15: Experimental setup of the proposed mode-locked 2 μm fiber laser using a hybrid

gain media in conjunction with a MWCNTs-PVA film SA.
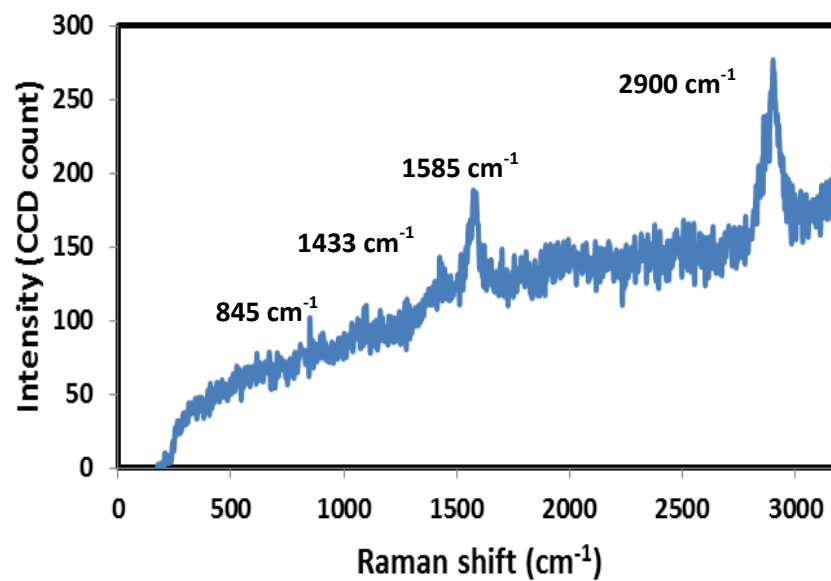
Figure 4.16: Raman spectrum obtained from the MWCNTs-PVA film.

4.5.2   Mode-locking performance of the 2 micron fiber laser

The output spectrum of the mode-locked laser was firstly monitored by an OSA whose resolution is limited to 0.05 nm. Figure 4.17 shows the optical spectrum when the 800 nm and 905 nm pump powers is fixed at 141.5 mW and 1.8 W respectively. The laser operates at the center wavelength of 1951.8 nm, which is relatively longer wavelength region, due to the use of TYDF, which provides a higher gain at longer wavelength due to energy transfer from Ytterbium to Thulium ions. The full-width at half maximum (FWHM) of the output spectra is obtained at ~1.3 nm, which is slightly broadened due to self-phase modulation (SPM) effect in the laser cavity.
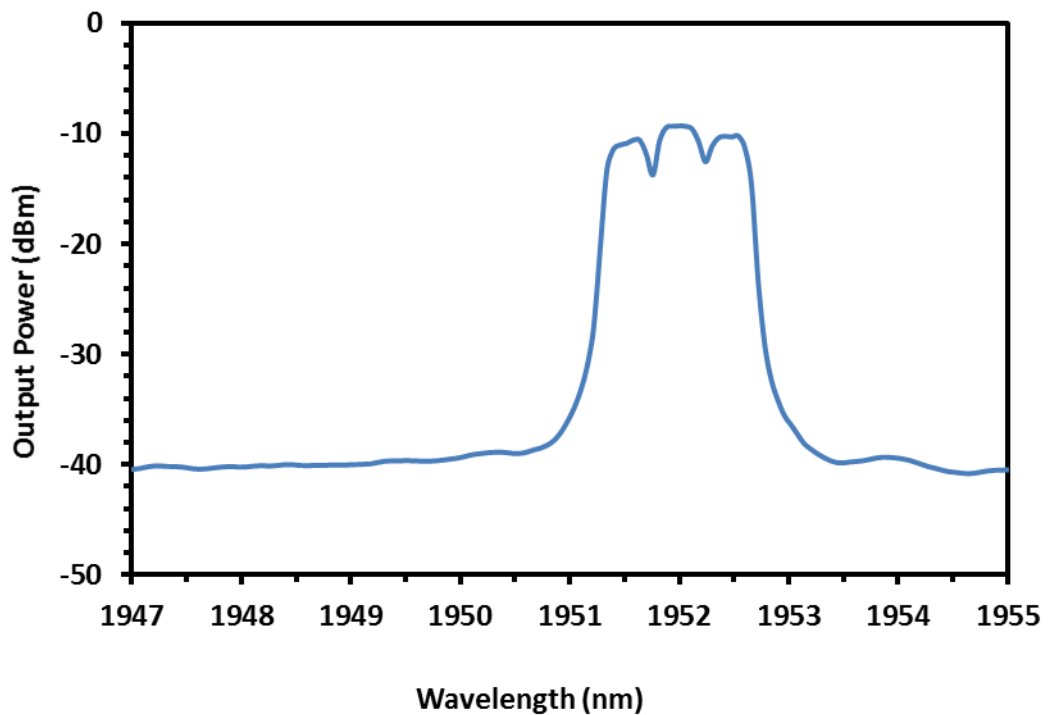
Figure 4.17: Optical spectrum of the mode-locked laser

A stable mode-locking of the laser was observed as the 905 nm multimode pump powers was varied within 1.8 – 2.2 W when the single-mode 800 nm pump power was fixed at 141.5 mW. At the beginning, the PC was slightly adjusted to initiate the mode-locking. Figure 4.18

illustrates a typical pulse train output from the mode-locked laser when the 800 nm and 905 nm pump powers is fixed at 141.5 mW and 2.2 W respectively. As shown in the figure, the peak to peak pulse duration for the laser is measured at 28.9 ns, which corresponds to a repetition rate of 34.6 MHz. The repetition rate is observed to be constant even when the multimode pump power is increased from 1.8 to 2.2 W. In order to show that the mode-locking operation was made possible by the MWCNTs SA, the same laser configuration was also tested without the MWCNTs film. But, no pulse train was observed in such configuration at any position of the PC.
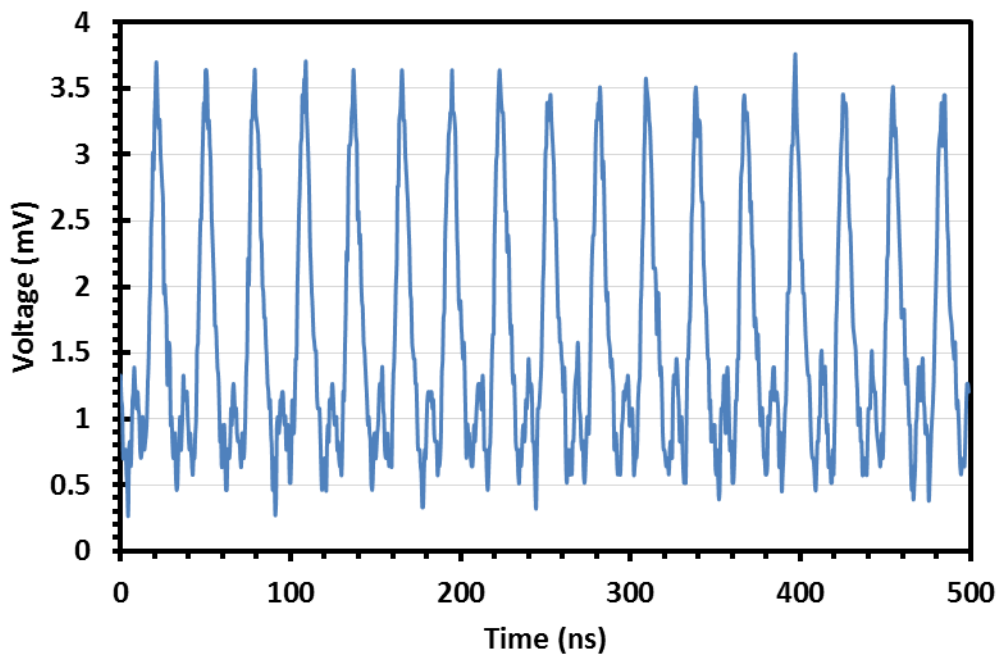
Figure 4.18: Oscilloscope trace of the typical pulse train from the mode-locked laser

Figure 4.19 shows a plot of a typical output second harmonic generation (SHG) autocorrelation trace, superimposed on the sech^2 fit. Assuming a sech^2 profile, the pulse duration is estimated to be around 10.79 ps. The time–bandwidth product (TBP) of the output pulses is ~11.05, with a major deviation from the value of 0.315 expected for transform-limited sech^2 pulses. This shows that the pulse is highly chirped by the

dispersion effect in the cavity, limiting the minimum achievable pulse width. Another limitation to shorter pulses could be due to spectral filtering effects introduced by the Thulium gain medium.
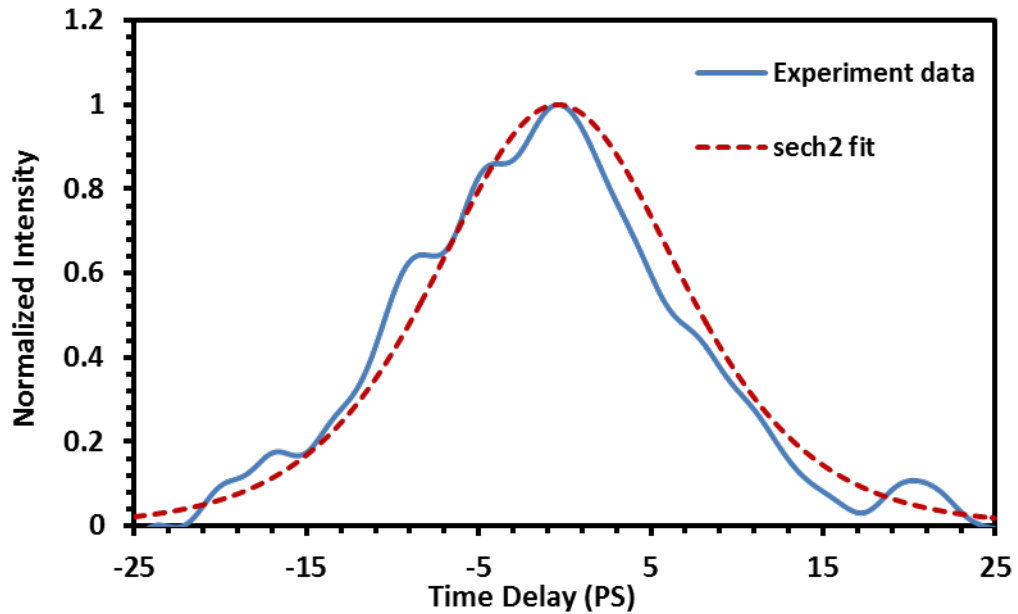
Figure 4.19: Autocorrelation trace, with sech^2 fit

It is also found that the average output power of the proposed mode-locked laser is linearly related with the pump power. It is observed that the output power increases from 0.31 mW to 0.59 mW as the 905 nm pump power rises from 1.8 to 2.2 W while the 800 nm pump power is fixed at 141.5 mW. At the maximum pump power, the pulse energy is calculated to around 17.0 pJ. The radio frequency (RF) spectrum was also investigated and the result is as depicted in Figure 4.20. The repetition rate of the laser is 34.6 MHz, which corresponds to the fourth order harmonic pulse with an approximately 23.5 m long cavity. A signal-to-noise ratio (SNR)of about 20-25 dB is observed, highlighting the moderate-amplitude fluctuation of the laser.
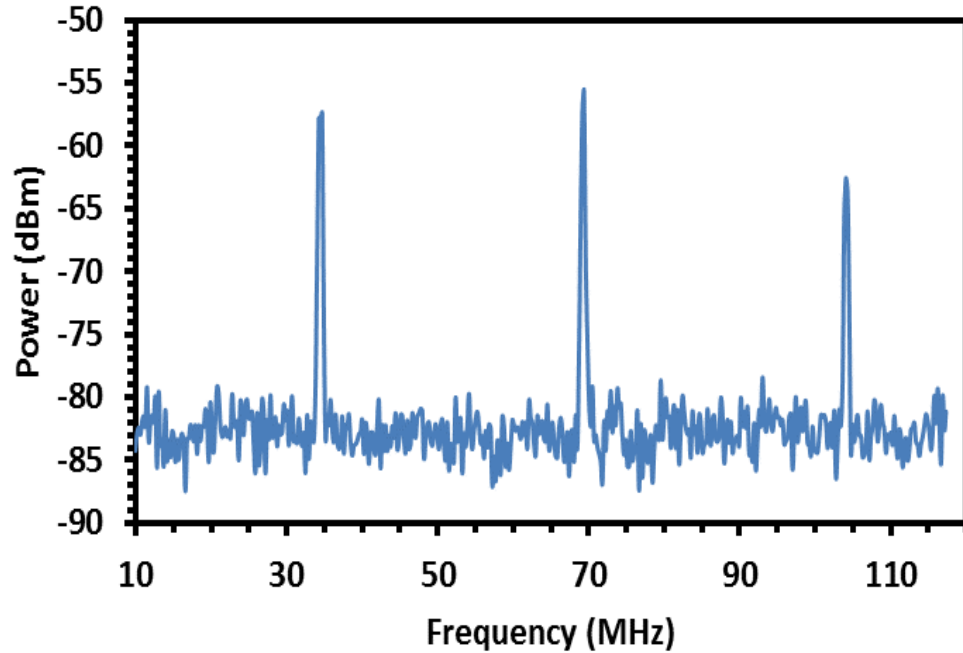
Figure 4.20: RF spectrum of the mode-locked fiber laser

4.6 Graphene Oxide Paper for Mode-locking

Up to now, most ultra-short pulse fiber lasers have adopted passive mode-locking technology, in which saturable absorbers (SAs) act as a key part. The improvement of lasers relies on the optical properties of SAs, for instance, transparency and optical non-linearity. In sections 4.3 and 4.5, mode-locked fiber lasers have been demonstrated using a NPR and multi-walled carbon nanotubes based SA, respectively. NPR currently dominate passive mode-locking especially in 1.5 µm region. However, it strongly depends on the polarization and phase evolution of the optical pulse in the laser cavity, so in a long cavity it can be easily overdriven and affected by the environmentally induced fiber birefringence (Keller, 2003; Sun et al., 2010). As a

promising SAs candidate, carbon nanotubes (CNTs) have advantages both in recovery time and saturable absorption. In order to achieve waveband tuning, CNTs with different diameters have to be mixed, resulting in extra linear losses, consequently increasing the difficulty of mode locking.(Hasan et al., 2009; Zhang et al., 2009). As an upcoming material in recent years, graphene has also emerged as a new saturable absorption material. It possesses favourable characteristics for SAs, similar to CNTs. As a result of gapless linear dispersion of Dirac electrons, graphene SAs would achieve wideband, tunable operation without the need of bandgap engineering or chirality/diameter control.(Bao et al., 2009; Bonaccorso et al., 2010; Hasan et al., 2009; Sun et al., 2010). However, the processability are the first issue for the graphene based materials.

The structure of graphene oxide (GO) is composed of sp^2-bonded areas with variable size, which are divided by surface oxidation in the form of carboxyl, hydroxyl or epoxy groups. The synthesis of GO is relatively easier than graphene, and more importantly, can be prepared in large quantities in both water and organic solvents (Hummers Jr & Offeman, 1958; Stankovich et al., 2007). Although the electric conductivity is highly influenced by the content of defect clusters, GO has good optical properties. Further investigation shows GO has ultrafast recovery time and strong saturable absorption, which is comparable to that of graphene (Loh et al., 2010). The reported research work on GO based SAs are realized by mirror (Xu et al., 2012; Xu et al., 2012), photonic crystal fiber filled with few-layered graphene oxide solution (Liu et al., 2011), fused silica windows with GO and reduced GO layers (Sobon et al., 2012), GO aqueous dispersion (Wang et al., 2012), reflective GO absorber with glass and copper (Feng et al., 2012), sandwich structured GO/PVA absorber (Wang et al., 2013) and GO membrane on microfiber (He et al., 2012).

Recently, a graphene oxide paper has also been developed and commercially available for various applications. It can be prepared by mixing graphite oxide in water. The oxygen atoms of graphite oxide repel water molecules, thus, undergoing complete exfoliation in water, producing a colloidal suspensions of almost entirely individual graphene oxide sheets. After filtering the exfoliated mixture through a membrane, these graphene oxide sheets could be made into paper-like material under a directional flow. A free-standing graphene oxide paper is obtained after drying. By changing the oxygen amount on the layers, the material can be an electrical insulator, semi-conductor or conductor. This material is uniform and dark brown in colour. (Dikin et al., 2007). In this section, a soliton mode-locked TYDFL is demonstrated using a commercially available graphene oxide (GO) paper as a saturable absorber (SA) for the first time. The SA is constructed by sandwiching the GO paper between two fiber connectors.

4.6.1 Experimental setup and Raman analysis for GO paper

The experimental setup for mode-locked TYDFL is schematically shown in Figure 4.21. It was constructed using a simple ring cavity, in which a 15 m long double-clad TYDF was used for the active medium and the GO paper based SA was used as a mode-locker. The set-up is almost similar to the previous work on NPR-based mode-locked TYDFL (Figure 4.6) except for the incorporation of SA. The fiber-type SA device was constructed by inserting a piece of GO paper in between two ferules. The TYDF was pumped by a 905 nm multimode laser diode via MMC. The length of total cavity is set at around 22.4 m so that the net cavity dispersion was anomalous for modelocking. The PC was used to adjust the polarisation state of the oscillating light and thus facilitate self- starting laser. The 10% port of a 90/10 coupler is used to monitor laser output.
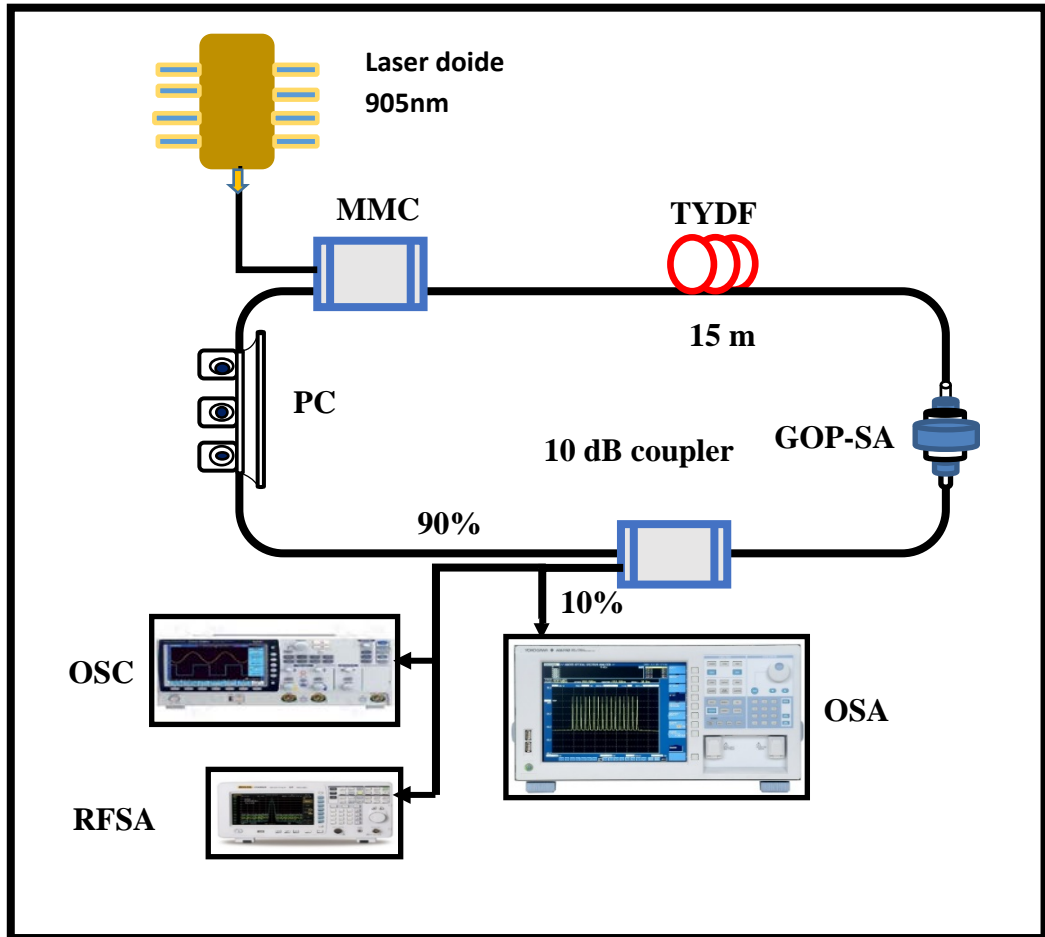
Figure 4.21: Experimental setup for the soliton mode-locked TYDFL

Figure 4.22 shows the result of Raman spectroscopy on graphene oxide paper, which was performed using 532 nm laser. The exposure time was set to 20 s. From the result, there are two distinctive peaks that can be observed; at 1349 cm^{-1} and 1588 cm^{-1}. These two peak corresponds to D-band and G-band respectively (Yang et al., 2009). The peak at D-band is caused by the hybridized vibrational mode related to graphene edges and it also reveal that there is disorder to the graphene structure. The G-band, also known as the graphite or tangential band, is due to the energy in the sp^2 bonded carbon in planar sheets. The in-plane optical vibration of the bond resulted in Raman spectrum at the frequency (Zhu et al., 2010).A bump at 2700 cm^{-1}, also known as G' or 2D band, is barely observable because the laser power is low. Because the intensity of G' band is

lower than the G band, it also shows that the GO paper has more than one graphene layer.
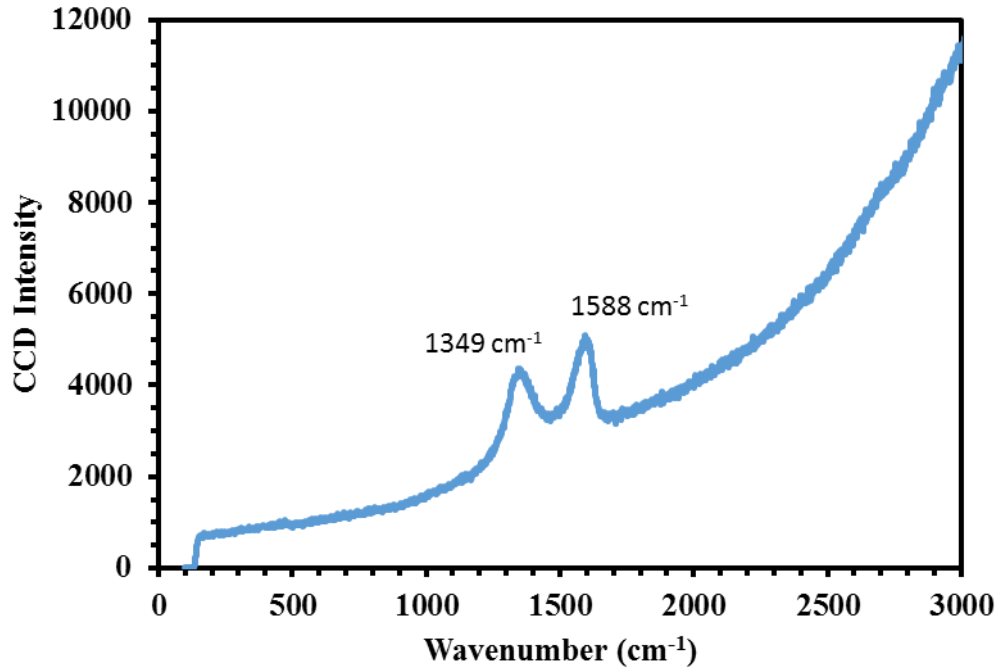
Figure 4.22: Raman spectroscopy result of graphene oxide paper

4.6.2 Performance of the GO paper based mode-locked TYDFL

Mode-locking was self-started by fine tuning the polarization controller when pumping at the threshold pump power of 1.8 W. The output spectrum of the laser when the laser was first mode-locked is shown in Figure 4.23. The output spectrum of the cw TYDFL, which was obtained by removing the SA is also presented for comparison purpose. As shown in the figure, the spectra were centered at about 1942.0 nm and 1943.5 nm as the TYDFL is configured with and without the SA, respectively. It is observed that the operating wavelength shifts to a shorter wavelength with the insertion of SA into the cavity due to the change in cavity loss. The oscillating laser shifts to shorter wavelength to acquire more gain to compensate the insertion loss of the SA. With the SA, the presence of soliton is also confirmed with a weak Kelly side bands at

1941.96 and 1942.15 nm as shown in the inset figure of Figure 4.23. This shows that this mode-locked fiber laser is operating in anomalous dispersion regime.
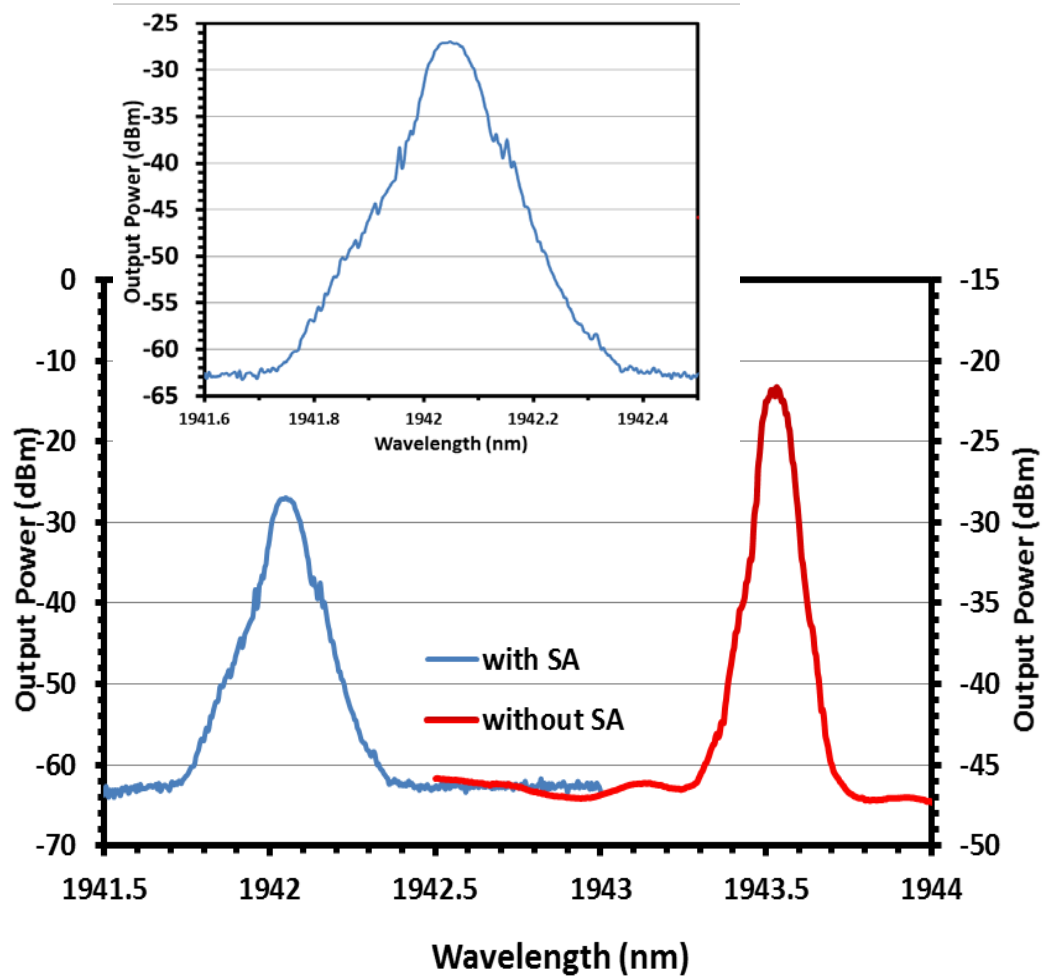
Figure 4.23: Output spectrum of the mode-locked TYDFL with and without SA

The total length of the laser cavity was measured to be approximately 22.4 m, comprising 15 m TYDF and 7.4 m SMF with estimated dispersions of -0.083 ps^2/m and -0.034 ps^2/m, respectively at 1942 nm. The total cavity dispersion comprises of the fiber dispersion and the material dispersion from graphene. Thereafter,

Total cavity dispersion = $(D_{SMF} \times L_{SMF}) + (D_{TYDF} \times L_{TYDF}) + D_{Graphene}$ (4.1)

The material dispersion from graphene could be roughly deduced

$$D_{\text{Graphene}} \approx -87 \times D_{\text{SMF}} \qquad = 2.958 \text{ ps}^2 \qquad (4.2)$$

Assuming that the output pulses possess a transform-limited, secant hyperbolic temporal shape, the pulse width of the soliton fiber laser could be estimated through the following equation:

$$\Delta\lambda = \pm\lambda_o \sqrt{\frac{2}{cDL} - 0.0787 \frac{\lambda_o^2}{(ct)^2}} \qquad (4.3)$$

Where $\Delta\lambda$ is the first order Kelly sideband separation, λ_o is the central wavelength, D is the average cavity dispersion parameter, L is the cavity length, c is the light velocity in vacuum and t is the soliton pulse width. Using experimentally observed parameters, including $\Delta\lambda = 0.1 nm$, $\lambda_o = 1942$ nm and D = 1.46 ps^2, the pulse width is estimated to be around 1.1 ns.

The typical pulse train of GO paper based passive mode-locked laser is shown in Figure 4.24 at 1.8 W pump power. It has a pulse-to-pulse separation of 44.8 ns, corresponding to a pulse repetition rate of 22.32 MHz which matches the fouth harmonic of the cavity roundtrip time with cavity length of 22.4 m. This indicates the well dispersed GO in the paper sheet exhibits saturable absorption for harmonic mode-locking operation. The modulation of the pulse amplitude is an artifact caused by the limited sampling points on the sampling oscilloscope, since the pulse duration is too narrow and the sampling rate of our oscilloscope is only 1 Gs/s. The RF spectrum of the mode-locked pulses was also measured as shown in Figure 4.25. Its forth harmonic peak locates at the frequency of 22.32 MHz and has a signal-to-noise ratio (SNR) of 18 dB, which further confirms the feasibility of mode-locking in operation. However, the stability of pulse trains is still low. The performance of the fiber laser was relatively stable during the measurement for half an hour. Compared to other functional materials, which is accompanied by special technical and engineering methods, the performances

of GO paper are not the best. However, GO paper is a competent material for optical applications with extra properties in ease of preparation, transparency, fluorescence, and optical non-linearity.
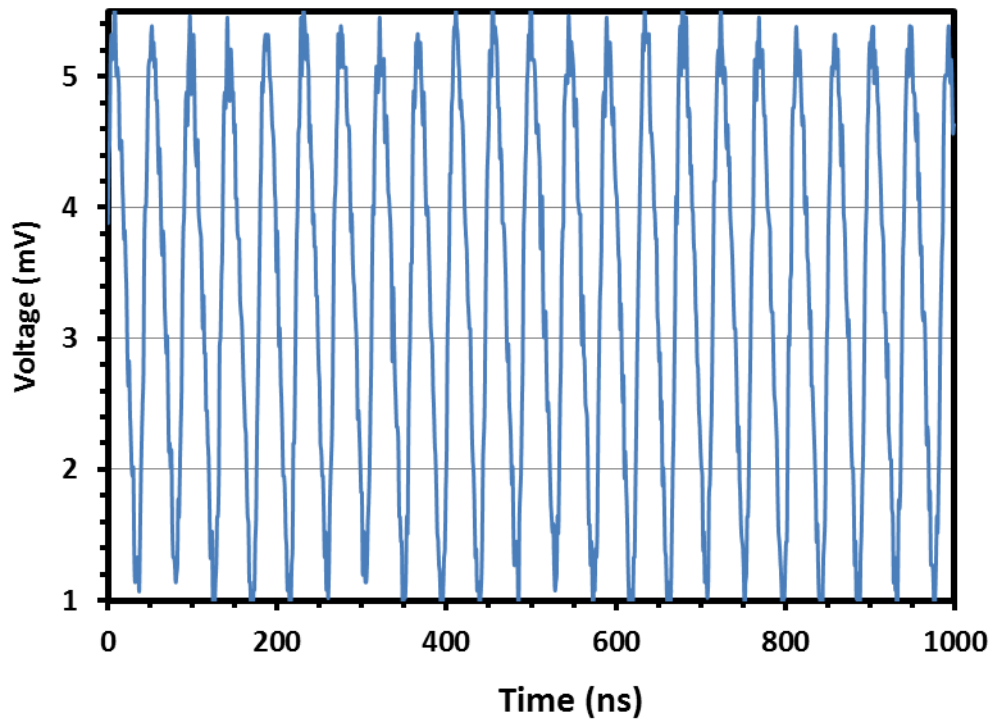
Figure 4.24: Typical pulse train for the mode-locked TYDFL
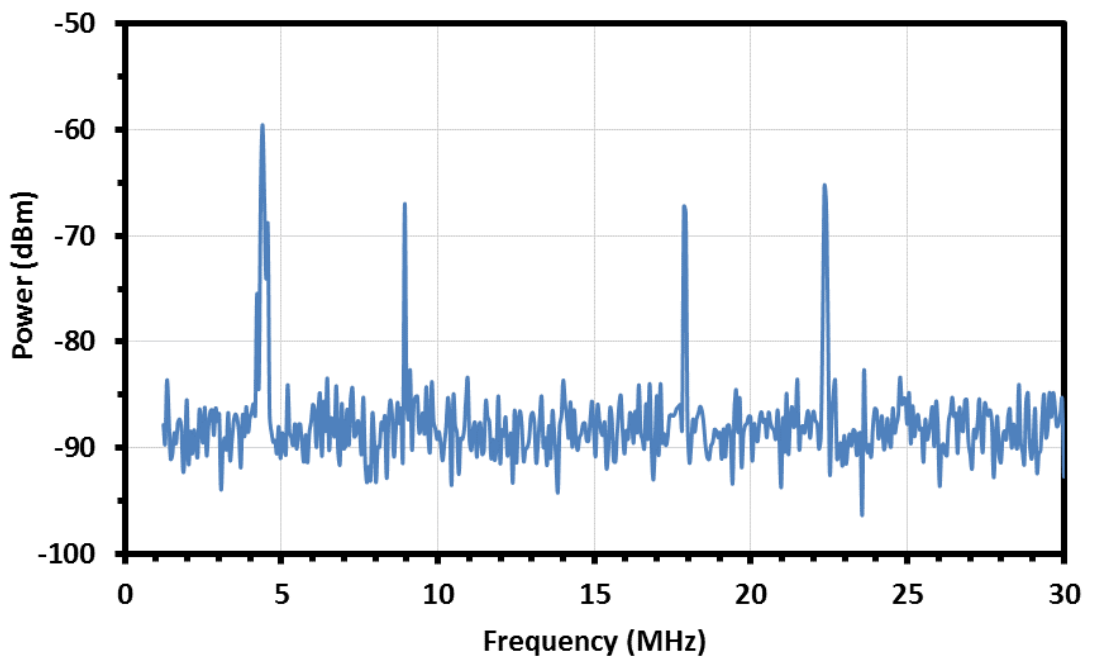
Figure 4.25: RF spectrum for the mode-locked TYDFL

4.7 Summary

A 2 micron pulsed laser has been succesfully demonstrated using either commercial TDF or a newly developed TYDF as the gain medium. At first, we propose and demonstrate a passively Q-switched fiber laser operating at 1949.0 nm using a commercial TDF and homemade double-clad TYDF as the gain media in a ring configuration based on NPR technique. The cavity consists of 2 m long TDF and a 15 m long TYDF which is pumped by a single-mode 800 nm and a multimode 905 nm, respectively. The combination of these gain media and multimode combiner functions as an artificial saturable absorber which enables the intensity-dependent transmission inside the cavity for the Q-switching. The proposed Q-switched laser produces a stable pulse train with a repetition rate of 13.49 kHz and pulse width of 3.089 μs when the 905 nm multimode pump power and 800 nm pump power are fixed at 2.3 W and 110.4 mW, respectively. The maximum pulse energy of the Q-switched laser is obtained at 11 nJ. An all-fiber mode-locked TYDFL operating at 1953.5 nm is then demonstrated using the NPR technique. The mode-locked pulse is self-started at threshold 905 nm pump power of 2.7 W. The pulse has repetition rate of 33.1 MHz, the calculated pulse width of 10 ps and pulse energy of 46.9 nJ at 2.7 W pump power.

We have also demonstrated a passive and stable Q-switched fiber laser operating in 1846.4 nm using a MWCNTs-PVA thin film based SA. The film was sandwiched between two ferrules and the SA was incorporated in the TDFL ring cavity to produce a stable pulse train with 10.58 kHz repetition rate, 17.52 μs pulse width and 11.34 nJ pulse energy at 121.1 mW pump power. A passively mode-locked fiber laser is also demonstrated using a MWCNTs-PVA film based SA. The laser is designed to operate at 1951.8 nm by using a cascaded gain media of TDF and TYDF. Stable mode-locking pulse with a repetition rate of 34.6 MHz and pulse width of 10.79 ps is obtained when the 905 nm multimode pump power reaches 1.8 – 2.2 W while the single-mode 800 nm

pump power is fixed at 141.5 mW. In addition to showing good Q-switching and mode-locking performances, the MWCNTs SA is also easy to fabricate at low cost.

Finally, a soliton mode-locked TYDFL is demonstrated operating at 1942.0 nm using a commercially available nonconductive graphene oxide paper as a saturable absorber. The paper which is sandwiched between two fiber ferrules acts as a mode-locker. The TYDFL generates a soliton mode-locked pulse train with a repetition rate of 22.32 MHz and calculated pulse-width of 1.1 ns. It is observed that the fiber laser has a low pulsing threshold (1.8 W) as well as low damage threshold. The easy fabrication of graphene oxide paper should promote its potential application in ultrafast photonics.

CHAPTER 5

Q-Switched Erbium-Doped Fiber Laser with Solid State Saturable Absorber Based on Thulium Doped Fiber

5.1   Introduction

Q-switched pulsed lasers operating in the "eye-safe" wavelength region above 1.5 μm have many potential applications such as in light detection and ranging (lidar) system, optical communication, sensor and instrumentations. Fiber lasers are suitable for such applications due to their excellent beam quality that can be made independent of the output power. Q-switched fiber lasers are normally achieved using active techniques such as acousto-optics modulators (Delgado-Pinar et al., 2006; Huang et al., 2000), piezoelectric actuators (Russo et al., 2002), or magnetostrictive transducers (Pérez-Millán et al., 2005) to modulate the Q-factor of the cavity. Besides, they can also be realized using passive approaches such as semiconductor saturable-absorber mirrors (SESAMs) (Paschotta et al., 1999), graphene (Ismail et al., 2013) and single-walled carbon nanotubes (CNTs) saturable absorbers (Hasan et al., 2009). However, SESAM's are complex, expensive to fabricate, operate in narrow wavelength band, require expensive clean room equipment and have low damage threshold and long recovery time. On the other hand, graphene and CNTs have a low damage threshold and thus limits the attainable pulse energy.

Q-switching can also be achieved by modulating cavity Q-factor using solid-state saturable-absorber fibers (Dvoyrin et al., 2007; Kurkov et al., 2009; Tsai et al., 2009). These saturable-absorber fibers are advantageous due to their ability to hold enormous gain excited in the fiber from lasing. They also have a high damage threshold suitable for generating high-power Q-switched pulses. Up to date, there is still a lack of research effort in this area and most of the works focus mainly on Ytterbium-doped fiber lasers (Dvoyrin et al., 2007; Kurkov et al., 2009). It is known that the energy

transition $^3H_6$ - $^3F_4$ of Tm^{3+} has a very broad emission and absorption band ranging from 1.6 - 2.1 µm and 1.5 - 1.9 µm respectively. It is reported that the absorption cross section of Thulium doped fibers (TDFs) are larger than the emission cross section of Erbium-doped fiber (EDF) at around 1.6 µm region. This suggests a possible application of TDF as SA in a passively Q-switched Erbium-doped fiber laser (EDFL).

In this chapter, various Q-switched EDFLs are proposed and demonstrated by using a short piece of TDF as a passive saturable absorber in a ring laser cavity. The performance of this laser is also compared with graphene oxide based SA, which was previously developed in Chapter 4. Finally, a dual-wavelength Q-switched EDFL is proposed using the solid state TDF SA.

5.2 All-fiber Q-switched EDFL operating at 1534.5 nm

Figure 5.1 shows the configuration of the proposed all-fiber Q-switched EDFL using a passive TDF SA. The laser resonator consists of a 3 m long EDF gain medium, a 980/1550 wavelength division multiplexer (WDM), an optical isolator, a 10 dB coupler and a 1 m long TDF as a SA. The EDF used has absorption coefficients of 23 and 35 dB/m at 980 and 1531 nm wavelength respectively. The numerical aperture (NA) of the EDF is 0.16 and its core and cladding diameters are 4 µm and 125 µm respectively. It is pumped by a commercial 980 nm laser diode with a maximum pump power of 125 mW via a WDM. The TDF has an initial absorption loss of 6 dB at around 1570 nm, NA of 0.16 and core diameter of 2.9 µm. An optical isolator is used to avoid the backward reflection and ensure unidirectional operation. The laser light is extracted from the ring resonator by a 10 dB fiber coupler which keeps 90% of the oscillating light in the cavity. An optical spectrum analyzer with wavelength resolution of 0.05 nm is used to capture the output laser spectrum while a 350 MHz oscilloscope in conjunction with 1.2 GHz bandwidth photo-detector is used to detect the pulse train. The length of the cavity is approximately 7 m.
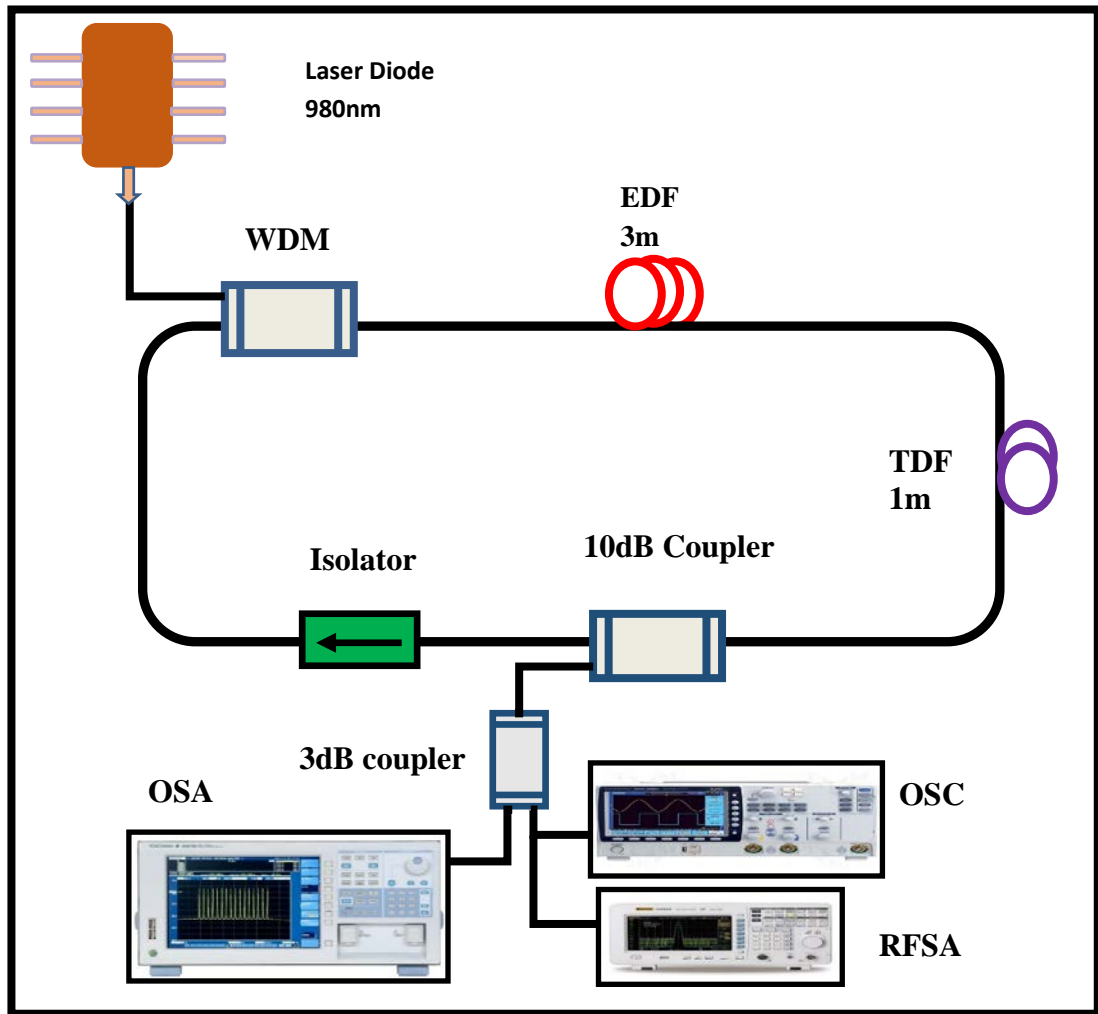
Figure 5.1: The configuration of the proposed Q-switched EDFL

Figure 5.2 shows the output spectra of the EDFL with and without the TDF SA. Without the TDF we observed a stable CW operation of EDFL at 1553.0 nm. After incorporating the 1 m long TDF in the cavity we obtained pulsed lasing. The operating wavelength of the pulsed laser is shifted to a shorter value (1534.5 nm) due to the cavity loss which increases with the incorporation of TDF. To compensate for the loss, the laser operates at a shorter wavelength which has a higher gain. Spectral broadening in the Q-switch fiber laser is attributed to self-phase modulation (SPM). A typical pulse train of the Q-switched laser generated at pump power of 75 mW is shown in Figure

5.3. From the figure, the peak to peak pulse separation is calculated at 38.6 µs, which is equivalent to a repetition rate of 25.9 kHz. The pulse width is 16.86 µs from the oscilloscope. The Q-switching pulse generation is due to gain-switching action provided by the Thulium ions interaction with the oscillating Erbium laser.
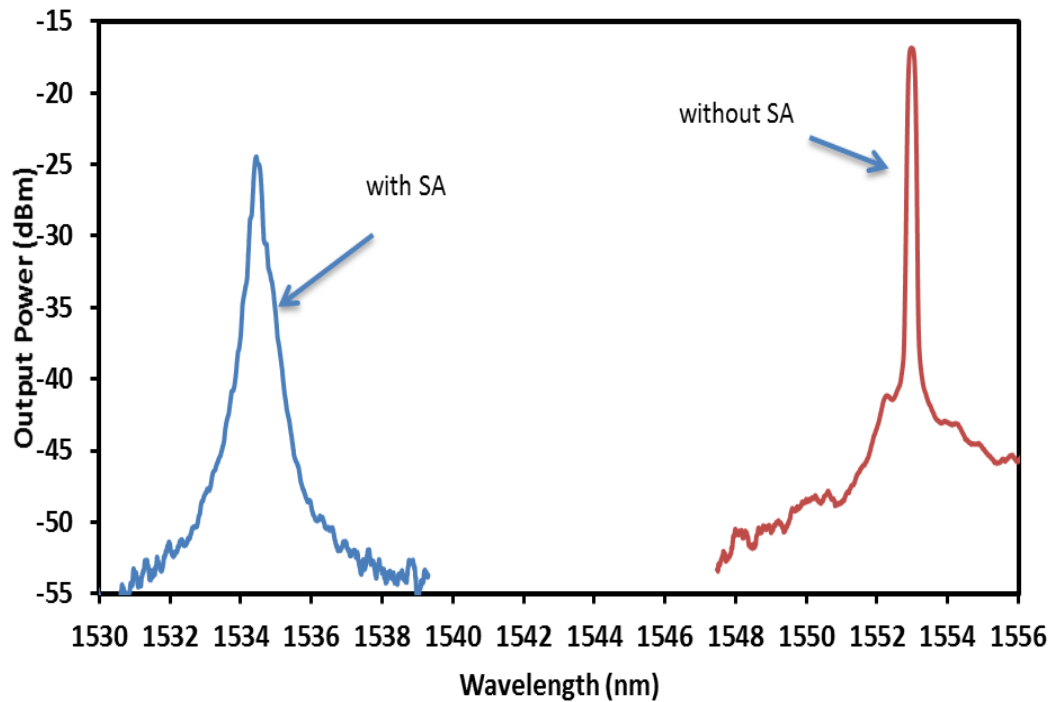
Figure 5.2: The output spectra with and without the TDF SA for the proposed EDFL
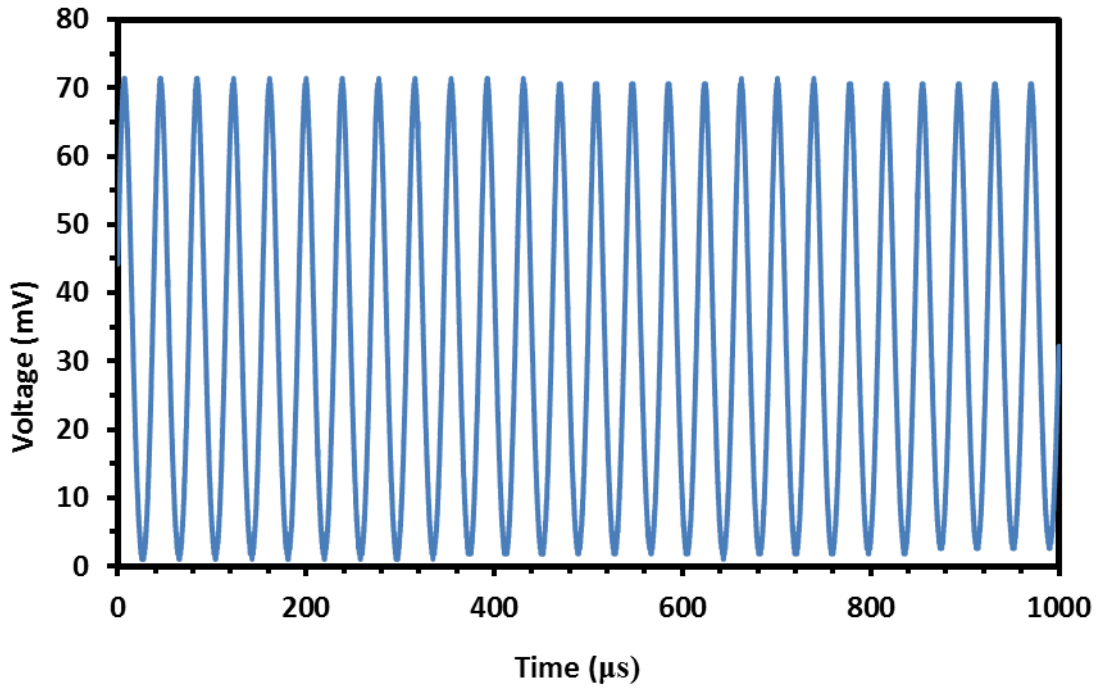
Figure 5.3: Typical pulse train at pump power of 75 mW.

Figure 5.4 shows the pulse repetition rate and pulse width against 980 nm pump power. As the pump power increases from 23 to 75 mW, the repetition rate of the Q-switched pulses monotonically grows from 11.0 to 25.9 kHz. At the same time, the pulse duration reduces from 37.56 to 16.86 μs as expected. We also measured the average output power and the corresponding calculated single-pulse energy at various pumping powers as shown in Figure 5.5. It is observed that both output power and pulse energy almost linearly increase with pump power from 23 to 75 mW. However, at above 75 mW pump power, the pulse train becomes unstable and disappears. This is due to the inability of the TDF SA to fully recover in time after a pulse and insufficient gain population for excitation before the next pulsing. It suggests that the relaxation lifetime ($^3F_4$) of the TDF is close to 0.039 ms which is calculated from the inversion of the largest repetition rate before disappearing. At the maximum pump power of 75 mW, an output power of 0.483 mW is obtained which corresponds to the maximum pulse energy of 18.6 nJ. Energy characteristics of the Q-switched laser allow possible

applications for various technological processes such as marking, trimming, micromachining and others. The laser can also find applications in medicine due to the relatively high absorption by biological tissue. The output power and energy are expected to further increase by the optimization of cavity design and saturable absorber. Inset of Figure 5.5 shows the RF spectrum of the Q-switched laser at pump power of 75 mW, which indicates a repetition rate of 25.9 kHz. The signal to noise ratio is measured to be around 50 dB, which indicates the stability of the Q-switching generation.
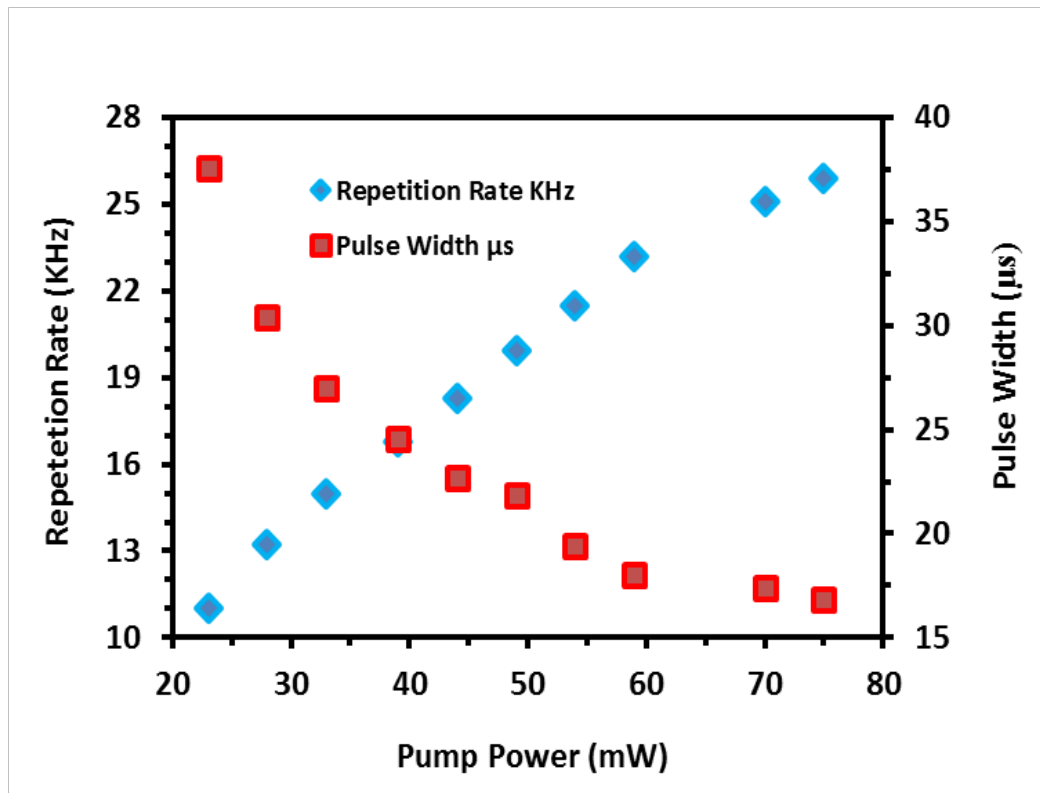
Figure 5.4: Repetition rate and pulse width against the 980nm pump power
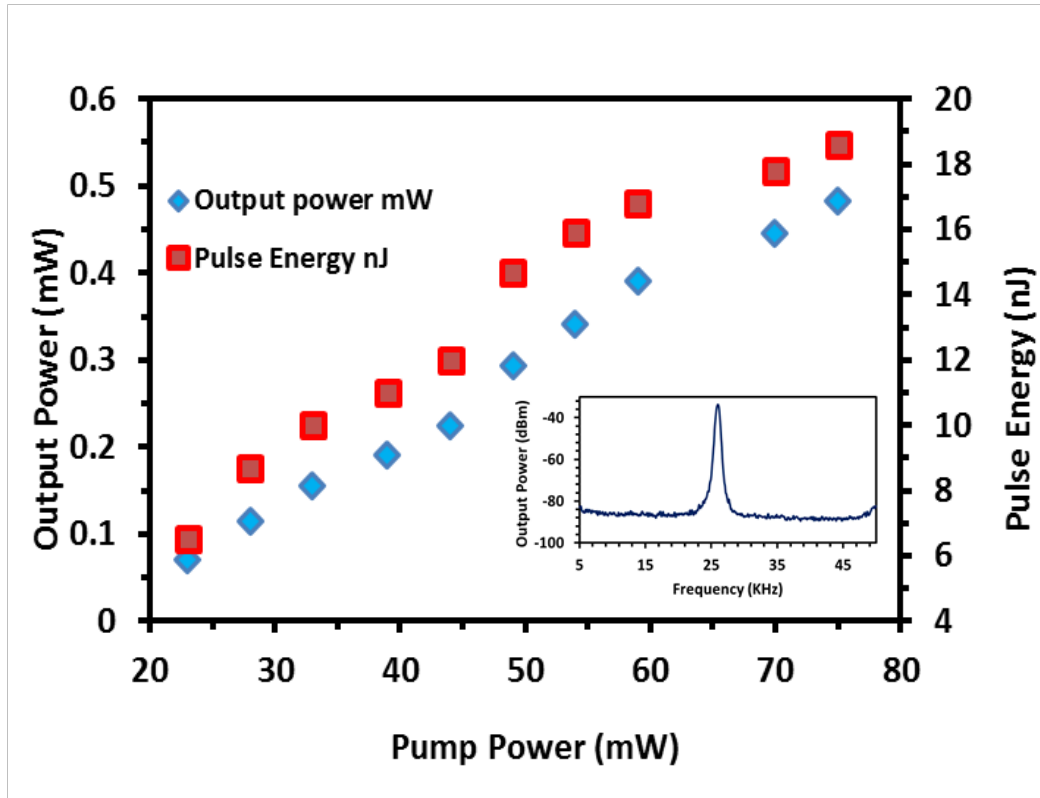
Figure 5.5: Average output power and pulse energy against the 980nm pump power.

5.3 Performance comparison with graphene oxide paper (GOP)

In Chapter 4, a soliton mode-locked Thulium Ytterbium co-doped fiber laser (TYDFL) was demonstrated using a commercially available graphene oxide (GO) paper as a SA. The choice of the commercial GO paper (GOP) as SA is due to the simpler manufacturing technology and the possibility of mass production which make GO much easier and common to obtain at a lower cost. Compared to graphene, GO shows no significant difference in the laser performance (Sobon et al., 2012). GO SA was also experimentally tested and reported to construct passively Q-switched Erbium-doped fiber laser (Ahmad et al., 2012). In this section, a new Q-switched EDFL is proposed and demonstrated using both TDF and GOP SAs as the Q-switcher for comparison purpose.

Figure 5.6 shows the experimental setup to compare the Q-switching performance between GOP and TDF SA. The resonator has the same components with

the previous setup of Figure 5.1. It uses a 0.8 m long EDF instead of 3 m as the gain medium. The EDF is pumped by a 980 nm laser diode via 980/1550 WDM. In this setup, the SA is placed between the isolator and WDM coupler to optimize the performance of the laser. The GOP used in this experiment is similar with the previous work in Chapter 4. The TDF used is also similar with the previous section. The TDF length is fixed at 0.25 m in this work to optimize the cavity loss. The laser output is tapped from 10 % port of the output coupler, before it is characterized using an OSA, oscilloscope and RF spectrum analyzer.
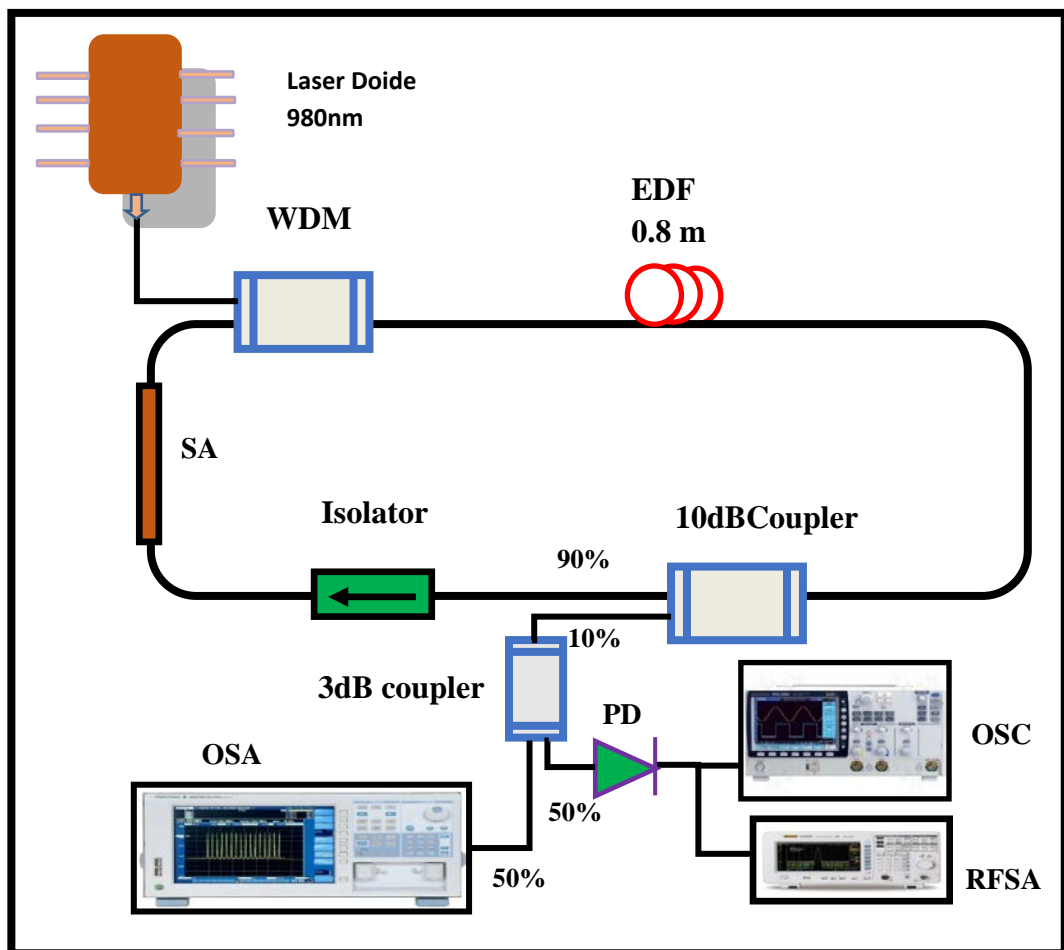
Figure 5.6: Experimental setup to compare the performance of the TDF with GOP as a saturable absorber in a Q-switched EDFL.

Initially, the continuous wave (CW) EDFL was investigated without the SA and the laser threshold was found to be at the pump power of 10 mW. As a GOP SA is incorporated in the cavity, CW lasing was obtained at slightly higher threshold pump power of 18 mW due to the insertion loss of the SA. A stable and self-starting Q-switched operation was observed as the pump power is further increased above 22 mW. It should be noted that no Q-switched operation occurs without the SA connected in the laser cavity. This shows that the Q-switched operation is mainly induced by the SA. As the GOP SA is replaced by 0.25 m long TDF, the Q-switching pulse is obtained at a lower threshold pump power of 14 mW. This is due to the insertion loss of the TDF, which is lower than GOP SA. Figure 5.7 shows the optical spectra of both Q-switched lasers with GOP and TDF, which are measured at 980 nm pump power of 50.5 and 25.4 mW, respectively. The optical spectrum of the CW laser, which was obtained by removing the SA is also shown in the figure for comparison purpose. In the CW laser, the pump power is fixed at 50.5 mW.

As can be seen in Figure 5.7, the EDFL cavity operates at 1557.7 nm, 1550.5 nm and 1534.5 nm as the laser is configured without SA, with TDF SA and with GOP, respectively. It is also observed that the operating wavelength of the laser shifted from 1557.7 nm to 1550.5 nm with the incorporation of TDF SA. This is attributed to the cavity loss, which increases with the incorporation of SA. Therefore, the laser operates at a shorter wavelength to acquire more gain to compensate for the loss. The operating wavelength is further shifted to a shorter wavelength as the TDF is replaced by GOP SA. This might be due to insertion loss of the GOP SA, which is higher than the TDF.
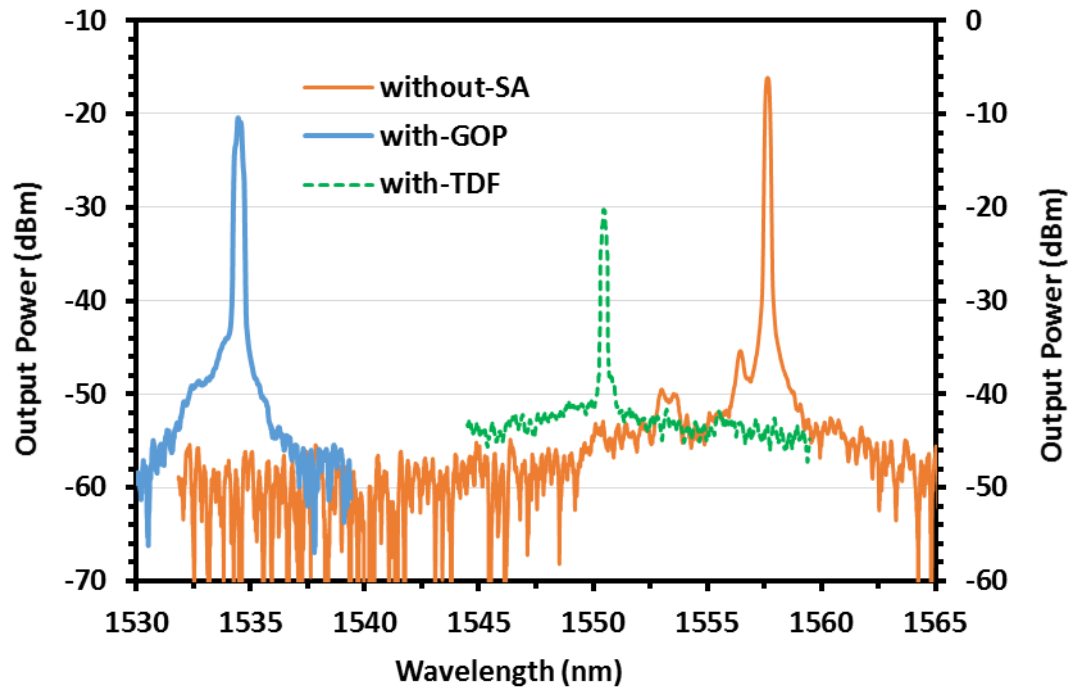
Figure 5.7: Comparison of output spectra from three different EDFL cavities

configured with and without SA.

The typical Q switched pulse train of the EDFL is presented in Figure 5.8 when the pump power is fixed at 25.4 and 50.5 mW for the laser configured with TDF and GOP, respectively. The repetition rates are obtained at 15.9 and 31.4 kHz with TDF and GOP, respectively. The corresponding pulse durations, which were measured directly from an oscillograph, are about 28.0 and 13.8 μs, respectively. This figure also shows no distinct amplitude modulation in each Q-switched envelop spectrum. This indicates that the self-mode locking effect on the Q-switching is weak for both lasers. Figure 5.9 shows how the repetition rate and pulse width of both lasers are related with the pump power. The pulsed operation was started at 14 mW with both repetition rate and pulse width are pump-dependent up to 26.7 mW for the EDFL configured with TDF. With GOP, the pulse operation is obtained within pump power of 22 mW to 50.5 mW, a typical signature of Q-switching. It is worthy to note that the GOP was burned when the pump power was further increase. In the proposed Q-switched EDFL with TDF SA, the repetition rate increases from 4.5 to 16.7 kHz while the pulse width reduces from 37.2

to 27.8 µs as the pump power is varied from 14.0 to 26.7 mW. The pulse repetition rate increases from 14.3 to 31.4 kHz with increasing pump power from 22.0 to 50.5 mW with the use of GOP SA. On the other hand, the pulse width decreases from 32.8 to 13.8 µs as the pump power is increased within the same range. This effect is due to gain compression in the Q-switched fiber laser.
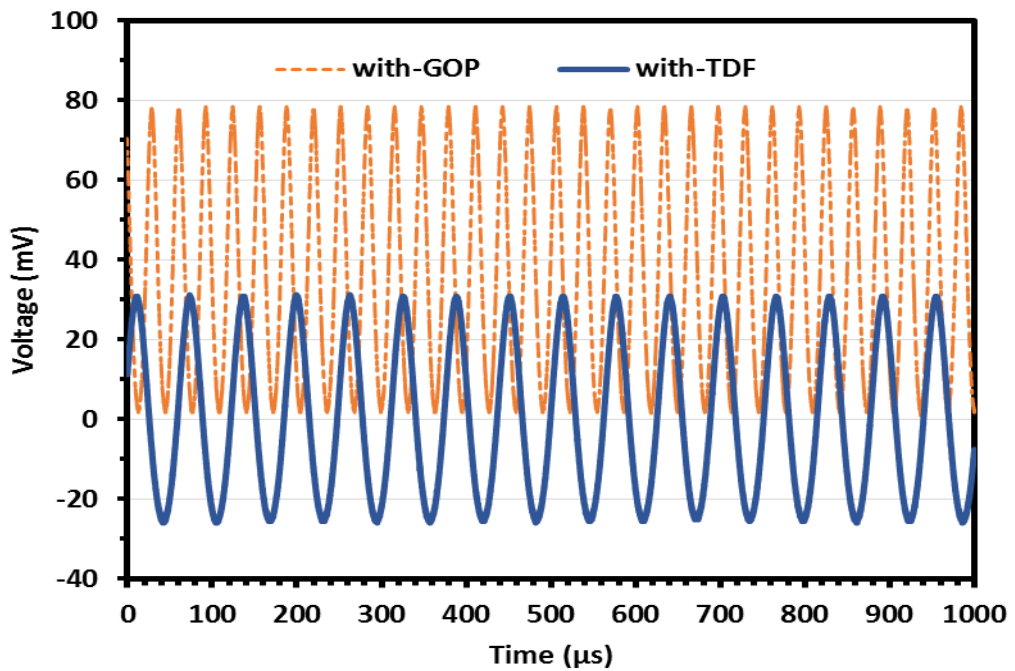
Figure 5.8: Typical pulse train of the EDFL with TDF and GOP at pump powers of 25.4 mW and 50.5 mW, respectively.
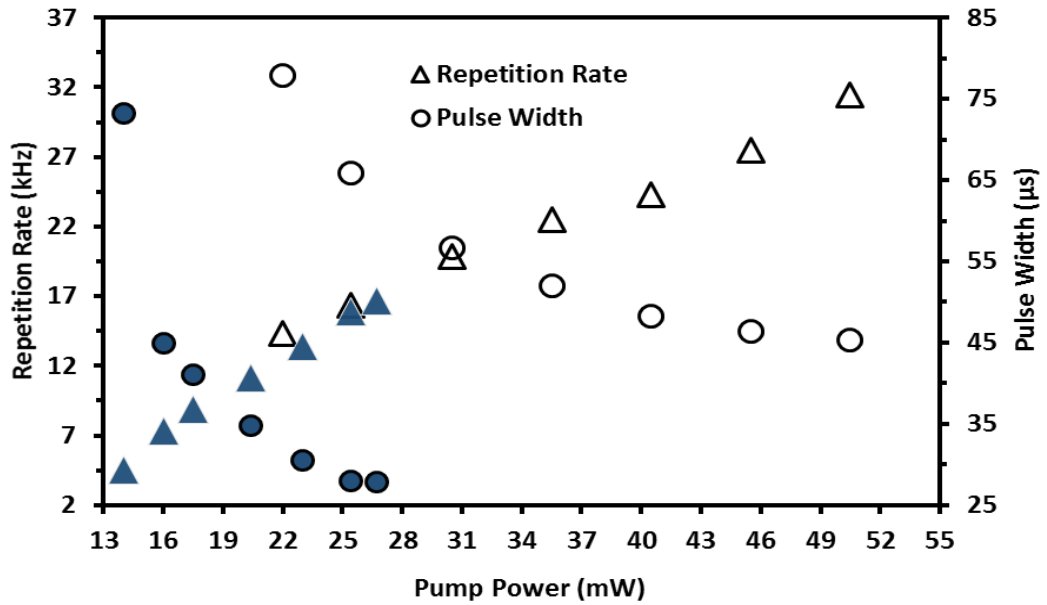
Figure 5.9: The repetition rate and pulse width as a function of input pump power for both EDFLs configured with TDF (solid symbols) and GOP SAs (hollow symbols).

Figure 5.10 shows the average output power and pulse energy as a function of 980 nm pump power for both EDFLs. The output power and pulse energy in both EDFLs show an increasing trend with the pump power. The maximum pulse energy of 15.8 nJ and 16.8 nJ are obtained at pump powers of 25.4 mW and 45.5 mW for the EDFL configured with TDF and GOP, respectively. This shows that the EDFL configured with TDF can achieve the same pulse energy at lower pump power compared to the use of GOP. The radio-frequency (RF) measurement of the output intensity for both EDFLs are shown in Figure 5.11. In the experiment, the pump power is fixed at 25.4 mW and 50.5 mW for the EDFL configured with TDF and GOP respectively. From the figure, the laser is observed to operate at frequencies of 15.9 kHz and 31.4 kHz, corresponding to a period of ~62.9 μs and 31.8 μs with the use of TDF and GOP, respectively as the SA. The signal to noise ratio (SNR) is obtained at around

20 and 12 dB with TDF and GOP, respectively. This shows that pulse stability is better
with the use of TDF SA in the proposed EDFL setup.
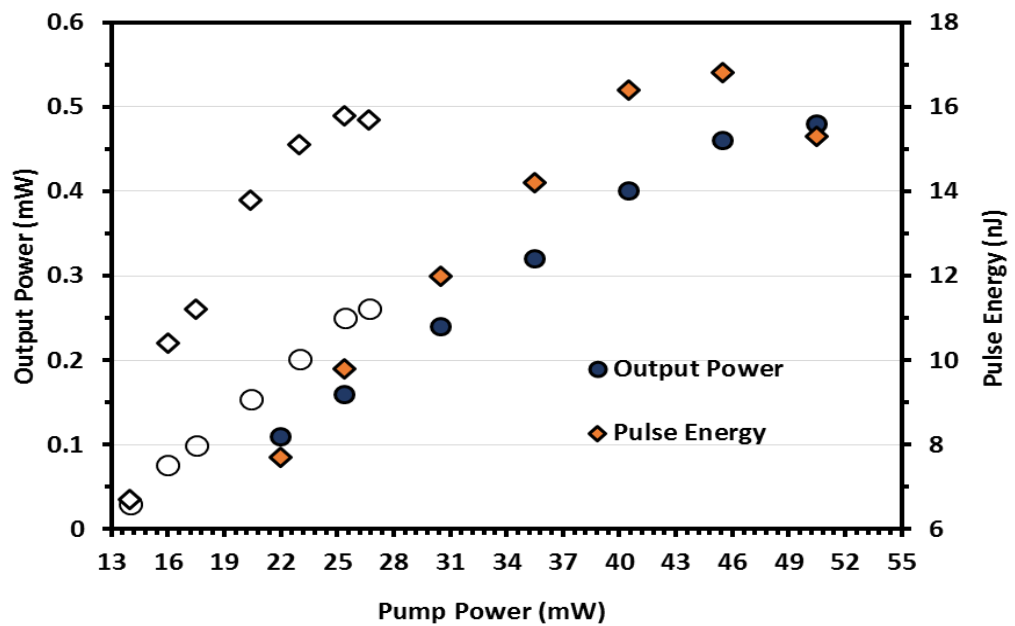
Figure 5.10: The average pump power and pulse energy as a function of input pump
power for both EDFLs configured with TDF (solid symbols) and GOP SAs (hollow
symbols).
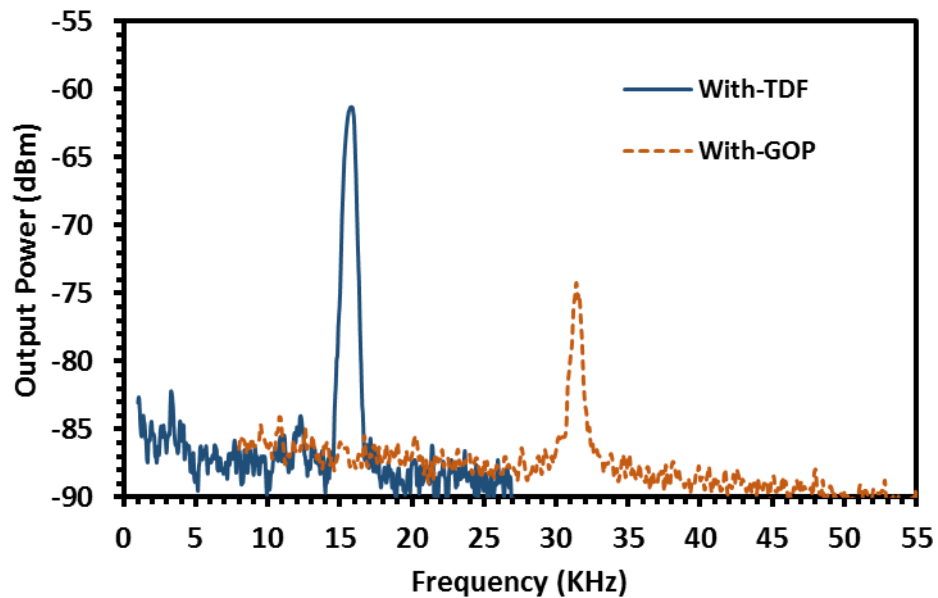
Figure 5.11: Comparison of output RF spectrum obtained with TDF and GOP SA.

5.4 Dual-wavelength Q-switched EDFL with TDF SA

Multi-wavelength Q-switching lasers show versatile applications in airborne Lidar, terahertz generation, microwave optics, biomedical diagnostics, telecommunication and sensing applications (Kurkov et al., 2010; Lou et al., 2008; Nawata et al., 2012; Urquhart, 1988). Some techniques had been proposed in Chapter 3 to deliver dual-wavelength fiber laser including spatial filtering effect, inline microfiber Mach Zehnder interferometer and multimode interference effect. Very recently, by using the birefringence-induced filtering effect, a dual-wavelength Q-switched EDF laser with a graphene saturable absorber has been reported (Wang et al., 2012). Leveraging the spectral gain peaks of the Yb-doped fiber wavelength, the dual-wavelength passively Q-switching operation has been demonstrated around 1µm wavelength, which uses Cr^{4+}:YAG as the saturable absorber (Pan et al., 2008). Based on the broad absorption spectrum of TDF, dual-wavelength Q-switched lasers are also possible to be realized with this kind of low-cost, fiber-compatible saturable absorbers. In this section, based on a TDF saturable absorber, without using any spectra filtering effect or modulation elements in the cavity, we experimentally demonstrate an all-fiber, passively Q-switched EDFL, which can simultaneously generate two pulse trains at different wavelengths over 16 nm apart. Generation of the dual-wavelength output is based on the spectral gain profile of the EDF that could possess two peaks under certain pump and signal conditions determined by the intra-cavity loss (Zhao et al., 2011).

5.4.1 Configuration of the proposed dual-wavelength EDFL

Figure 5.12 shows the experimental setup of TDF SA based passively Q-switched dual-wavelength EDFL. The laser resonator is similar with Fig. 5.1 except for TDF length, which is fixed at 0.7 m to reduce the mode competition and allows dual-wavelength simultaneous lasing to take place in the cavity. A 980/1550 nm WDM is used to launch the 980 nm pump light into the laser cavity. A 10% coupler is employed

to couple out light. The 3 m long EDF is pumped by a 980 nm laser diode. The total cavity length is measured to be around 6.7 m. The output pulse trains are passed through a tunable pass filter with the filtering bandwidth of 1 nm and an insertion loss of around 1.1 dB. It was split into two paths via a 3 dB coupler so that the spectrum and temporal characteristics of the output light can be analyzed simultaneously by an OSA and a 350 MHz oscilloscope via a photodetector, respectively. We note that there is no device with large birefringence or polarization dependence in the cavity and little birefringence induced-filtering effect is observed in our setup.
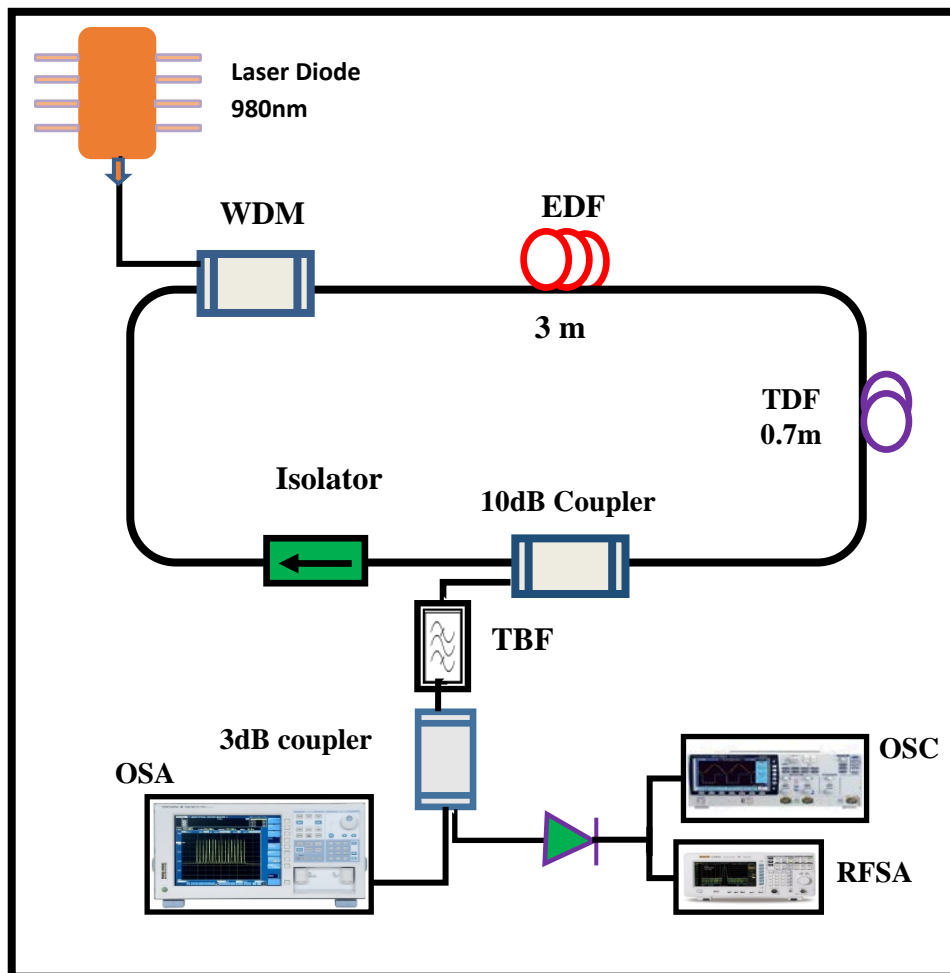
Figure 5.12: Experimental setup of the dual-wavelength Q-switched EDFL

5.4.2 Experimental results and discussion

Q-switching operation in our fiber laser is achieved by the TDF SA. CW state of dual-wavelength operation is obtained at a pump power above 13.8 mW, corresponding to the laser threshold. The laser can operate on dual-wavelength Q-switching once the pump power exceeds 25 mW. Figure 5.13 shows the output spectrum of the EDFL at three different pump powers. The output spectrum for the CW laser without the SA at pump power of 41 mW is also included in the figure for comparison purpose. As shown in Figure 5.13, the EDFL operates at 1558.52 nm without the SA in the cavity. As the SA is incorporated in the cavity, the laser starts to generate simultaneous dual-wavelength output at shorter wavelength region when the pump power exceeds 13.8 mW. This is attributed to the absorption characteristic of the TDF, which alter the gain spectrum shape of the EDF. It is observed that the EDF can possess two gain peaks that the magnitude can vary with the pump power, one near 1534.8 nm and the other near 1551.64 nm, which could enable dual-wavelength Q-switching (DWQS) operation of the laser. At the pump power of 41 mW, the two lasing peaks of the EDFL have nearly the same magnitude, and thus a stable dual wavelength Q-switched (DWQS) operation is achieved with the highest repetition rate and pulse energy. Stable dual-wavelength Q-switched mode can be maintained within the pump power range of 25–41 mW.
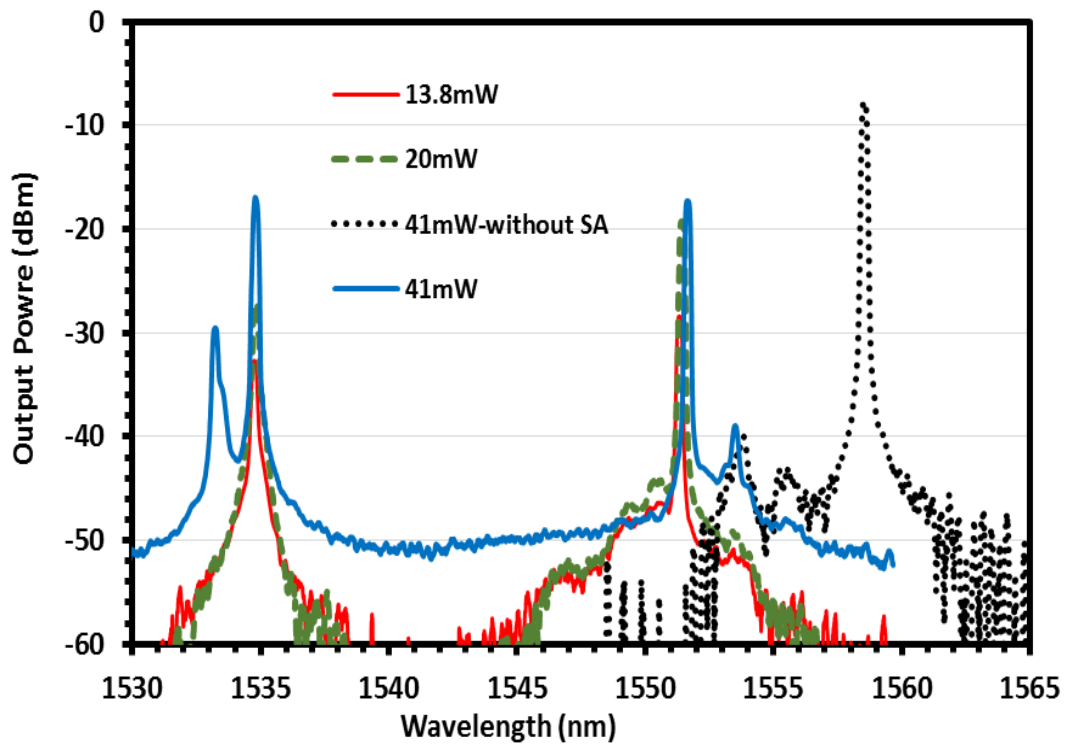
Figure 5.13 shows the output spectrum of the EDFL at three different pump powers.

Figure 5.14 shows the pulse traces measured by the oscilloscope at the pump power of 41 mW as the outputs at different wavelengths are connected to the scope consecutively. The amplitudes of the traces are normalized to clearly show. So that the detailed characteristics of the dual-wavelength pulse trains can be compared. The pulses at the two wavelengths have almost the same repetition rate, and, as the pump power reduces, both repetition rates reduce. The pulse repetition rate and pulsewidth of both Q-switching lasers are shown in Figure 5.15 at varying pump powers. Similar to many other passively Q-switched lasers, the repetition rate is closely related to the pump level,which means that
 the higher the pump power, the higher the repetition rate is. That is because high pump power leads to a shorter time for the inversion number of the gain medium to reach the threshold. For 1551.64 nm laser, repetition rates from 14.7 kHz to 21.6 kHz can be achieved, when the pump power is increased from 25 mW to 41 mW. The laser operates

at the repetition rates of 15.8 to 22.8 kHz at the same pump power range for 1534.8 nm laser. The slight change of the repetition rate is observed due to the refractive index of the core, which is wavelength dependent.

The pulse width, on the other hand, reduces with the pump power. For instance, the pulse width of the 1551.64 nm signal can be varied from 30.1 μs to 21.8 μs by increasing the pump power from 25 mW to 41 mW. As indicated in the previous work (Song, 2012), the long pulse duration obtained is due to the long cavity lifetime related to the long length of the cavity, which can be reduced by decreasing the cavity length with a highly doped EDF or other more compact components. In our experiment, we observe that the pulse durations of these two pulse trains at different center wavelengths are somewhat different. The pulses at 1534.8 nm are typically slightly shorter than those at 1551.64 nm. The difference is due to the different absorption and emission parameters at the two wavelengths as the ground- and excited-state populations vary.

The radio-frequency (RF) measurement of the output intensity for both wavelengths is also investigated at a fixed pump power of 41 mW. Figure 5.16 shows the result, which indicates that the laser at frequencies of 21.6 kHz and 22.8 kHz for the operating wavelength of 1551.64 nm and 1534.8 nm, respectively. The signal to noise ratio (SNR) of the laser is obtained at around 10 and 13 dB for 1551. nm and 1534.8 nm signal, respectively. This shows that both pulse trains are stable.

The proposed dual-wavelength Q-switched EDFL based on a TDF SA could find applications where multiple synchronized short optical pulses are needed. The proposed laser provides the advantages of all-fiber structure, simple realization, robust and low cost.
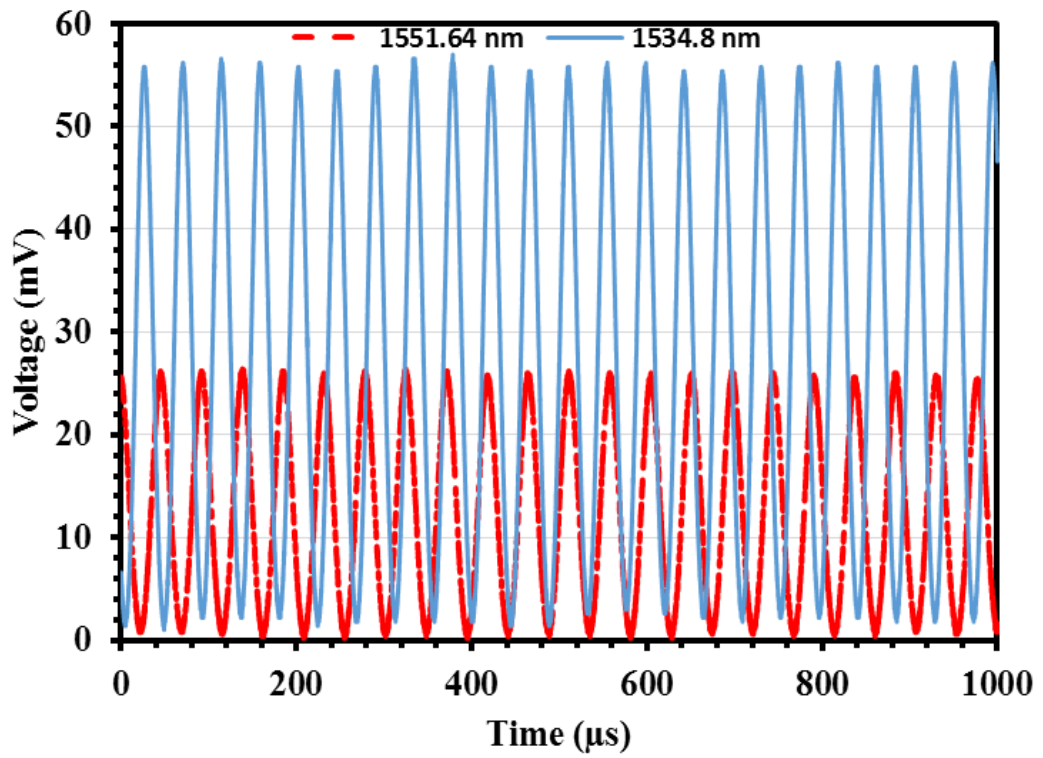
Figure 5. 14: The pulse traces measured by the oscilloscope at the pump power of 41

mW
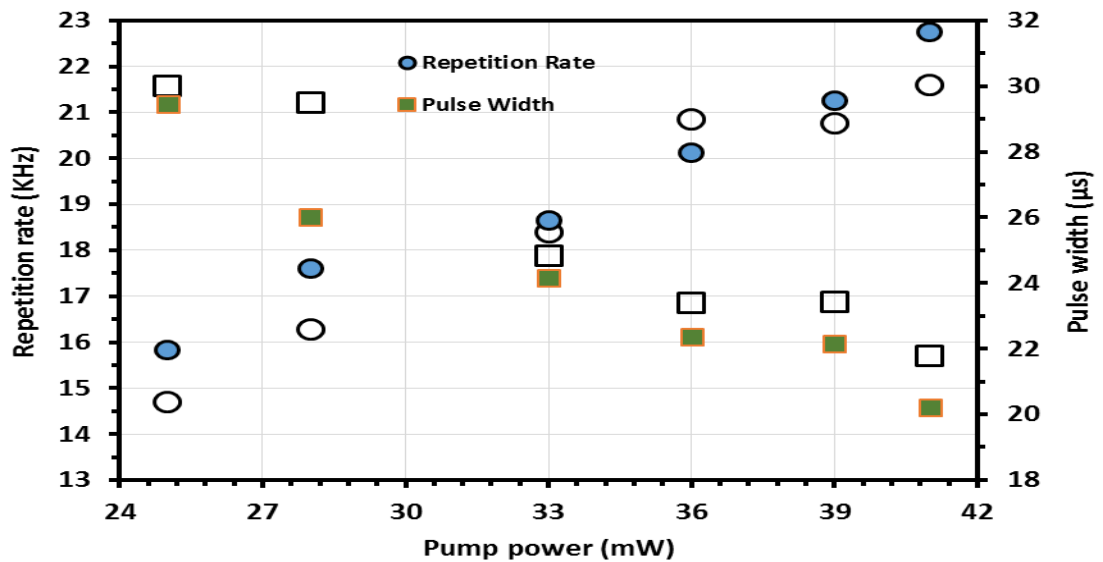
Figure 5.15: The repetition rate and pulse width of Q-switching lasers as a function of

input pump power for both EDFLs wavelengthes 1551.64 nm (hollow symbols) and

1534.8 nm (solid symbols).
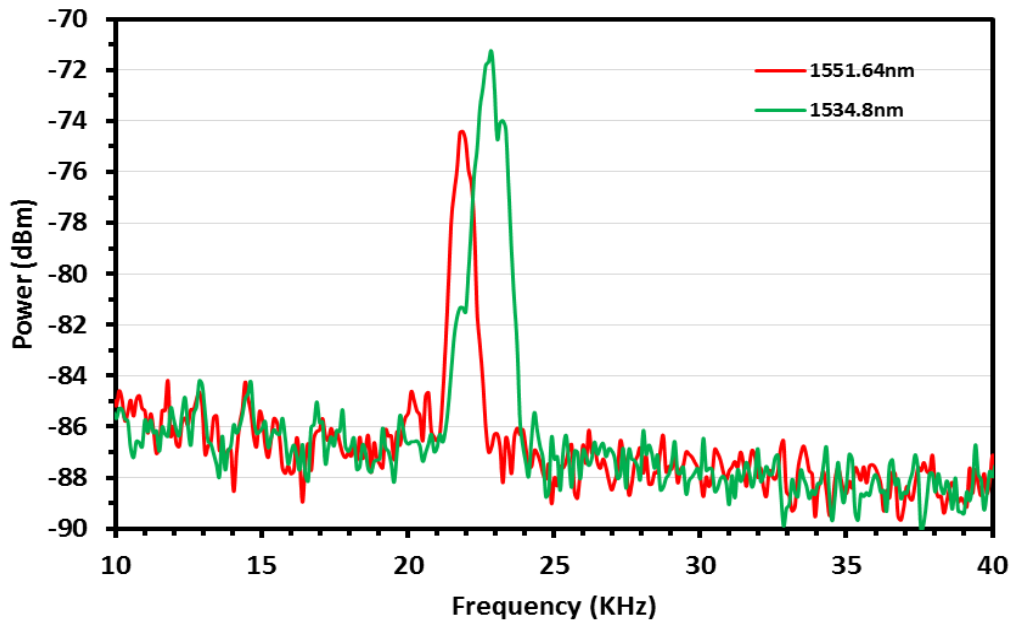
Figure 5.16: Output RF spectrum for both wavelengthes

5.5   Summary

In this chapter, we have successfully demonstrated various Q-switched EDFLs

by using a short piece of TDF as a passive saturable absorber in a ring laser cavity. At

first, we have demonstrated the passive Q-switched EDFL laser operating at 1534.5 nm.

In this experiment, The EDF and TDF lengths are fixed at 3 m and 1 m, respectively.

The EDFL generates Q-switching pulse at a threshold pump power as small as 23 mW.

By increasing the pump power from the threshold power to 75 mW, the repetition rate

can be varied from 11.0 kHz to 25.9 kHz, whereas the corresponding pulse width drops

from 37.56 μs to 16.86 μs. At pump power of 75 mW, the maximum pulse energy of

18.6 nJ is obtained. The second Q-switched EDFL is based on similar configuration but

uses 0.8 m long EDF as the gain medium in conjunction with 0.25 m long TDF as the

SA to reduce the pump power threshold. The performance of this laser was also

investigated with GO paper SA for comparison purpose. With TDF SA, the repetition

rate of the Q-switched EDFL increases from 4.5 to 16.7 kHz while the pulse width

reduces from 37.2 to 27.8 μs as the pump power is varied from 14.0 to 26.7 mW. In

case of GOP, the pulse repetition rate increases from 14.3 to 31.4 kHz while the pulse width reduces 32.8 to 13.8 µs with the change of pump power from 22.0 to 50.5 mW. The maximum pulse energy of 15.8 nJ and 16.8 nJ are obtained at pump powers of 25.4 mW and 45.5 mW for the EDFL configured with TDF and GOP, respectively. This shows that the EDFL configured with TDF can achieve the same pulse energy at lower pump power compared to the use of GOP. The RF spectrum shows the SNR of approximately 20 and 12 dB with TDF and GOP, respectively, which indicates that the pulse was more stable with the use of TDF SA. Finally, we demonstrated a dual-wavelength Q-switched EDFL operating at 1551.64 nm and 1534.8 nm using a TDF SA. The laser resonator uses a shorter length of TDF (0.7 m) to reduce the mode competition and allows dual-wavelength simultaneous lasing to taking place in the cavity. The repetition rate of 1551.64 nm laser changes from 14.7 kHz to 21.6 kHz as the pump power is increased from 25 mW to 41 mW. The repetition rate varies from 15.8 to 22.8 kHz at the same pump power range for 1534.8 nm laser. On the other hand, the pulse width for both lasing lines reduces with the pump power. For instance, the pulse width of the 1551.64 nm signal can be varied from 30.1 µs to 21.8 µs by increasing the pump power from 25 mW to 41 mW. We also observe that the pulse width at 1534.8 nm is typically slightly shorter than those at 1551.64 nm. The difference is due to the different absorption and emission parameters at the two wavelengths as the ground- and excited-state populations vary. The RF measurement shows that the SNR of the laser is obtained at around 10 and 13 dB for 1551.64 nm and 1534.8 nm signal respectively, which indicates the stability of both pulse trains. The laser has a good potential in industrial and medical applications.

CHAPTER 6

Conclusion and Future Works

6.1   Conclusion

This thesis presented the study of two applications of Thulium fiber as gain medium and saturable absorber (SA). In this work, two types of Thulium fibers were used; a commercial Thulium-doped fiber (TDF) and a newly developed Thulium-Ytterbium co-doped fiber (TYDF). TDF laser (TDFL) operates near 2 µm using the $^3F_4$ $\rightarrow$ $^3H_6$ pump transition of thulium ions in the vicinity of 800 nm. Efficient lasing was achieved as a result of a so-called cross-relaxation process, where two ground-level thulium ions can be excited to the upper lasing level of the $^3F_4$ $\rightarrow$ $^3H_6$ transition by absorbing a single pumping photon with the energy corresponding to approximately 800 nm. This suggests that every excited Tm^{3+} ion located at the $^3H_4$ level can produce two Tm^{3+} ions at the upper lasing level $^3F_4$. On the other hand, the TYDF pumped by a commercial 905−980 nm laser diode. This is due to the $^3H_5$ level of Tm^3+, which is (quasi-) resonant with the excited Yb^{3+} level ($^2F_{5/2}$) and thus allows the energy transfer to create a population inversion between the $^3F_4$ and $^3H_6$ energy levels of Thulium ions.

Besides amplification, the Thulium fibers can also function as a solid-state SA. This is attributed to the energy transition $^3H_6$ - $^3F_4$ of Tm^{3+}, which has a very broad emission and absorption band ranging from 1.6 - 2.1 µm and 1.5 - 1.9 µm respectively. The absorption cross section of TDFs are larger than the emission cross section of Erbium-doped fiber (EDF) at around 1.6 µm region. This suggests a possible application of TDF as SA in a passively Q-switched Erbium-doped fiber laser (EDFL). In this work, we also demonstrated various Q-switched EDFLs based on TDF SA.

The following are highlights of the achievements of this thesis with details to follow;

1-New all-fiber dual-wavelength 2 μm fiber lasers were succesfully demonstrated based on three simple approaches; spatial filtering effect, inline microfiber Mach Zehnder Interferometer and multimode interference effect.

2-Various Q-switched and mode-locked fiber lasers operating in 2 micron region were demonstrated using either commercial Thulium-doped fiber (TDF) or a newly developed Thulium-Ytterbium co-doped fiber (TYDF) as the gain medium. In this work both artificial and passive saturable absorbers were used as Q-switcher or mode-locker.

3-Various Q-switched EDFLs are proposed and demonstrated by using a short piece of TDF as a passive saturable absorber in a ring laser cavity. A dual-wavelength Q-switched EDFL was also demonstrated using the solid state TDF as the SA.

With regards to dual-wavelength fiber lasers, three new approaches; spatial filtering effect, inline microfiber Mach Zehnder Interferometer (MMZI) and multimode interference (Snitzer et al.) effect were proposed and demonstrated in Chapter 3. At first, we developed a room-temperature all-fiber dual-wavelength TDFL operating near 1900 nm, which uses a simpler approach based on a spatial mode-beating filter generated due to mismatch at the splicing points of a TDF. By pumping the gain medium with an 800 nm laser and controlling the phase mismatch at the splicing points of a thulium-doped fiber, the two output lines are obtained at 1844.8 and 1852.0 nm, with the corresponding signal-to-noise ratios of 30 and 21 dB. The threshold pump power is 109.3 mW. At the maximum pump power of 131.7 mW, the output powers are 0.297 and 0.038 mW for the 1844.8 and 1852.0 nm laser lines, respectively.

The second approach used an inline MMZI in the laser cavity to act as a comb filter to realize a room temperature all-fiber dual-wavelength fiber laser operating in 1955 nm region. The proposed laser used a cascaded commercial TDF and homemade double-clad Thulium-Ytterbium co-doped fiber (TYDF), which was forward pumped by

a single-mode 800 nm and a multimode 905 nm pumps respectively as a gain medium. The inline MMZI filter was fabricated using a flame brushing technique to realize two transmission peaks at 1952.93 and 1956.68 nm with the extinction ratio of more than 10 dB based on modal interference. By pumping the TDF and TYDF with a fixed 800 nm and 905 nm pumps at 110 mW and 2.0 W, respectively, dual-wavelength output lines were succesfully obtained at these two wavelengths with a signal to noise ratio of more than 35 dB. The dual-wavelength operation was stable for more than two hours and could be tunable since the laser wavelength is only determined by the function of the MMZI filter.

An all-fiber dual-wavelength fiber laser operating at room temperature in 1950 nm region was also reported using MMI filter in a ring configuration. It uses a commercial TDF and homemade double-clad TYDF as gain media. The MMI filter consists of a 13.5 cm long multimode fiber (MMF) axially spliced at both its ends to identical single mode fibers to realize two transmission peaks at 1939.68 and 1959.60 nm with the maximum extinction ratio based on modal interference. By pumping the TDF and TYDF with a fixed 800 nm and 905 nm pumps at 143 mW and 1.5 W, respectively, dual-wavelength output lines were obtained at these two wavelengths with a signal to noise ratio of more than 27 dB, respectively. The laser was stable for more than two hours and the dual wavelength operation could be tuned by adjusting the parameters of the MMI filter. The proposed dual-wavelength fiber lasers have potential applications in microwave photonics, fiber sensing systems, optical instrument testing, and optical signal processing

In chapter 4, a 2 micron pulsed laser has been succesfully demonstrated using either commercial TDF or a newly developed TYDF as the gain medium. At first, a Q-switched fiber laser operating at 1949.0 nm is demonstrated based on nonlinear polarization rotation (NPR) technique. NPR was widely used especially in Erbium-

doped fiber laser (EDFL) setups to initiate and shape the pulses especially for mode-locking. In fact, the NPR technique can produce the intensity-dependent transmission by self-phase modulation mechanism to provide an artificial SA effect in a fiber ring laser. In our work, we use a 2 m long a commercial TDF and a 15 m long homemade TYDF which is pumped by a single-mode 800 nm and a multimode 905 nm, respectively as the active media. The combination of these gain media and multimode combiner functions as an artificial saturable absorber (SA) which enables the intensity-dependent transmission inside the cavity for the Q-switching. Stable Q-switched pulse train with a repetition rate of 13.49 kHz and pulse width of 3.089 µs is obtained when the 905 nm multimode pump power and 800 nm pump power are fixed at 2.3 W and 110.4 mW, respectively. The maximum pulse energy of 11 nJ is obtained at 800 nm single mode and 905 nm multimode pump powers of 110.4 mW and 2.5 W, respectively. An all-fiber mode-locked TYDFL operating at 1953.5 nm is also demonstrated using the NPR technique. The mode-locked pulse is self-started at threshold 905 nm pump power of 2.7 W. The pulse has repetition rate of 33.1 MHz, the calculated pulse width of 10 ps and pulse energy of 46.9 nJ at 2.7 W pump power.

We have also demonstrated a simple, compact and low cost Q-switched fiber lasers based on TDF to operate at 1846.4 nm by exploiting a multi-walled carbon nanotubes (MWCNTs) polymer composite film based SA. The composite is prepared by mixing the MWCNTs homogeneous solution into a dilute polyvinyl alcohol polymer solution before it is left to dry at room temperature to produce thin film. Then the film is sandwiched between two FC/PC fiber connectors and integrated into the laser cavity for Q-switching pulse generation. The TDFL generates a stable pulse train with 10.38 kHz repetition rate, 17.52 µs pulse width and 11.34 nJ pulse energy at 121.1 mW 800 nm pump power. A passively mode-locked fiber laser is also demonstrated using a MWCNTs-PVA film based SA. The laser is designed to operate at 1951.8 nm by using

a cascaded gain media of TDF and TYDF. Stable mode-locking pulse with a repetition rate of 34.6 MHz and pulse width of 10.79 ps is obtained when the 905 nm multimode pump power reaches 1.8 – 2.2 W while the single-mode 800 nm pump power is fixed at 141.5 mW. Beside showing good Q-switching and mode-locking performances, the MWCNTs SA is also easy to fabricate and low cost. A higher performance Q switching and mode-locking are expected to be achieved with the optimization of the MWCNTs SA and laser cavity.

A mode-locked TYDFL is proposed and demonstrated in Chapter 4 by using a commercial graphene oxide (GO) paper as SA. The GO paper is sandwiched between two fiber ferrules and incorporates a ring laser cavity to generate soliton pulse train operating at 1942.0 nm at a threshold multimode pump power as low as 1.8W. The mode-locked TYDFL has a repetition rate of 22.32 MHz and the calculated pulse width of 1.1 ns. Even though the SA has a low damage threshold, the easy fabrication of GO paper should promote its potential application in ultrafast photonics in 2 micron region.

Besides carbon nanotubes and graphene, solid-state fibers can also be used as a SA. The advantages of this fiber SA are their ability to hold enormous gain excited in the gain fiber from lasing and their high damage threshold for high-power Q-switched pulses. The energy transition $^3H_6$ - $^3F_4$ of Tm^{3+} has a very broad absorption band ranging from 1.5 to 1.9 µm. The absorption cross section of TDFs are larger than the emission cross sections of Erbium-doped fiber (EDF) at 1.6 µm region, suggesting a possible realization of a passively Q-switched EDFL using a TDF as a passive SA. In Chapter 5, we have demonstrated various Q-switched EDFLs by using a short length of TDF as a SA in a ring laser cavity. At first, a Q-switched EDFL operating at 1534.5 nm is proposed and demonstrated using a TDF SA. In this experiment, The EDF and TDF lengths are fixed at 3 m and 1 m, respectively. With the SA, the laser produces a stable pulse train with a repetition rate and pulse width ranging from 11.0 to 25.9 kHz and

37.56 to 16.86 µs while varying the 980 nm pump power from 23 mW to 75 mW. The Q-switched also produces the highest pulse energy of 18.6 nJ at pump power of 75 mW.

The second Q-switched EDFL is based on similar configuration but uses 0.8 m long EDF as the gain medium in conjunction with 0.25 m long TDF as the SA to reduce the pump power threshold. The performance of this laser was also investigated with GO paper SA for comparison purpose. With TDF SA, the repetition rate of the Q-switched EDFL increases from 4.5 to 16.7 kHz while the pulse width reduces from 37.2 to 27.8 µs as the pump power is varied from 14.0 to 26.7 mW. In case of GOP, the pulse repetition rate increases from 14.3 to 31.4 kHz while the pulse width reduces 32.8 to 13.8 µs with the change of pump power from 22.0 to 50.5 mW. The maximum pulse energy of 15.8 nJ and 16.8 nJ are obtained at pump powers of 25.4 mW and 45.5 mW for the EDFL configured with TDF and GOP, respectively. This shows that the EDFL configured with TDF can achieve the same pulse energy at lower pump power compared to the use of GOP. The RF spectrum shows the SNR of approximately 20 and 12 dB with TDF and GOP, respectively, which indicates that the pulse was more stable with the use of TDF SA.

Finally, we demonstrated a dual-wavelength Q-switched EDFL operating at 1551.64 nm and 1534.8 nm using a TDF SA. The laser resonator uses a shorter length of TDF (0.7 m) to reduce the mode competition and allows dual-wavelength simultaneous lasing to taking place in the cavity. The repetition rate of 1551.64 nm laser changes from 14.7 kHz to 21.6 kHz as the pump power is increased from 25 mW to 41 mW. The repetition rate varies from 15.8 to 22.8 kHz at the same pump power range for 1534.8 nm laser. On the other hand, the pulse width for both lasing lines reduces with the pump power. For instance, the pulse width of the 1551.64 nm signal can be varied from 30.1 µs to 21.8 µs by increasing the pump power from 25 mW to 41 mW. We also observe that the pulse width at 1534.8 nm is typically slightly shorter than

those at 1551.64 nm. The difference is due to the different absorption and emission parameters at the two wavelengths as the ground- and excited-state populations vary. The RF measurement shows that the SNR of the laser is obtained at around 10 and 13 dB for 1551.64 nm and 1534.8 nm signal respectively, which indicates the stability of both pulse trains.

Finally, we demonstrate a dual-wavelength, all-fiber, passively Q-switched EDFL based on a TDF SA. Generation of the dual-wavelength output is based on the spectral gain profile of the EDF, which produces two peaks with incorporation of TDF. Our experimental results show that the fiber laser can simultaneously generate Q-switched microsecond pulses at 1534.8 nm and 1551.6 nm. The repetition rate of 1551.64 nm laser changes from 14.7 kHz to 21.6 kHz as the pump power is increased from 25 mW to 41 mW. The repetition rate varies from 15.8 to 22.8 kHz at the same pump power range for 1534.8 nm laser. On the other hand, the pulse width for both lasing lines reduces with the pump power. The pulse width of 20.2 µs and 21.8 µs are achieved for 1534.8 nm and 1551.6 nm lasers, respectively at pump power of 41 mW. We also observe that the pulse width at 1534.8 nm is typically slightly shorter than those at 1551.64 nm. The difference is due to the different absorption and emission parameters at the two wavelengths as the ground- and excited-state populations vary. The RF measurement shows that the SNR of the laser is obtained at around 10 and 13 dB for 1551.64 nm and 1534.8 nm signal respectively, which indicates the stability of both pulse trains.

The final conclusion is that both TDF and TYDF can be effectively used as the gain medium for 2 micron fiber lasers while the TDF was successfully demonstrated as a Q-switcher in EDFL system. Dual wavelength fiber lasers operating in 2 micron region have been demonstrated using various interferometer filters. 2 micron Q-switched and mode-locked fiber lasers have also been demonstrated using passive

technique such as NPR, MWCNTs and GO paper SAs. All proposed fiber laser schemes are quite simple to implement at a low cost. The proposed fiber lasers have a good potential in industrial and medical applications.

6.2   Future research

The research work in this thesis has shown some exciting results and drawn several important conclusions on the use of Thulium fibers as gain medium and SA. It also reveals several challenges. This section discusses some suggestions for future work.

1.   A more comprehensive theoretical model needs to be developed to include the influences of up conversion and reverse cross relaxation energy transfer.

2.   The concentration quenching of $^3F_4$ states needs to be investigated and avoided in the fabrication process. This allows the development of a high concentration Thulium fibers, which is essential in a development of a compact lasers such as distributed feedback fiber lasers.

3.   Most of application of 2 micron fiber laser is in the high power region, working under either CW or pulsed condition. Research focuses needs to be shifted onto fabrication of efficient high power TDFL and TYDFL.

BIBLIOGRAPHY

Agger, S., Povlsen, J. H., & Varming, P. (2004). Single-frequency thulium-doped distributed-feedback fiber laser. *Optics letters, 29*(13), 1503-1505.

Agrawal, G. (2001). *Applications of nonlinear fiber optics*: Academic press.

Ahmad, F., Harun, S., Nor, R., Zulkepely, N., Muhammad, F., Arof, H., & Ahmad, H. (2014). Mode-locked soliton erbium-doped fiber laser using a single-walled carbon nanotubes embedded in polyethylene oxide thin film saturable absorber. *Journal of Modern Optics, 61*(6), 541-545.

Ahmad, H., Muhammad, F., Zulkifli, M., & Harun, S. (2012). Graphene-Oxide-Based Saturable Absorber for All-Fiber Q-Switching With a Simple Optical Deposition Technique. *Photonics Journal, IEEE, 4*(6), 2205-2213.

Ahmad, H., Zulkifli, M., Latif, A., & Harun, S. (2009). Tunable dual wavelength fiber laser incorporating AWG and optical channel selector by controlling the cavity loss. *Optics Communications, 282*(24), 4771-4775.

Allen, R., Esterowitz, L., & Aggarwal, I. (1993). An efficient 1.46 μm thulium fiber laser via a cascade process. *Quantum Electronics, IEEE Journal of, 29*(2), 303-306.

Álvarez-Tamayo, R., Durán-Sánchez, M., Pottiez, O., Kuzin, E., Ibarra-Escamilla, B., & Flores-Rosas, A. (2011). Theoretical and experimental analysis of tunable Sagnac high-birefringence loop filter for dual-wavelength laser application. *Applied optics, 50*(3), 253-260.

Andrews, R., Jacques, D., Qian, D., & Rantell, T. (2002). Multiwall carbon nanotubes: synthesis and application. *Accounts of Chemical Research, 35*(12), 1008-1017.

Anyi, C., Ali, N., Rahman, A., Harun, S., & Arof, H. (2013). Multi-wavelength Q-switched erbium-doped fiber laser using saturable absorber based on carbon nanotube film. *Ukr. J. Phys. Opt, 14*(4), 213.

Bae, S., Kim, H., Lee, Y., Xu, X., Park, J.-S., Zheng, Y., . . . Song, Y. I. (2010). Roll-to-roll production of 30-inch graphene films for transparent electrodes. *Nature nanotechnology, 5*(8), 574-578.

Bajwa, N., Li, X., Ajayan, P. M., & Vajtai, R. (2008). Mechanisms for catalytic CVD growth of multiwalled carbon nanotubes. *Journal of nanoscience and nanotechnology, 8*(11), 6054-6064.

Banhart, F. (1999). Irradiation effects in carbon nanostructures. *Reports on Progress in Physics, 62*(8), 1181.

Bao, Q., Zhang, H., Wang, Y., Ni, Z., Yan, Y., Shen, Z. X., . . . Tang, D. Y. (2009). Atomic-Layer Graphene as a Saturable Absorber for Ultrafast Pulsed Lasers. *Advanced Functional Materials, 19*(19), 3077-3083.

Baudelet, M., Willis, C. C., Shah, L., & Richardson, M. (2010). Laser-induced breakdown spectroscopy of copper with a 2 μm thulium fiber laser. *Optics express, 18*(8), 7905-7910.

Berger, C., Song, Z., Li, X., Wu, X., Brown, N., Naud, C., . . . Marchenkov, A. N. (2006). Electronic confinement and coherence in patterned epitaxial graphene. *Science, 312*(5777), 1191-1196.

Bommeli, F., Degiorgi, L., Wachter, P., Bacsa, W., De Heer, W., & Forro, L. (1997). The optical response of carbon nanotubes. *Synthetic Metals, 86*(1), 2307-2308.

Bonaccorso, F., Sun, Z., Hasan, T., & Ferrari, A. (2010). Graphene photonics and optoelectronics. *Nature Photonics, 4*(9), 611-622.

Bose, S., Gayen, S., & Behera, S. (2005). Theory of the tangential G-band feature in the Raman spectra of metallic carbon nanotubes. *Physical Review B, 72*(15), 153402.

Bradley, D., & O'neill, F. (1969). Passive mode-locking of flashlamp pumped rhodamine dye-lasers. *Opto-electronics, 1*(2), 69-74.

Bridges, W. B. (1964). Laser oscillation in singly ionized argon in the visible spectrum. *Applied Physics Letters, 4*(7), 128-130.

Brown, S., Jorio, A., Dresselhaus, M., & Dresselhaus, G. (2001). Observations of the D-band feature in the Raman spectra of carbon nanotubes. *Physical Review B, 64*(7), 073403.

Chan, K. (1997). Erbium-doped fiber lasers for dual wavelength operation. *Electronics Letters, 33*(1), 52-53.

Chen, L., Zhang, M., Zhou, C., Cai, Y., Ren, L., & Zhang, Z. (2009). Ultra-low repetition rate linear-cavity erbium-doped fiber laser modelocked with semiconductor saturable absorber mirror. *Electronics Letters, 45*(14), 731-733.

Chen, Y.-C., Raravikar, N., Schadler, L., Ajayan, P., Zhao, Y.-P., Lu, T.-M., . . . Zhang, X.-C. (2002). Ultrafast optical switching properties of single-wall carbon nanotube polymer composites at 1.55 μm. *Applied Physics Letters, 81*(6), 975-977.

Colbert, D., Zhang, J., McClure, S., Nikolaev, P., Chen, Z., Hafner, J., . . . Weaver, J. (1994). Growth and sintering of fullerene nanotubes. *Science, 266*(5188), 1218-1222.

Das, A., Chakraborty, B., & Sood, A. (2008). Raman spectroscopy of graphene on different substrates and influence of defects. *Bulletin of Materials Science, 31*(3), 579-584.

Dausinger, F., Lichtner, F., & Lubatschowski, H. (2004). *Femtosecond technology for technical and medical applications* (Vol. 96): Springer.

Delgado-Pinar, M., Zalvidea, D., Diez, A., Perez-Millan, P., & Andres, M. (2006). Q-switching of an all-fiber laser by acousto-optic modulation of a fiber Bragg grating. *Optics express, 14*(3), 1106-1112.

Digonnet, M. J. (2002). *Rare-earth-doped fiber lasers and amplifiers, revised and expanded*: CRC press.

Dikin, D. A., Stankovich, S., Zimney, E. J., Piner, R. D., Dommett, G. H., Evmenenko, G., . . . Ruoff, R. S. (2007). Preparation and characterization of graphene oxide paper. *Nature, 448*(7152), 457-460.

DiLeo, R. A., Landi, B. J., & Raffaelle, R. P. (2007). Purity assessment of multiwalled carbon nanotubes by Raman spectroscopy. *Journal of Applied Physics, 101*(6), 064307.

Dingle, R., & Henry, C. H. (1976). Quantum effects in heterostructure lasers: Google Patents.

Dong, B., Hao, J., Hu, J., & Liaw, C.-y. (2011). Short linear-cavity Q-switched fiber laser with a compact short carbon nanotube based saturable absorber. *Optical Fiber Technology, 17*(2), 105-107.

Doorn, S., Heller, D., Barone, P., Usrey, M., & Strano, M. (2004). Resonant Raman excitation profiles of individually dispersed single walled carbon nanotubes in solution. *Applied Physics A, 78*(8), 1147-1155.

Dresselhaus, M., Dresselhaus, G., & (ed), A. P. (2001). Carbon nanotubes: synthesis, structure, properties and applications. *Topics in Applied Physics, 80*.

Dvoyrin, V. V., Mashinsky, V. M., & Dianov, E. (2007). Yb-Bi pulsed fiber lasers. *Optics letters, 32*(5), 451-453.

El-Sherif, A. F., & King, T. A. (2003). High-energy, high-brightness Q-switched Tm^{3+}-doped fiber laser using an electro-optic modulator. *Optics Communications, 218*(4), 337-344.

Esterowitz, L. (1990). Diode-pumped holmium, thulium, and erbium lasers between 2 and 3 m operating cw at room temperature. *Opt. Eng, 29*(6), 676-680.

Fan, S., Chapline, M. G., Franklin, N. R., Tombler, T. W., Cassell, A. M., & Dai, H. (1999). Self-oriented regular arrays of carbon nanotubes and their field emission properties. *Science, 283*(5401), 512-514.

Fang, Q., Shi, W., Petersen, E., Kieu, K., Chavez-Pirson, A., & Peyghambarian, N. (2012). Half-mJ All-Fiber-Based Single-Frequency Nanosecond Pulsed Fiber Laser at 2. *Photonics Technology Letters, IEEE, 24*(5), 353-355.

Fantini, C., Jorio, A., Souza, M., Strano, M., Dresselhaus, M., & Pimenta, M. (2004). Optical transition energies for carbon nanotubes from resonant Raman spectroscopy: Environment and temperature effects. *Physical Review Letters, 93*(14), 147406.

Feng, C., Liu, D., & Liu, J. (2012). Graphene oxide saturable absorber on golden reflective film for Tm: YAP Q-switched mode-locking laser at 2 μm. *Journal of Modern Optics, 59*(21), 1825-1828.

Fermann, M. E., Galvanauskas, A., & Sucha, G. (2002). *Ultrafast lasers: Technology and applications* (Vol. 80): CRC Press.

Ferrari, A., Meyer, J., Scardaci, V., Casiraghi, C., Lazzeri, M., Mauri, F., . . . Roth, S. (2006). Raman spectrum of graphene and graphene layers. *Physical Review Letters, 97*(18), 187401.

Forro, L., & Schoenenberger, C. (2001). Physical properties of multi-wall nanotubes *Carbon Nanotubes* (pp. 329-391): Springer.

Fried, N. M., & Murray, K. E. (2005). High-power thulium fiber laser ablation of urinary tissues at 1.94 um. *Journal of endourology, 19*(1), 25-31.

Gandy, H., Ginther, R., & Weller, J. (1967). Stimulated emission of Tm3+ radiation in silicate glass. *Journal of Applied Physics, 38*(7), 3030-3031.

Geim, A. K., & MacDonald, A. (2007). Graphene: Exploring carbon flatland.

Geusic, J., Marcos, H., & Van Uitert, L. (1964). Laser oscillations in Nd-doped yttrium aluminum, yttrium gallium and gadolinium garnets. *Applied Physics Letters, 4*(10), 182-184.

Going, R., Popa, D., Torrisi, F., Sun, Z., Hasan, T., Wang, F., & Ferrari, A. (2012). 500fs wideband tunable fiber laser mode-locked by nanotubes. *Physica E: Low-dimensional Systems and Nanostructures, 44*(6), 1078-1081.

Grubb, S., Bennett, K., Cannon, R., & Humer, W. (1992). CW room-temperature blue upconversion fiber laser. *Electronics Letters, 28*(13), 1243-1244.

Guo, T., Nikolaev, P., Thess, A., Colbert, D., & Smalley, R. (1995). Catalytic growth of single-walled manotubes by laser vaporization. *Chemical Physics Letters, 243*(1), 49-54.

Halder, A., Paul, M. C., Damanhuri, S., Huri, N., Hamzah, A., Harun, S., . . . Bhadra, S. K. (2012). Upconversion luminescence in Tm3+/Yb3+ co-doped double-clad silica fibers under 980 nm cladding pumping. *Journal of Modern Optics, 59*(6), 527-532.

Hall, R., Fenner, G., Kingsley, J., Soltys, T., & Carlson, R. (1962). Coherent Light Emission from Ga-As Junctions. *Phys. Rev. Lett, 9*, 366.

Hamzah, A., Paul, M. C., Awang, N., Ahmad, H., Pal, M., Das, S., . . . Harun, S. (2013). Passively mode-locked erbium doped zirconia fiber laser using a nonlinear polarisation rotation technique. *Optics & Laser Technology, 47*, 22-25.

Han, Y. G., & Lee, J. H. (2007). Switchable dual wavelength erbium-doped fiber laser at room temperature. *Microwave and Optical Technology Letters, 49*(6), 1433-1435.

Hanna, D., Jauncey, I., Percival, R., Perry, I., Smart, R., Suni, P., . . . Tropper, A. (1988). Continuous-wave oscillation of a monomode thulium-doped fiber laser. *Electronics Letters, 24*(19), 1222-1223.

Hanna, D., Percival, R., Smart, R., & Tropper, A. (1990). Efficient and tunable operation of a Tm-doped fiber laser. *Optics Communications, 75*(3), 283-286.

Hanna, D., Perry, I., Lincoln, J., & Townsend, J. (1990). A 1-Watt thulium-doped cw fiber laser operating at 2 μm. *Optics Communications, 80*(1), 52-56.

Hároz, E., Duque, J., Rice, W., Densmore, C., Kono, J., & Doorn, S. (2011). Resonant Raman spectroscopy of armchair carbon nanotubes: Absence of broad G-feature. *Physical Review B, 84*(12), 121403.

Harun, S., Halder, A., Paul, M. C., Ali, S., Saidin, N., Damanhuri, S., . . . Bhadra, S. K. (2012). Ytterbium-sensitized thulium-doped fiber laser with a single-mode output operating at 1 900-nm region. *Chinese Optics Letters, 10*(10), 101401-101401.

Harun, S., Ismail, M., Ahmad, F., Ismail, M., Nor, R., Zulkepely, N., & Ahmad, H. (2012). A Q-switched erbium-doped fiber laser with a carbon nanotube based saturable absorber. *Chinese Physics Letters, 29*(11), 114202.

Harun, S., Saidin, N., Damanhuri, S., Ahmad, H., Halder, A., Paul, M. C., . . . Bhadra, S. K. (2012). Fiber laser at 2 micron region using double-clad thulium/ytterbium co-doped yttria-alumino-silicate fiber. *Laser Physics Letters, 9*(1), 50.

Harun, S., Samsuri, N. M., & Ahmad, H. (2005). Gain enhancement in partial double-pass l-band edfa system using a band-pass filter. *Laser Physics Letters, 2*(1), 36.

Hasan, T., Scardaci, V., Tan, P., Bonaccorso, F., Rozhin, A., Sun, Z., & Ferrari, A. (2011). Nanotube and graphene polymer composites for photonics and optoelectronics *Molecular-and Nano-Tubes* (pp. 279-354): Springer.

Hasan, T., Sun, Z., Wang, F., Bonaccorso, F., Tan, P. H., Rozhin, A. G., & Ferrari, A. C. (2009). Nanotube–polymer composites for ultrafast photonics. *Advanced Materials, 21*(38-39), 3874-3899.

He, X., Liu, Z.-B., Wang, D., Yang, M., Liao, C., & Zhao, X. (2012). Passively mode-locked fiber laser based on reduced graphene oxide on microfiber for ultra-wide-band doublet pulse generation. *Journal of lightwave technology, 30*(7), 984-989.

Hecht, J. (2010). Short history of laser development. *Optical engineering, 49*(9), 091002-091002-091023.

Henderson, S. W., Suni, P. J., Hale, C. P., Hannon, S. M., Magee, J. R., Bruns, D. L., & Yuen, E. H. (1993). Coherent laser radar at 2 μm using solid-state lasers. *Geoscience and Remote Sensing, IEEE Transactions on, 31*(1), 4-15.

Herda, R., Kivistö, S., & Okhotnikov, O. G. (2008). Dynamic gain induced pulse shortening in Q-switched lasers. *Optics letters, 33*(9), 1011-1013.

Holonyak Jr, N., & Bevacqua, S. (1962). Coherent (visible) light emission from Ga (As1− xPx) junctions. *Applied Physics Letters, 1*(4), 82-83.

Huang, D.-W., Liu, W.-F., & Yang, C. (2000). Q-switched all-fiber laser with an acoustically modulated fiber attenuator. *Photonics Technology Letters, IEEE, 12*(9), 1153-1155.

Huang, J., Huang, W., Zhuang, W., Su, K., Chen, Y., & Huang, K. (2009). High-pulse-energy, passively Q-switched Yb-doped fiber laser with AlGaInAs quantum wells as a saturable absorber. *Optics letters, 34*(15), 2360-2362.

Huang, P. L., Lin, S.-C., Yeh, C.-Y., Kuo, H.-H., Huang, S.-H., Lin, G.-R., . . . Cheng, W.-H. (2012). Stable mode-locked fiber laser based on CVD fabricated graphene saturable absorber. *Optics express, 20*(3), 2460-2465.

Hummers Jr, W. S., & Offeman, R. E. (1958). Preparation of graphitic oxide. *Journal of the American Chemical Society, 80*(6), 1339-1339.

Iijima, S. (1991). Helical microtubules of graphitic carbon. *Nature, 354*(6348), 56-58.

Iijima, S., Wakabayashi, T., & Achiba, Y. (1996). Structures of carbon soot prepared by laser ablation. *The Journal of Physical Chemistry, 100*(14), 5839-5843.

Inc., M.-W. (2004). *Merriam-Webster's collegiate dictionary*: Merriam-Webster.

Ismail, M., Ahmad, F., Harun, S., Arof, H., & Ahmad, H. (2013). A Q-switched erbium-doped fiber laser with a graphene saturable absorber. *Laser Physics Letters, 10*(2), 025102.

Ivanov, V., Nagy, J., Lambin, P., Lucas, A., Zhang, X., Zhang, X., . . . Van Landuyt, J. (1994). The study of carbon nanotubules produced by catalytic method. *Chemical Physics Letters, 223*(4), 329-335.

Javan, A., Bennett Jr, W. R., & Herriott, D. R. (1961). Population inversion and continuous optical maser oscillation in a gas discharge containing a He-Ne mixture. *Physical Review Letters, 6*(3), 106.

Jeon, M. Y., Kim, N., Jaeheon Shin, Jong Sool Jeong, Sang-Pil Han, Chul Wook Lee, . . . Park, K. H. (2010). Widely tunable dual-wavelength Er3+-doped fiber laser for tunable continuous-wave terahertz radiation *Optics Communications, 282*(24), 4771-4775.

Ji, F., Xin, L., & Ming, H. (2007). *Passively mode-locked fiber laser using SESAM*. Paper presented at the SPIE.

Jiang, M., Ma, H., Ren, Z., Chen, X., Long, J., Qi, M., . . . Bai, J. (2013). A graphene Q-switched nanosecond Tm-doped fiber laser at 2 μm. *Laser Physics Letters, 10*(5), 055103.

Jiang, M., Ren, Z., Zhang, Y., Lu, B., Wan, L., & Bai, J. (2011). Graphene-based passively Q-switched diode-side-pumped Nd: YAG solid laser. *Optics Communications, 284*(22), 5353-5356.

Jiang, S. (2011). *Recent progress on 2-micron fiber lasers.* Paper presented at the 2011 Optical Fiber Communication Conference and Exposition and the National Fiber Optic Engineers Conference.

Jishi, R., Venkataraman, L., Dresselhaus, M., & Dresselhaus, G. (1993). Phonon modes in carbon nanotubules. *Chemical Physics Letters, 209*(1), 77-82.

Johnson, L. F. (1962). Optical maser characteristics of Nd3+ in CaF2. *Journal of Applied Physics, 33*(2), 756-756.

Jong Lee, S., Koo Baik, H., Yoo, J.-e., & Hoon Han, J. (2002). Large scale synthesis of carbon nanotubes by plasma rotating arc discharge technique. *Diamond and related Materials, 11*(3), 914-917.

Jorio, A., Dresselhaus, G., & Dresselhaus, M. S. (2007). *Carbon nanotubes: advanced topics in the synthesis, structure, properties and applications* (Vol. 111): Springer.

Jorio, A., Pimenta, M., Souza Filho, A., Saito, R., Dresselhaus, G., & Dresselhaus, M. (2003). Characterizing carbon nanotube samples with resonance Raman scattering. *New Journal of Physics, 5*(1), 139.

Jung, I., Kärtner, F., Matuschek, N., Sutter, D., Morier-Genoud, F., Shi, Z., . . . Keller, U. (1997). Semiconductor saturable absorber mirrors supporting sub-10-fs pulses. *Applied Physics B: Lasers and Optics, 65*(2), 137-150.

Kapron, F., Keck, D. B., & Maurer, R. D. (1970). Radiation losses in glass optical waveguides. *Applied Physics Letters, 17*(10), 423-425.

Kashiwagi, K., & Yamashita, S. (2010). Optical Deposition of Carbon Nanotubes for Fiber-based Device Fabrication.

Kastner, J., Pichler, T., Kuzmany, H., Curran, S., Blau, W., Weldon, D., . . . Zandbergen, H. (1994). Resonance Raman and infrared spectroscopy of carbon nanotubes. *Chemical Physics Letters, 221*(1), 53-58.

Kataura, H., Kumazawa, Y., Maniwa, Y., Umezu, I., Suzuki, S., Ohtsuka, Y., & Achiba, Y. (1999). Optical properties of single-wall carbon nanotubes. *Synthetic Metals, 103*(1), 2555-2558.

Kee, H. H., Lees, G. P., & Newson, T. P. (1998). Narrow linewidth CW and Q-switched erbium-doped fiber loop laser. *Electronics Letters, 34*(13), 1318-1319.

Keller, U. (2003). Recent developments in compact ultrafast lasers. *Nature, 424*(6950), 831-838.

Keller, U. (2004). Ultrafast solid-state lasers. *Progress in Optics, 46*, 1-116.

Keller, U. (2010). Ultrafast solid-state laser oscillators: a success story for the last 20 years with no end in sight. *Applied Physics B, 100*(1), 15-28.

Kieu, K., & Wise, F. (2009). Soliton thulium-doped fiber laser with carbon nanotube saturable absorber. *IEEE photonics technology letters: a publication of the IEEE Laser and Electro-optics Society, 21*(3), 128.

Kim, K. S., Zhao, Y., Jang, H., Lee, S. Y., Kim, J. M., Kim, K. S., . . . Hong, B. H. (2009). Large-scale pattern growth of graphene films for stretchable transparent electrodes. *Nature, 457*(7230), 706-710.

Kim, P., Shi, L., Majumdar, A., & McEuen, P. (2001). Thermal transport measurements of individual multiwalled nanotubes. *Physical Review Letters, 87*(21), 215502.

Kind, H., Bonard, J. M., Emmenegger, C., Nilsson, L. O., Hernadi, K., Maillard-Schaller, E., . . . Kern, K. (1999). Patterned films of nanotubes using microcontact printing of catalysts. *Advanced Materials, 11*(15), 1285-1289.

Kivistö, S., Koskinen, R., Paajaste, J., Jackson, S. D., Guina, M., & Okhotnikov, O. G. (2008). Passively Q-switched Tm3+, Ho3+-doped silica fiber laser using a highly nonlinear saturable absorber and dynamic gain pulse compression. *Optics express, 16*(26), 22058-22063.

Koester, C. J., & Snitzer, E. (1964). Amplification in a fiber laser. *Applied optics, 3*(10), 1182-1186.

Kurkov, A., Sadovnikova, Y. E., Marakulin, A., & Sholokhov, E. (2010). All fiber Er-Tm Q-switched laser. *Laser Physics Letters, 7*(11), 795-797.

Kurkov, A., Sholokhov, E., & Medvedkov, O. (2009). All fiber Yb-Ho pulsed laser. *Laser Physics Letters, 6*(2), 135-138.

Kürti, J., Zólyomi, V., Grüneis, A., & Kuzmany, H. (2002). Double resonant Raman phenomena enhanced by van Hove singularities in single-wall carbon nanotubes. *Physical Review B, 65*(16), 165433.

Lacerda, L., Raffa, S., Prato, M., Bianco, A., & Kostarelos, K. (2007). Cell-penetrating CNTs for delivery of therapeutics. *Nano Today, 2*(6), 38-43.

Latif, A., Ahmad, H., Awang, N., Zulkifli, M., Pua, C., Ghani, Z., & Harun, S. (2011). Tunable high power fiber laser using an AWG as the tuning element. *Laser Physics, 21*(4), 712-717.

Lehman, J. H., Terrones, M., Mansfield, E., Hurst, K. E., & Meunier, V. (2011). Evaluating the characteristics of multiwall carbon nanotubes. *Carbon, 49*(8), 2581-2602.

Léonard, F. o. (2009). The physics of carbon nanotube devices.

Li, S., Ngo, N. Q., Tjin, S. C., & Binh, L. N. (2004). Tunable and switchable optical bandpass filters using a single linearly chirped fiber Bragg grating. *Optics Communications, 239*(4), 339-344.

Li, X., Cai, W., An, J., Kim, S., Nah, J., Yang, D., . . . Tutuc, E. (2009). Large-area synthesis of high-quality and uniform graphene films on copper foils. *Science, 324*(5932), 1312-1314.

Lim, K. S., Pua, C. H., Awang, N. A., Harun, S. W., & Ahmad, H. (2009). Fiber loop mirror filter with two-stage high birefringence fibers. *Progress In Electromagnetics Research C, 9*, 101-108.

Lin, X. C., Zhang, L., Tsang, Y. H., Wang, Y. G., Yu, H. J., Yan, S. L., . . . Hou, W. (2013). Multi-walled carbon nanotube as a saturable absorber for a passively mode-locked Nd: YVO4 laser. *Laser Physics Letters, 10*(5), 055805.

Liu, D., Ngo, N., Liu, H., & Liu, D. (2009). Microwave generation using an all polarization-maintaining linear cavity dual-wavelength fiber laser with tunable wavelength spacing. *Optics Communications, 282*(8), 1611-1614.

Liu, D., Ngo, N. Q., Tjin, S. C., & Dong, X. (2007). A dual-wavelength fiber laser sensor system for measurement of temperature and strain. *Photonics Technology Letters, IEEE, 19*(15), 1148-1150.

Liu, H., Chow, K., Yamashita, S., & Set, S. (2013). Carbon-nanotube-based passively Q-switched fiber laser for high energy pulse generation. *Optics & Laser Technology, 45*, 713-716.

Liu, J. R., Luo, Z. C., Luo, A. P., Yin, H. S., & Xu, W. C. (2011). Switchable dual-wavelength passively Q-switched erbium-doped fiber ring laser using nonlinear polarization rotation technique. *Microwave and Optical Technology Letters, 53*(5), 1000-1003.

Liu, L., Zhao, Q., Zhou, G., Zhang, H., Chen, S., Zhao, L., . . . Dong, X. (2004). Study on an optical filter constituted by concatenated Hi-Bi fiber loop mirrors. *Microwave and Optical Technology Letters, 43*(1), 23-26.

Liu, X., Wang, T., Shu, C., Wang, L., Lin, A., Lu, K., . . . Zhao, W. (2008). Passively harmonic mode-locked erbium-doped fiber soliton laser with a nonlinear polarization rotation. *Laser Physics, 18*(11), 1357-1361.

Liu, Z.-B., He, X., & Wang, D. (2011). Passively mode-locked fiber laser based on a hollow-core photonic crystal fiber filled with few-layered graphene oxide solution. *Optics letters, 36*(16), 3024-3026.

Liu, Z., Liu, Y.-g., Du, J., Yuan, S., & Dong, X. (2007). Switchable triple-wavelength erbium-doped fiber laser using a single fiber Bragg grating in polarization-maintaining fiber. *Optics Communications, 279*(1), 168-172.

Loh, K. P., Bao, Q., Eda, G., & Chhowalla, M. (2010). Graphene oxide as a chemically tunable platform for optical applications. *Nature chemistry, 2*(12), 1015-1024.

Lou, Q., Zhou, J., He, B., & Zhou, H. (2008). Fiber lasers and their coherent beam combination. *Optics and Photonics News, 19*(5), 46-51.

Lu, B., Chen, H., Jiang, M., Chen, X., Ren, Z., & Bai, J. (2013). Graphene-based passive Q-switching for a 2 μm thulium-doped fiber laser. *Laser Physics, 23*(4), 045111.

Maiman, T. H. (1960). Stimulated optical radiation in ruby.

Mao, Q., & Lit, J. W. (2002). Switchable multiwavelength erbium-doped fiber laser with cascaded fiber grating cavities. *Photonics Technology Letters, IEEE, 14*(5), 612-614.

Maultzsch, J., Telg, H., Reich, S., & Thomsen, C. (2005). Radial breathing mode of single-walled carbon nanotubes: Optical transition energies and chiral-index assignment. *Physical Review B, 72*(20), 205438.

Miazato, K., De Sousa, D., Delben, A., Delben, J., De Oliveira, S., & Nunes, L. (2000). Upconversion mechanisms in Tm3+ -doped lead fluoroindogallate glasses. *Journal of non-crystalline solids, 273*(1), 246-251.

Moghaddam, M., Harun, S., Akbari, R., & Ahmad, H. (2011). Stable mode-locked fiber laser using 49 cm long bismuth oxide based erbium doped fiber and slow saturable absorber. *Laser Physics, 21*(5), 913-918.

Moore, P. J., Chaboyer, Z. J., & Das, G. (2009). Tunable dual-wavelength fiber laser. *Optical Fiber Technology, 15*(4), 377-379.

Moulton, P. F. (1986). Spectroscopic and laser characteristics of Ti: Al2 O3 *JOSA B, 3*(1), 125-133.

Myslinski, P., Pan, X., Chrostowski, J., Bayon, J.-F., Sullivan, B. T., & Barnard, C. W. (1993). Q-switched thulium-doped fiber laser. *Optical engineering, 32*(9), 2025-2030.

Nawata, K., Notake, T., Kawamata, H., Matsukawa, T., Qi, F., & Minamide, H. (2012). *High-power tunable terahertz-wave source pumped by dual-wavelength injection-seeded optical parametric generator.* Paper presented at the CLEO: Science and Innovations.

Nelson, L., Ippen, E., & Haus, H. (1995). Broadly tunable sub-500 fs pulses from an additive-pulse mode-locked thulium-doped fiber ring laser. *Applied Physics Letters, 67*(1), 19-21.

Novoselov, K. S., Geim, A. K., Morozov, S., Jiang, D., Zhang, Y., Dubonos, S., . . . Firsov, A. (2004). Electric field effect in atomically thin carbon films. *Science, 306*(5696), 666-669.

Okoshi, T. (1982). Optical Fibers, : Academic Press, Inc.

Osswald, S., Flahaut, E., Ye, H., & Gogotsi, Y. (2005). Elimination of D-band in Raman spectra of double-wall carbon nanotubes by oxidation. *Chemical Physics Letters, 402*(4), 422-427.

Pal, A., Dhar, A., Das, S., Chen, S. Y., Sun, T., Sen, R., & Grattan, K. T. (2010). Ytterbium-sensitized Thulium-doped fiber laser in the near-IR with 980 nm pumping. *Optics express, 18*(5), 5068-5074.

Pan, L., Utkin, I., & Fedosejevs, R. (2007). Passively Q-switched Ytterbium-Doped Double-Clad Fiber Laser With a Cr 4+: YAG Saturable Absorber. *Photonics Technology Letters, IEEE, 19*(24), 1979-1981.

Pan, L., Utkin, I., & Fedosejevs, R. (2008). Two-wavelength passively Q-switched ytterbium doped fiber laser. *Optics express, 16*(16), 11858-11870.

Parvizi, R., Harun, S., Ali, N., Shahabuddin, N., & Ahmad, H. (2011). Photonic crystal fiber-based multi-wavelength Brillouin fiber laser with dual-pass amplification configuration. *Chinese Optics Letters, 9*(2), 021403.

Paschotta, R., Häring, R., Gini, E., Melchior, H., Keller, U., Offerhaus, H., & Richardson, D. (1999). Passively Q-switched 0.1-mJ fiber laser system at 1.53 μm. *Optics letters, 24*(6), 388-390.

Patel, C. K. N. (1964). Continuous-Wave Laser Action on Vibrational-Rotational Transitions of C O 2. *Physical review, 136*(5A), A1187.

Pérez-Millán, P., Díez, A., Andrés, M., Zalvidea, D., & Duchowicz, R. (2005). Q-switched all-fiber laser based on magnetostriction modulation of a Bragg grating. *Optics express, 13*(13), 5046-5051.

Philippov, V., Kir'yanov, A., & Unger, S. (2004). Advanced configuration of erbium fiber passively Q-switched laser with Co 2+: ZnSe crystal as saturable absorber. *Photonics Technology Letters, IEEE, 16*(1), 57-59.

Piscanec, S., Lazzeri, M., Robertson, J., Ferrari, A. C., & Mauri, F. (2007). Optical phonons in carbon nanotubes: Kohn anomalies, Peierls distortions, and dynamic effects. *Physical Review B, 75*(3), 035427.

Popa, D., Sun, Z., Hasan, T., Torrisi, F., Wang, F., & Ferrari, A. (2010). Graphene Q-switched, tunable fiber laser. *arXiv preprint arXiv:1011.0115*.

Popa, D., Sun, Z., Torrisi, F., Hasan, T., Wang, F., & Ferrari, A. (2010). Sub 200 fs pulse generation from a graphene mode-locked fiber laser. *Applied Physics Letters, 97*(20), 203106.

Qamar, F. Z., & King, T. A. (2005). Passive Q-switching of the Tm-silica fiber laser near 2μm by a Cr2+: ZnSe saturable absorber crystal. *Optics Communications, 248*(4), 501-508.

Ramadurai, K., Cromer, C. L., Lewis, L. A., Hurst, K. E., Dillon, A. C., Mahajan, R. L., & Lehman, J. H. (2008). High-performance carbon nanotube coatings for high-power laser radiometry. *Journal of Applied Physics, 103*(1), 013103.

Rao, A., Eklund, P., Bandow, S., Thess, A., & Smalley, R. E. (1997). Evidence for charge transfer in doped carbon nanotube bundles from Raman scattering. *Nature, 388*(6639), 257-259.

Richards, B. D., Tsang, Y. H., Binks, D. J., Lousteau, J., & Jha, A. (2008). *CW and Q-switched 2.1 µm Tm3+/Ho3+/Yb3+-triply-doped tellurite fiber lasers.* Paper presented at the SPIE Remote Sensing.

Riesbeck, T., & Lux, O. (2009). AOM fourfold pass for efficient Q-switching and stable high peak power laser pulses. *Optics Communications, 282*(18), 3789-3792.

Rulliere, C. (2005). *Femtosecond laser pulses*: Springer.

Russo, N., Duchowicz, R., Mora, J., Cruz, J., & Andrés, M. (2002). High-efficiency Q-switched erbium fiber laser using a Bragg grating-based modulator. *Optics Communications, 210*(3), 361-366.

Saito, R., Jorio, A., Souza Filho, A., Dresselhaus, G., Dresselhaus, M., & Pimenta, M. (2001). Probing phonon dispersion relations of graphite by double resonance Raman scattering. *Physical Review Letters, 88*(2), 027401.

Sakakibara, Y., Rozhin, A. G., Kataura, H., Achiba, Y., & Tokumoto, M. (2005). Carbon nanotube-poly (vinylalcohol) nanocomposite film devices: Applications for femtosecond fiber laser mode lockers and optical amplifier noise suppressors. *Japanese journal of applied physics, 44*(4R), 1621.

Schadler, L., Giannaris, S., & Ajayan, P. (1998). Load transfer in carbon nanotube epoxy composites. *Applied Physics Letters, 73*(26), 3842-3844.

Schmidt, A., Rivier, S., Cho, W. B., Yim, J. H., Choi, S. Y., Lee, S., . . . Petrov, V. (2009). Sub-100 fs single-walled carbon nanotube saturable absorber mode-locked Yb-laser operation near 1 µm. *Optics express, 17*(22), 20109-20116.

Set, S. Y., Yaguchi, H., Tanaka, Y., & Jablonski, M. (2004). Laser mode locking using a saturable absorber incorporating carbon nanotubes. *Journal of lightwave technology, 22*(1), 51.

Shang, L., Ning, J., & Yang, X. (2012). An experimental study of an acousto-optic Q-switched Yb3+-doped all-fiber laser. *Optik-International Journal for Light and Electron Optics, 123*(12), 1061-1062.

Sharp, R., Spock, D., Pan, N., & Elliot, J. (1996). 190-fs passively mode-locked thulium fiber laser with a low threshold. *Optics letters, 21*(12), 881-883.

Snitzer, E. (1961A). Proposed fiber cavities for optical masers. *Journal of Applied Physics, 32*(1), 36-39.

Snitzer, E. (1961B). Optical maser action of Nd+ 3 in a barium crown glass. *Physical Review Letters, 7*(12), 444.

Snitzer, E., Po, H., Hakimi, F., Tumminelli, R., & McCollum, B. (1988). *Double clad, offset core Nd fiber laser.* Paper presented at the Optical Fiber Sensors.

Sobon, G., Sotor, J., Jagiello, J., Kozinski, R., Librant, K., Zdrojek, M., . . . Abramski, K. M. (2012). Linearly polarized, Q-switched Er-doped fiber laser based on reduced graphene oxide saturable absorber. *Applied Physics Letters, 101*(24), 241106.

Sobon, G., Sotor, J., Jagiello, J., Kozinski, R., Zdrojek, M., Holdynski, M., . . . Abramski, K. M. (2012). Graphene oxide vs. reduced graphene oxide as saturable absorbers for Er-doped passively mode-locked fiber laser. *Optics express, 20*(17), 19463-19473.

Solodyankin, M. A., Obraztsova, E. D., Lobach, A. S., Chernov, A. I., Tausenev, A. V., Konov, V. I., & Dianov, E. M. (2008). Mode-locked 1.93 μm thulium fiber laser with a carbon nanotube absorber. *Optics letters, 33*(12), 1336-1338.

Song, Y.-W. (2012). Q-switched fiber lasers with carbon nanotubes hosted in ceramics. *Applied optics, 51*(3), 290-294.

Sorokin, P., & Lankard, J. (1966). Stimulated emission observed from an organic dye, chloro-aluminum phthalocyanine. *IBM Journal of Research and Development, 10*(2), 162-163.

Sotor, J., Sobon, G., Krzempek, K., & Abramski, K. M. (2012). Fundamental and harmonic mode-locking in erbium-doped fiber laser based on graphene saturable absorber. *Optics Communications, 285*(13), 3174-3178.

Stankovich, S., Dikin, D. A., Piner, R. D., Kohlhaas, K. A., Kleinhammes, A., Jia, Y., . . . Ruoff, R. S. (2007). Synthesis of graphene-based nanosheets via chemical reduction of exfoliated graphite oxide. *Carbon, 45*(7), 1558-1565.

Stoneman, R., & Esterowitz, L. (1990). Efficient, broadly tunable, laser-pumped Tm: YAG and Tm: YSGG cw lasers. *Optics letters, 15*(9), 486-488.

Su, L., Wang, Y., Liu, J., Zheng, L., Su, L., & Xu, J. (2012). Double-wall carbon nanotube absorber for passively mode-locked Yb3+: Sc2SiO5 laser. *Laser Physics Letters, 9*(2), 120-125.

Sun, Z., Hasan, T., Torrisi, F., Popa, D., Privitera, G., Wang, F., . . . Ferrari, A. C. (2010). Graphene mode-locked ultrafast laser. *ACS nano, 4*(2), 803-810.

Sun, Z., Hasan, T., Wang, F., Rozhin, A. G., White, I. H., & Ferrari, A. C. (2010). Ultrafast stretched-pulse fiber laser mode-locked by carbon nanotubes. *Nano Research, 3*(6), 404-411.

Sun, Z., Rozhin, A., Wang, F., Scardaci, V., Milne, W., White, I., . . . Ferrari, A. (2008). L-band ultrafast fiber laser mode locked by carbon nanotubes. *Applied Physics Letters, 93*(6), 61114.

Szlauer, R., Götschl, R., Razmaria, A., Paras, L., & Schmeller, N. T. (2009). Endoscopic Vaporesection of the Prostate Using the Continuous-Wave 2-Microm Thulium Laser: Outcome and Demonstration of the Surgical Technique Editorial Comment: ELSEVIER SCIENCE INC 360 PARK AVE SOUTH, NEW YORK, NY 10010-1710 USA.

Taccheo, S., Laporta, P., Longhi, S., Svelto, O., & Svelto, C. (1996). Diode-pumped bulk erbium-ytterbium lasers. *Applied Physics B, 63*(5), 425-436.

Talaverano, L., Abad, S., Jarabo, S., & Lopez-Amo, M. (2001). Multiwavelength fiber laser sources with Bragg-grating sensor multiplexing capability. *Journal of lightwave technology, 19*(4), 553.

Tan, P., Rozhin, A., Hasan, T., Hu, P., Scardaci, V., Milne, W., & Ferrari, A. (2007). Photoluminescence spectroscopy of carbon nanotube bundles: Evidence for exciton energy transfer. *Physical Review Letters, 99*(13), 137402.

Tanaka, K., Sato, T., Yamabe, T., Okahara, K., Uchida, K., Yumura, M., . . . Yase, K. (1994). Electronic properties of carbon nanotube. *Chemical Physics Letters, 223*(1), 65-68.

Tang, Y., Yang, Y., Xu, J., & Hang, Y. (2008). Passive Q-switching of short-length Tm3+-doped silica fiber lasers by polycrystalline Cr2+: ZnSe microchips. *Optics Communications, 281*(22), 5588-5591.

Telg, H., Maultzsch, J., Reich, S., Hennrich, F., & Thomsen, C. (2004). Chirality distribution and transition energies of carbon nanotubes. *Physical Review Letters, 93*(17), 177401.

Theisen-Kunde, D., Tedsen, S., Herrmann, K., Danicke, V., & Brinkmann, R. (2007). *Partial Kidney Resection Based on 1.94 μm Fiber Laser System.* Paper presented at the European Conference on Biomedical Optics.

Thess, A., Lee, R., Nikolaev, P., Dai, H., Petit, P., Robert, J., . . . Rinzler, A. G. (1996). Crystalline ropes of metallic carbon nanotubes. *Science-AAAS-Weekly Paper Edition, 273*(5274), 483-487.

Tsai, T.-Y., Fang, Y.-C., Lee, Z.-C., & Tsao, H.-X. (2009). All-fiber passively Q-switched erbium laser using mismatch of mode field areas and a saturable-amplifier pump switch. *Optics letters, 34*(19), 2891-2893.

Tu, C., Guo, W., Li, Y., Zhang, S., & Lu, F. (2007). Stable multiwavelength and passively mode-locked Yb-doped fiber laser based on nonlinear polarization rotation. *Optics Communications, 280*(2), 448-452.

Urquhart, P. (1988). Review of rare earth doped fiber lasers and amplifiers. *IEE Proceedings J (Optoelectronics), 135*(6), 385-407.

Vodopyanov, I. S. K. (2003). Solid-state mid-infrared laser sources. *Topics in Applied Physics–Springer, 89*, 221.

Wakabayashi, T., Kasuya, D., Shiromaru, H., Suzuki, S., Kikuchi, K., & Achiba, Y. (1997). Towards the selective formation of specific isomers of fullerenes: T-and p-dependence in the yield of various isomers of fullerenes C60–C84. *Zeitschrift für Physik D Atoms, Molecules and Clusters, 40*(1), 414-417.

Wang, F., Rozhin, A., Scardaci, V., Sun, Z., Hennrich, F., White, I., . . . Ferrari, A. C. (2008). Wideband-tuneable, nanotube mode-locked, fiber laser. *Nature nanotechnology, 3*(12), 738-742.

Wang, F., Rozhin, A., Sun, Z., Scardaci, V., Penty, R., White, I., & Ferrari, A. (2008). Fabrication, characterization and mode locking application of single-walled carbon nanotube/polymer composite saturable absorbers. *International Journal of Material Forming, 1*(2), 107-112.

Wang, F., Rozhin, A., Sun, Z., Scardaci, V., White, I., & Ferrari, A. (2008). Soliton fiber laser mode-locked by a single-wall carbon nanotube-polymer composite. *physica status solidi (b), 245*(10), 2319-2322.

Wang, L., Xu, W., Luo, Z., Cao, W., Luo, A., Dong, J., & Wang, H. (2011). Passively Q-switched mode-locking erbium-doped fiber laser with net-normal dispersion using nonlinear polarization rotation technique. *Laser Physics, 21*(10), 1808-1812.

Wang, Q., Geng, J., Jiang, Z., Luo, T., & Jiang, S. (2011). Mode-Locked Tm–Ho-Codoped Fiber Laser at 2.06 m. *Photonics Technology Letters, IEEE, 23*(11), 682-684.

Wang, Q., Geng, J., Luo, T., & Jiang, S. (2009). Mode-locked 2 μm laser with highly thulium-doped silicate fiber. *Optics letters, 34*(23), 3616-3618.

Wang, Q., Teng, H., Zou, Y., Zhang, Z., Li, D., Wang, R., . . . Wei, Z. (2012). Graphene on SiC as a Q-switcher for a 2 μm laser. *Optics letters, 37*(3), 395-397.

Wang, Y., Chen, H., Hsieh, W., & Tsang, Y. (2013). Mode-locked Nd: GdVO4 laser with graphene oxide/polyvinyl alcohol composite material absorber as well as an output coupler. *Optics Communications, 289*, 119-122.

Wang, Y., Qu, Z., Liu, J., & Tsang, Y. H. (2012). Graphene Oxide Absorbers for Watt-Level High-Power Passive Mode-Locked Nd: GdVO Laser Operating at 1 m. *Lightwave Technology, Journal of, 30*(20), 3259-3262.

Wang, Z., Chen, Y., Zhao, C., Zhang, H., & Wen, S. (2012). Switchable dual-wavelength synchronously Q-switched erbium-doped fiber laser based on graphene saturable absorber. *Photonics Journal, IEEE, 4*(3), 869-876.

Wei, L., Zhou, D.-P., Fan, H. Y., & Liu, W.-K. (2012). Graphene-based-switched erbium-doped fiber laser with wide pulse-repetition-rate range. *Photonics Technology Letters, IEEE, 24*(4), 309-311.

Wu, J. (2005). Thulium doped microsphere laser and fiber laser.

Wu, Y., Maultzsch, J., Knoesel, E., Chandra, B., Huang, M., Sfeir, M. Y., . . . Heinz, T. F. (2007). Variable electron-phonon coupling in isolated metallic carbon nanotubes observed by Raman scattering. *Physical Review Letters, 99*(2), 027402.

Xinju, L. (2010). Laser technology.

Xu, J., Liu, J., Wu, S., Yang, Q.-H., & Wang, P. (2012). Graphene oxide mode-locked femtosecond erbium-doped fiber lasers. *Optics express, 20*(14), 15474-15480.

Xu, J., Wu, S., Li, H., Liu, J., Sun, R., Tan, F., . . . Wang, P. (2012). Dissipative soliton generation from a graphene oxide mode-locked Er-doped fiber laser. *Optics express, 20*(21), 23653-23658.

Yamashita, S. (2012). A tutorial on nonlinear photonic applications of carbon nanotube and graphene. *Journal of lightwave technology, 30*(4), 427-447.

Yang, D., Velamakanni, A., Bozoklu, G., Park, S., Stoller, M., Piner, R. D., . . . Ventrice Jr, C. A. (2009). Chemical analysis of graphene oxide films after heat and chemical treatments by X-ray photoelectron and micro-Raman spectroscopy. *Carbon, 47*(1), 145-152.

Yap, Y., De La Rue, R. M., Pua, C., Harun, S., & Ahmad, H. (2012). Graphene-based Q-switched pulsed fiber laser in a linear configuration. *Chinese Optics Letters, 10*(4), 041405.

Yap, Y., Huang, N., Harun, S., & Ahmad, H. (2013). Graphene oxide-based Q-switched erbium-doped fiber laser. *Chinese Physics Letters, 30*(2), 024208.

Zeller, W., Naehle, L., Fuchs, P., Gerschuetz, F., Hildebrandt, L., & Koeth, J. (2010). DFB Lasers Between 760 nm and 16 µm for Sensing Applications. *Sensors, 10*(4), 2492-2510.

Zhang, C., Yao, B., Li, G., Wang, Q., Ju, Y., & Wang, Y. (2010). 2041.3 nm/2054.6 nm simultaneous dual-wavelength single-longitudinal-mode Tm, Ho: YVO4 microchip laser. *Laser Physics, 20*(7), 1564-1567.

Zhang, H., Bao, Q., Tang, D., Zhao, L., & Loh, K. (2009). Large energy soliton erbium-doped fiber laser with a graphene-polymer composite mode locker. *Applied Physics Letters, 95*(14), 141103.

Zhang, L., Wang, Y., Yu, H., Sun, L., Hou, W., Lin, X., & Li, J. (2011). Passive mode-locked Nd: YVO4 laser using a multi-walled carbon nanotube saturable absorber. *Laser Physics, 21*(8), 1382-1386.

Zhang, L., Zhuo, Z., Wang, J., & Wang, Y. (2012). Passively Q-switched fiber laser based on graphene saturable absorber. *Laser Physics, 22*(2), 433-436.

Zhang, Z., Boyland, A., Sahu, J., Clarkson, W., & Ibsen, M. (2011). High-power single-frequency thulium-doped fiber DBR laser at 1943 nm. *Photonics Technology Letters, IEEE, 23*(7), 417-419.

Zhang, Z., Sang, M., Ye, Z., & Nie, Y. (2008). Passively Q-switched erbium-doped fiber laser based on nonlinear polarization rotation. *Microwave and Optical Technology Letters, 50*(3), 694-696.

Zhao, X., Zheng, Z., Liu, L., Liu, Y., Jiang, Y., Yang, X., & Zhu, J. (2011). Switchable, dual-wavelength passively mode-locked ultrafast fiber laser based on a single-wall carbon nanotube modelocker and intracavity loss tuning. *Optics express, 19*(2), 1168-1173.

Zhou, P., Wang, X., Ma, Y., Han, K., & Liu, Z. (2011). Stable all-fiber dual-wavelength thulium-doped fiber laser and its coherent beam combination. *Laser Physics, 21*(1), 184-187.

Zhu, Y., Murali, S., Cai, W., Li, X., Suk, J. W., Potts, J. R., & Ruoff, R. S. (2010). Graphene and graphene oxide: synthesis, properties, and applications. *Advanced Materials, 22*(35), 3906-3924.

Zitter, R. N. (1969). Saturated optical absorption through band filling in semiconductors. *Applied Physics Letters, 14*(2), 73-74.

LIST OF PUBLICATIONS

1- **Azooz, S. M**., Harun, S. W., Ahmad, H., Halder, A., Paul, M. C., Pal, M., & Bhadra, S. K. (2015). Mode-Locked Thulium Ytterbium Co-Doped Fiber Laser with Graphene Oxide Paper Saturable Absorber. Chinese Physics Letters, 32(1), 014204.

2- **Azooz, S. M**., Jasim, A. A., Hamida, B. A., Ahmad, H., Harun, S. W., Halder, A., ... & Bhadra, S. K. (2014). All-fiber dual-wavelength fiber laser operating at 1950 nm region based on multimode interference effect. Laser, 2, 800nm.

3- **Azooz, S. M**., Hamida, B. A., Khan, S., Eltaif, T., Jasim, A. A., Ahmad, H., & Harun, S. W. (2014). All-fibre dual-wavelength thulium-doped fibre laser based on spatial filtering effect. Ukr. J. Phys. Opt, 15, 79-83.

4- **Azooz, S. M**., Ahmad, F., Ahmad, H., Harun, S. W., Hamida, B. A., Khan, S., ... & Bhadra, S. K. (2015). Mode-locked 2 μm fiber laser with a multi-walled carbon nanotube as a saturable absorber. Chinese Optics Letters, 13(3), 030602-030602.

5- **Azooz, S**., Harun, S., Ahmad, H., Halder, A., Paul, M., Das, S., & Bhadra, S. (2015). A Q-switched fibre laser operating in the 2 um region based on nonlinear polarization rotation technique. Ukrainian Journal of Physical Optics, 16, 32.